Role of the VAsodilator-Stimulated Phosphoprotein (VASP) in brown fat cell differentiation and function

Dissertation

zur

Erlangung des Doktorgrades (Dr. rer. nat.)

der

Mathematisch-Naturwissenschaftlichen Fakultät

der

Rheinischen Friedrich-Wilhelms-Universität Bonn

vorgelegt von

Katja Jennißen

aus

Zwickau

Bonn, September 2011

Angefertigt mit Genehmigung der Mathematisch-Naturwissenschaftlichen Fakultät der Rheinischen Friedrich-Wilhelms-Universität Bonn.

1. Gutachter: Prof. Dr. Alexander Pfeifer
2. Gutachter: Prof. Dr. Dieter O. Fürst
Tag der Promotion: 07. Mai 2012
Erscheinungsjahr: 2012

Für meine Familie

Danksagung

An erster Stelle danke ich Herrn Prof. Dr. Alexander Pfeifer für die hervorragende Betreuung, die stetige Unterstützung und das Wecken meiner Leidenschaft für die Wissenschaft - für jeden Tag, der stets etwas Neues brachte.

Auch Herrn Prof. Dr. Fürst gilt besonderer Dank für die Übernahme des Zweitgutachtens der vorliegenden Arbeit sowie Herrn Prof. Dr. Witke und Herrn Prof. Dr. Mohr in ihrer Funktion als Mitglieder meiner Promotionskommission.

Ebenso danke ich Herrn Prof. Dr. Kunz für seine Hilfe, für die vielen guten Ratschläge und die Möglichkeit, in seinem Labor Respirationsmessungen erlernen und durchführen zu dürfen.

Ein herzliches Dankeschön geht an Michaela-Rosemarie Hermann für den Beistand an der VASP-Front in jeglicher Hinsicht – für die fachliche und menschliche Unterstützung in guten wie in schlechten Zeiten.

Herzlich danke ich auch all meinen momentanen und ehemaligen Arbeitskollegen am Institut für Pharmakologie und Toxikologie, besonders Dr. Ana Kilič und Dr. Franziska Siegel sowie Dr. Anita John, Jutta Mülich, Regina Müller, Daniela Scholz, Tanja Stevens, Kristina Weyer, Gabi Wolff, Dr. Katrin Zimmermann, Dr. Andreas Hofmann und Dr. Bodo Haas, für die vielfältige Unterstützung. Besonders hervorheben möchte ich an dieser Stelle Stefanie Kipschull – vielen Dank für die hervorragende technische Unterstützung!

Ein weiterer herzlicher Dank geht an meine Eltern und Großeltern, die stets an mich glaubten, mir beistanden und mir dieses Studium erst ermöglichten.

Doch der größte Dank gilt meinem Mann André für all die Unterstützung, die Toleranz, die Ermutigung und die Geduld, so schwer es auch manchmal war. Er hat mit mir gelacht und geweint, gelernt, gekämpft, gelitten, sich gefreut und noch so vieles mehr – er war einfach da – immer! Vielen Dank dafür!

And last but not least I want to thank my best friend and trusted advisor Prof. Dr. Joseph Anders Beavo for the boundless support and constant encouragement during the last two years. Thank you for being there! I will never give up hope.

Abbreviations

8-Br-cAMP	8- Bromoadenosine- 3', 5'- cyclic monophosphate
8-pCPT-cGMP	8- (4- Chlorophenylthio)guanosine- 3', 5'- cyclic monophosphate
β-ox	β-oxidation
ADP	adenosine 5’-diphosphate
Akt	protein kinase B
ANP	atrial natriuretic peptide
aP2	fatty acid-binding protein 4
APS	ammonium persulfate
AR	adrenergic receptor
ATP	adenosine 5’-triphosphate
BAT	brown adipose tissue
BAT-MSC	brown adipose tissue derived mesenchymal stem cell
BNP	B-type natriuretic peptide
BSA	bovine serum albumin
CAC	citric acid cycle
cAMP	cyclic adenosine-3’, 5’-monophosphate
cDNA	complementary deoxyribonucleic acid
C/EBP	CCAAT/enhancer-binding protein
cGMP	cyclic guanosine-3’, 5’-monophosphate
CMV	cytomegalovirus
CNG	cyclic nucleotide-gated
CNP	C-type natriuretic peptide
cntr	control
CP	crossing point
cPPT	central polypurine tract
Cytc	cytochrome c
d	day
DEA-NO	diethylamine NONOate sodium salt hydrate
Dexa	dexamethasone
dig	digitonin
DM	differentiation medium
DMEM	Dulbecco’s modified Eagle’s medium
DMSO	dimethyl sulfoxide

DNA	deoxyribonucleic acid
dNTP	deoxynucleotide triphosphate
ECL	enhanced chemiluminescence
EDTA	ethylene diamine tetraacetic acid
EGTA	ethylene glycol tetraacetic acid
Ena	Drosophila protein Enabled
eNOS	endothelial nitric oxide synthase
ERK	extracellular signaling-regulated kinase
EVH	Ena/VASP homology
Evl	Ena/VASP-like protein
FBS	foetal bovine serum
FFA	free fatty acid
FP4	four copies of a proline-rich motif
GC	guanylyl cyclase
glu/mal	glutamate/malate
GLUT-4	glucose transporter type 4
GST	glutathione S-transferase
GTP	guanosine 5’-triphosphate
H/E	hematoxylin/eosin
HEPES	N-(2-hydroxyethyl)-piperazine-N’-2-ethansulfonic acid
HIV	human immune deficiency virus
hMSC	human mesenchymal stem cell
HPRT	hypoxanthine-guanine-phosphoribosyltransferase
HRP	horseradish peroxidase
HSL	hormone-sensitive lipase
HuR	human-antigen R
IBMX	3-isobutyl-1-methylxanthine
IM	induction medium
iNOS	inducible nitric oxide synthase
IRAG	IP_3 receptor-associated cGMP kinase substrate
IRS-1	insulin receptor substrate-1
kb	kilo base
kDa	kilo Dalton
LB	lysogeny broth

LTR	long terminal repeat
LV	lentivirus
LV-cntr	lentivirus containing no promoter and no transgene
LV-RacL61	lentivirus containing mutant constitutively active Rac-1
LV-RacN17	lentivirus containing mutant dominant negative Rac-1
LV-sGCβ1	lentivirus containing the β1 subunit of the soluble guanylyl cyclase
LV-sicntr	lentivirus containing a control small interfering ribonucleic acid
LV-siERK1	lentivirus containing a small interfering ribonucleic acid against the extracellular signaling-regulated kinase1
LV-VASP	lentivirus containing the VAsodilator-Stimulated Phosphoprotein
MAPK	mitogen-activated protein kinase
MAPKK	mitogen-activated protein kinase kinase
MAPKKK	mitogen-activated protein kinase kinase kinase
max	maximal mitochondrial respiration
MEF	mouse embryonic fibroblast
Mena	mammalian Enabled protein
mRNA	messenger ribonucleic acid
MSC	mesenchymal stem cell
n	number
NE	norepinephrine
nNOS	neuronal nitric oxide synthase
NO	nitric oxide
NOS	nitric oxide synthase
NP	natriuretic peptide
ODQ	1H-[1,2,4]oxadiazolo[4,3-a]quinoxalin-1-one
oligo	oligomycin
PAGE	polyacrylamide gel electrophoresis
PAK	p21-activated kinase
PAK-CRIB	biotinylated Rac/Cdc42 binding motif of p21-activated kinase
PBS	phosphate-buffered saline
PCR	polymerase chain reaction
PDE	phosphodiesterase
PFA	paraformaldehyde
pGC	particulate guanylyl cyclase

PGC-1α	peroxisome proliferator-activated receptor γ-coactivator-1α
PGK	phosphoglycerate kinase
PI3K	phosphatidylinositol 3-kinase
PKA	cAMP-dependent protein kinase, protein kinase A
PKG	cGMP-dependent protein kinase, protein kinase G
Plin	perilipin
PPARγ	peroxisome proliferator-activated receptor γ
PRDM16	PRD1-BF-1-RIZ1 homologous domain containing protein-16
PRR	proline-rich region
P/S	penicillin/streptomycin
PVDF	polyvinylidenfluoride
RacL61	mutant constitutively active Rac-1
RacN17	mutant dominant negative Rac-1
rel.	relative
RIPA	radioimmunoprecipitation assay
RNA	ribonucleic acid
ROCK	RhoA-activated protein kinase
rpm	rotations per minute
RQ	quantitative real-time
RSV	respiratory syncytial virus
RT	room temperature
SDS	sodium dodecyl sulphate
SEM	standard error of the mean
sGC	soluble guanylyl cyclase
SIN	self-inactivating
siRNA	small interfering ribonucleic acid
succ	succinate
SV40	simian virus 40
T3	triiodothyronine
TAE	Tris-acetic acid-ethylene diamine tetraacetic acid
TBS	Tris-buffered saline
TBST	Tris-buffered saline supplemented with Tween-20
TEMED	N, N, N’, N’-tetramethylethylenediamine
TG	triglyceride

TK	thymidine kinase
UCP-1	uncoupling protein-1
UCP-1d	uncoupling protein-1-dependent fraction of total mitochondrial respiration
VASP	VAsodilator-Stimulated Phophoprotein
$VASP^{-/-}$	VAsodilator-Stimulated Phosphoprotein knock out
WAT	white adipose tissue
WPRE	posttranscriptional regulatory element of the woodchuck hepatitis virus
wt	wild type

Table of Contents

1. Introduction

1.1. The NO/cGMP signaling cascade

The Nitric Oxide (NO) / cyclic guanosine-3', 5'-monophosphate (cGMP) signaling cascade plays an important role in a variety of physiological processes such as smooth muscle relaxation, platelet aggregation and cell differentiation (Ignarro et al., 1999; Knowles and Moncada, 1992; Pfeifer et al., 1999). Enzymes responsible for cellular NO formation are the endothelial, neuronal and inducible NO synthases (eNOS, nNOS and iNOS) (Francis et al., 2010). They catalyze the production of NO from the amino acid L-arginine with stoechiometric production of L-citrullin (Figure 1). eNOS and nNOS synthesize nanomolar amounts of NO in a calcium dependent manner (Tsutsui et al., 2009) and are expressed in neurons (nNOS) and endothelial cells (eNOS). The third isoform, iNOS, is activated during immune response and produces NO at micromolar concentrations (Culmsee et al., 2005; MacMicking et al., 1995).

NO diffuses through the membrane into the target cell, where it activates the NO sensitive, cytosolic guanylyl cyclase (GC) known as soluble GC (sGC) (Friebe and Koesling, 2003). sGC activation induces the production of the second messenger cGMP from guanosine-5'-triphosphate (GTP) (Furchgott and Vanhoutte, 1989). In addition, cGMP is also generated by the membrane bound, particulate guanylyl cyclases (pGCs) such as GC-A and GC-B, which are stimulated by natriuretic peptides (NPs), namely the atrial NP (ANP), the B-type NP (BNP) and the C-type NP (CNP) (Garbers and Lowe, 1994).

cGMP exerts its influence on various cell functions via three different receptors: cyclic nucleotide-dependent phosphodiesterases (PDEs) (Sonnenburg and Beavo, 1994), cyclic nucleotide-gated (CNG) cation channels (Biel et al., 1999) and cGMP-dependent protein kinases (PKGs) (Pfeifer et al., 1999). PKGs mediate cGMP effects by phosphorylation of serine/threonine residues of target proteins. One of the major substrates of PKGs is the VAsodilator-Stimulated Phosphoprotein (VASP) (Butt et al., 1994) (Figure 1).

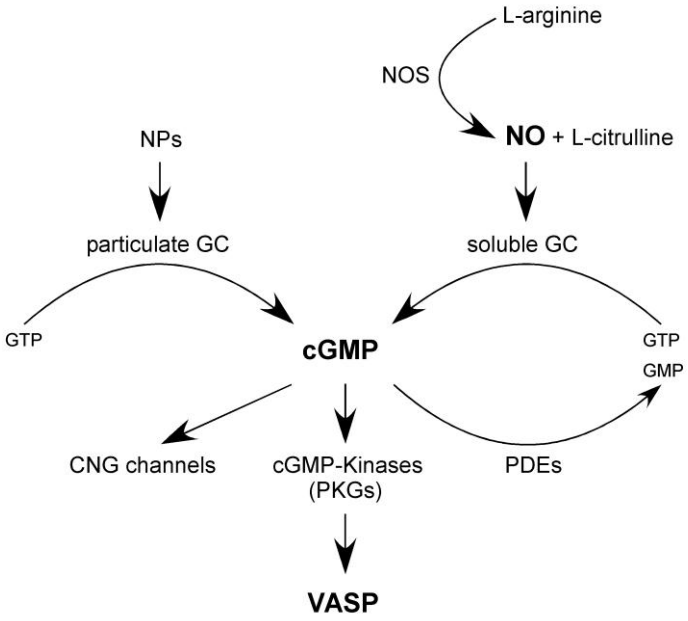

Figure 1: The NO/cGMP signaling cascade and the involvement of VASP.
NO, synthesized by NO synthases (NOS), and NPs increase cellular cGMP production by activation of soluble and particulate GCs, respectively. Effects of cGMP are mediated by CNG channels, PKGs and PDEs. VASP is one of the major substrates of PKGs.

1.2. Structure, expression and function of VASP

1.2.1. Structure and expression of VASP

VASP is an actin binding protein (Huttelmaier et al., 1999) that was initially isolated from human platelets (Halbrugge and Walter, 1989). Expression analysis in mouse revealed that VASP is ubiquitously expressed. The highest concentrations are found in platelets, lung, spleen, the gastrointestinal tract and blood vessels (Aszodi et al., 1999; Gambaryan et al., 2001).

VASP consists of 380 amino acids in human and 375 amino acids in mouse with a predicted molecular mass of 39.8 kDa and 39.7 kDa, respectively. It runs as a 46 kDa protein in sodium dodecyl sulphate polyacrylamide gel electrophoresis (SDS-PAGE) and is shifted to an apparent molecular mass of 50 kDa by phosphorylation. VASP is phosphorylated *in vitro* and in intact cells both by PKGs and cyclic adenosine-3', 5'-monophosphate (cAMP)-dependent protein kinase (PKA) (Butt et al., 1994). Murine VASP contains three phosphorylation sites: Ser153, Ser235 and Thr274 (Ser157, Ser239 and Thr278 in human). The preferred sites for PKA and PKG are Ser153 and Ser235, respectively (Figure 2). Phosphorylation of Thr274 by PKA and PKG requires prior phosphorylation of Ser153 and Ser235.

In its native state, VASP forms homo-tetramers and is associated with highly dynamic membrane structures, focal adhesions and cell-cell-contacts in various cell types (Reinhard et al., 1992).

VASP is a member of the proline-rich protein family of Ena/VASP proteins (Reinhard et al., 2001). In addition to VASP, this family comprises the Drosophila protein Ena, its mammalian homolog Mena and the Ena/VASP-like protein Evl (Gertler et al., 1996). All members of the Ena/VASP family are characterized by a tripartite domain structure including the highly homologous N-terminal and C-terminal Ena/VASP homology domains 1 and 2 (EVH1 and EVH2) and a central proline-rich region (PRR) domain (Bachmann et al., 1999; Gertler et al., 1995; Haffner et al., 1995; Reinhard et al., 2001) (Figure 2). The EVH1 domain mediates interactions of VASP with proteins containing domains that include four copies of a proline-rich (FP4) motif, like vinculin, zyxin and ActA. The EVH2 domain is responsible for tetramerization as well as F-actin binding and bundling (Bachmann et al., 1999; Chakraborty et al., 1995; Gertler et al., 1996; Huttelmaier et al., 1999; Huttelmaier et al., 1998; Reinhard et al., 1995; Reinhard et al., 2001; Reinhard et al., 1996). Moreover, VASP is not only able to bind proline-rich domains via the EVH1 domain, but is also a proline-rich protein itself, thus being able to interact with proline-binding proteins like profilin via its central PRR domain (Gertler et al., 1996). Therefore, VASP is believed to act as a molecular adaptor linking polymerization competent profilin–actin (profilactin) complexes to subcellular sites containing FP4 motif exhibiting proteins.

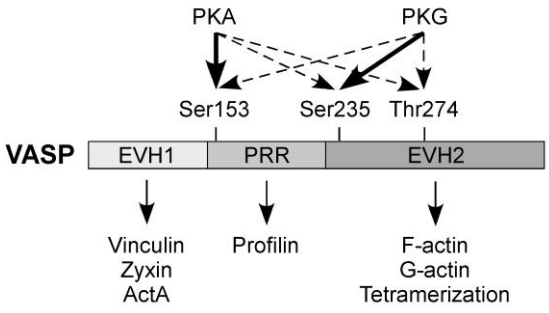

Figure 2: Scheme of the structure and phosphorylation sites of murine VASP.
The EVH1 domain binds FP4 motif containing proteins, the PRR domain binds profilin and the EVH2 domain is responsible for actin binding and tetramerization. VASP contains three phosphorylation sites as indicated. The preferred sites for PKA and PKG are indicated by bold arrows.

1.2.2. Function of VASP

VASP regulates cell motility in a variety of cells (Anderson et al., 2003; Bear et al., 2000; Garcia Arguinzonis et al., 2002; Goh et al., 2002). In fibroblasts, Ena/VASP proteins regulate the protrusive step of motility by controlling the geometry of actin networks within lamellipodia (Bear et al., 2002). Ena/VASP proteins are also implicated in many other actin-dependent processes including axon guidance (Lanier et al., 1999), attenuation of platelet aggregation (Aszodi et al., 1999), T-cell activation (Krause et al., 2000) and cell-cell adhesion (Vasioukhin et al., 2000). A potential link between Ena/VASP proteins and actin dynamics involves their ability to bind the actin monomer-binding protein profilin via the PRR domains. Profilin promotes the formation of polymerization competent ATP-actin monomers, which can be added on to free, rapidly growing (barbed) ends of actin filaments (Pollard and Borisy, 2003). Therefore, Ena/VASP proteins function to recruit profilin-actin complexes to sites of actin assembly. Moreover, evidence has been provided that the biochemical properties of profilin-actin complexes are altered when bound to Ena/VASP proteins, suggesting a functional relevance of this interaction including more than simple recruitment (Jonckheere et al., 1999). Furthermore, Ena/VASP proteins function to antagonize the activity of capping protein. Ena/VASP proteins bind to free actin filament barbed ends and permit continued monomer addition while blocking the ability of capping protein to terminate filament elongation (Bear et al., 2002).

Small GTPases of the Rho family, namely Rho, Rac and Cdc42, were suggested to be potential targets of VASP, because they regulate cell polarity and motility (Jaffe and Hall, 2005). Similar to VASP, they are regulated by PKG (Hou et al., 2004). RhoA controls stress fibre and focal adhesion assembly. Rac regulates the formation of lamellipodia protrusions and membrane ruffles and Cdc42 governs the extension of filopodia or microspikes at the cell periphery (Hall, 1998). Furthermore, it is known that Rho GTPases mediate several of the cytoskeletal processes that are impaired in VASP-deficient cells, indicating an interaction of VASP with these proteins.

Although VASP has been extensively studied in the context of the actin cytoskeleton, platelet aggregation and neural development, up to now, its role in adipose tissue and the differentiation of adipocytes is unknown.

1.3. Brown adipose tissue (BAT)

Adipose tissue plays an important role in energy storage. In mammals, adipose tissue is divided into two functionally distinct forms. White adipose tissue (WAT) is both the major site of energy storage and an endocrine organ, which produces and releases leptin and a variety of other regulators of energy balance (Galic et al.). In contrast, brown adipose tissue (BAT), which is specific to mammals, is responsible for non-shivering thermogenesis as a defense against cold. BAT is mainly found in the interscapular neck region and in supraclavicular regions of newborn mammals and is histologically distinguishable from WAT. Whereas white fat cells contain one major – unilocular – lipid droplet occupying almost the whole cytoplasm, brown fat cells contain numerous, small – multilocular – lipid droplets (Cinti, 2005). Moreover, BAT is highly vascularized, densely packed with mitochondria and heavily innervated by the sympathetic branch of the autonomic nervous system (Cannon and Nedergaard, 2004). In mammals, BAT allows for energy expenditure in form of heat. This thermogenic function of BAT is critically associated with uncoupling protein-1 (UCP-1), which is exclusively expressed in this tissue and therefore, is a molecular marker of BAT. UCP-1 serves as a proton transporter in the inner mitochondrial membrane that disrupts the electrochemical proton gradient and allows for uncoupling of respiration from adenosine 5'- triphosphate (ATP) synthesis (Cannon and Nedergaard, 2004).

BAT thermogenesis *in vivo* is activated by cold and mediated through noradrenaline/norepinephrine (NE) release from the sympathetic nervous system, which stimulates β3-adrenergic receptors (β3-ARs) in murine BAT, thereby increasing intracellular cAMP levels (Figure 3).

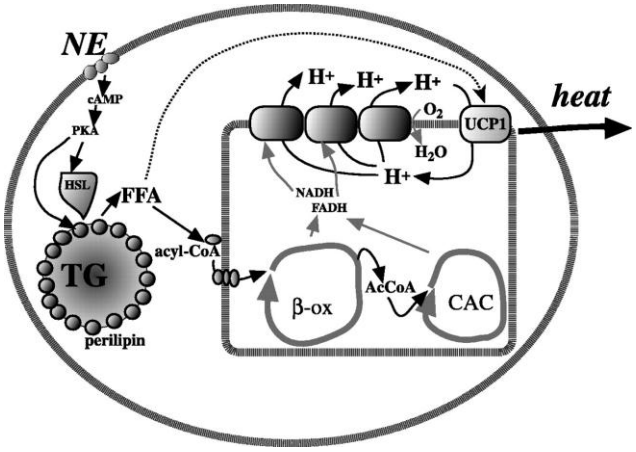

Figure 3: NE-induced stimulation of thermogenesis in brown adipocytes (Cannon and Nedergaard, 2004). NE stimulates β3-ARs, thereby increasing intracellular cAMP levels, leading to an activation of PKA. PKA phosphorylates the hormone-sensitive lipase (HSL), resulting in a release of free fatty acids (FFA). These FFAs activate UCP-1. β-ox, β-oxidation; CAC, citric acid cycle.

Recently, NO was identified as a key regulator of BAT mitochondrial biogenesis through activation of cGMP-dependent mechanisms (Nisoli et al., 2003; Nisoli et al., 1998). Moreover, our laboratory has unravelled a key role for PKGI in BAT differentiation and function demonstrating that PKGI is an essential permissive factor of insulin signaling in BAT. Ablation of PKGI results in the abrogation of cGMP signaling as well as insulin resistance and thus the suppression of BAT differentiation and function (Haas et al., 2009) (Figure 4).

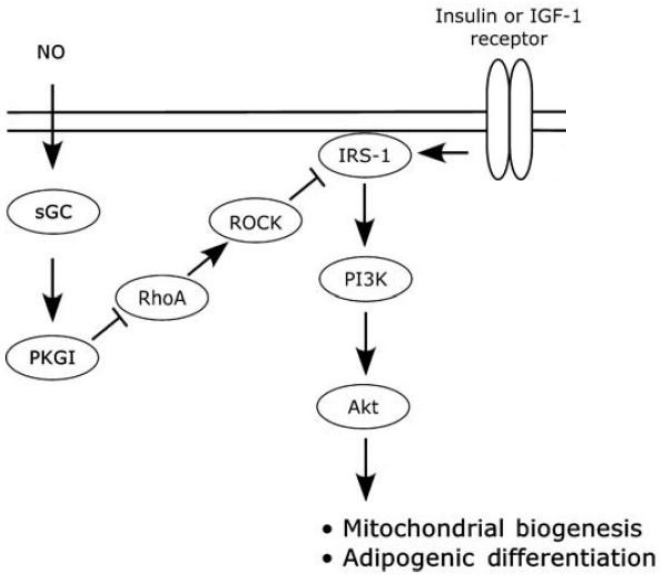

Figure 4: Scheme of the crosstalk of PKGI with the RhoA and insulin signaling pathways in brown fat cells (modified from Haas et al., 2009).
RhoA is an important target for PKG phosphorylation, which leads to an inhibition of the RhoA-activated protein kinase (ROCK). This inhibition of ROCK activity results in a decreased phosphorylation of the ROCK target insulin receptor substrate-1 (IRS-1), which leads to an increase in insulin receptor signaling and activation of phosphatidylinositol 3-kinase (PI3K) and protein kinase B /Akt.

Although BAT content decreases after birth, recent studies using positron emission tomography indicate that adult humans also possess metabolically active BAT (Cypess et al., 2009; Nedergaard et al., 2007; Saito et al., 2009; van Marken Lichtenbelt et al., 2009; Virtanen et al., 2009). Therefore, strategies aiming at the regulation of BAT activity and abundance are of great interest to reduce obesity and associated metabolic disorders.

1.4. Adipogenic differentiation of mesenchymal stem cells (MSCs)

Depending on their differentiation potential, stem cells are divided into four groups. Totipotent stem cells are found in zygotes and give rise to the embryo and the throphoblast (embryonic stem cells). Pluripotent stem cells, derived from blastocysts, can differentiate into all three germ layers: ectoderm, endoderm and mesoderm, but can not give rise to a whole organism. Multipotent stem cells differentiate into various cell types of one germ layer and are responsible for building up and self-renewal of the tissue (adult stem cells). In contrast, unipotent stem cells can only give rise to one single cell type.
Mesenchymal stem cells (MSCs) are multipotent stem cells, which can differentiate into a variety of lineages of mesenchymal origin including osteoblasts, chondrocytes, endothelial cells, adipocytes, myocytes and hematopoietic cells depending on the *in vitro* cell culture

conditions (Baksh et al., 2004; Guilak et al., 2004; Hattori et al., 2004; Safford et al., 2004; Zuk et al., 2002) (Figure 5). They can be found, for example, in umbilical cord blood, placenta, bone marrow and in a variety of fetal tissues as well as adipose tissue (Bieback et al., 2004; Campagnoli et al., 2001; In 't Anker et al., 2004; Pittenger et al., 1999; Zuk et al., 2002).

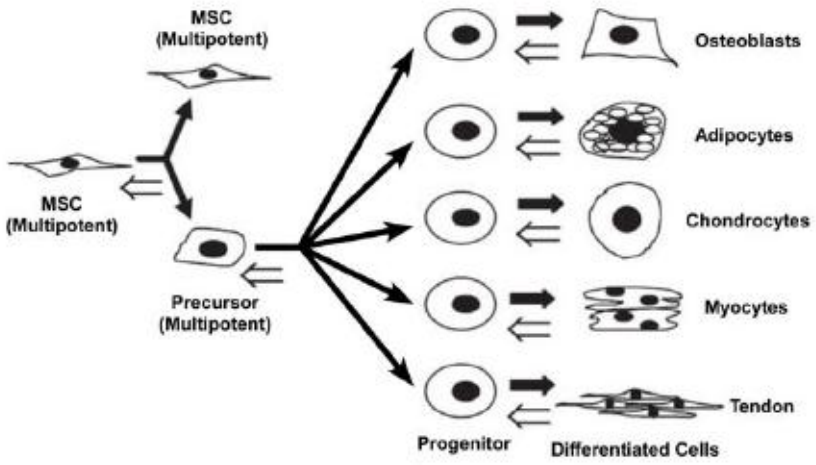

Figure 5: Scheme of MSC differentiation (modified from Baksh et al., 2004).
MSCs are multipotent stem cells, which can give rise to a variety of different cell types of mesenchymal origin.

MSCs, derived from adipose tissue, are considered to be the multipotent fraction of adherent cells that can be isolated from the adipose stroma-vascular fraction. After isolation, these cells attach to the surface of culture dishes and grow as a heterogenous population of fibroblast-like cells. Interestingly, they can be isolated from both WAT and BAT with a similar differentiation potential (Prunet-Marcassus et al., 2006).
MSCs, used in this study, were derived from BAT of newborn mice (BAT derived mesenchymal stem cells, BAT-MSCs) (2.4.3.) and were differentiated into brown adipocytes (2.4.6.).

1.5. Transcriptional control of BAT development

As WAT and BAT share many features, these tissues have been assumed to share a direct common progenitor. However, recent studies have shown that brown adipocytes are developmentally closer related to skeletal muscles than to white adipocytes. Both brown adipocytes and skeletal muscle cells arise from Myf5 expressing cells, a gene previously assumed to be present almost exclusively in committed skeletal muscle precursors (Seale et

al., 2008). In addition, global gene expression analysis revealed that brown - but not white - precursor cells exhibit a gene expression profile related to that of skeletal muscle cells (Timmons et al., 2007). Moreover, the mitochondrial proteom signature of BAT is highly related to that of skeletal muscle (Forner et al., 2009). Therefore, it was suggested that BAT shares a direct common upstream precursor with skeletal muscle cells.

Despite the differences in the developmental origin and functions of brown and white adipocytes, both cell types share a similar transcriptional cascade that controls adipogenic differentiation. The peroxisome proliferator-activated receptor γ (PPARγ) has been demonstrated to be absolutely necessary for both white and brown fat cell development. CCAAT/enhancer-binding proteins (C/EBPs) function cooperatively with PPARγ to promote and maintain a stable differentiation into adipocytes. C/EBPα and PPARγ stimulate the expression of downstream adipogenic genes (Rosen et al., 2000), namely UCP-1 in BAT and the fatty acid-binding protein 4 (aP2) in BAT and WAT. C/EBPβ and C/EBPδ also participate in the transcriptional control of adipogenesis by regulating PPARγ gene expression. But although brown fat cell differentiation requires PPARγ, this factor alone is not sufficient to drive MSC differentiation into the brown fat cell program. For example, the PPARγ-coactivator-1α (PGC-1α) activates UCP-1 transcription and is essential for BAT thermogenesis and mitochondrial biogenesis but not for adipogenic differentiation (Uldry et al., 2006). In contrast, the PRD1-BF-1-RIZ1 homologous domain containing protein-16 (PRDM16) is both necessary and sufficient to stimulate the development of brown fat cells by interacting with PGC-1α to increase its transcriptional activity (Seale et al., 2007) as well as by interaction with PPARγ and several members of the C/EBP family (Kajimura et al., 2009; Seale et al., 2008). PRDM16 forms a transcriptional complex with C/EBPβ, which controls the initiating events of brown adipogenic differentiation (Kajimura et al., 2010) (Figure 6). Surprisingly, the combination of PRDM16 and C/EBPβ is also sufficient to induce a fully functional brown fat program in non-adipogenic cells such as embryonic and skin fibroblasts (Kajimura et al., 2009).

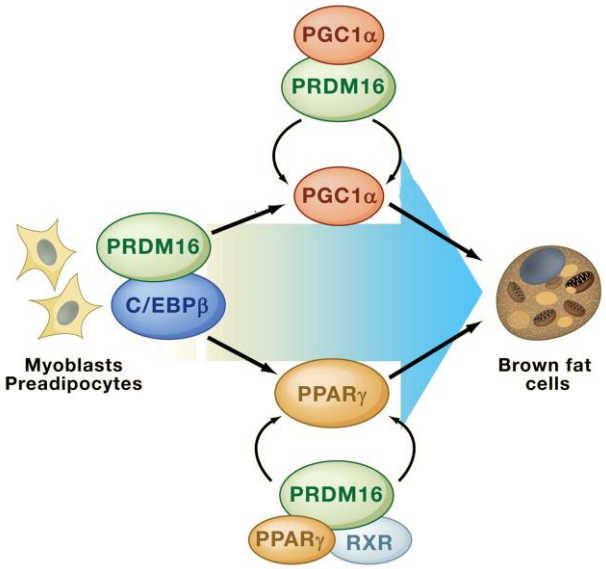

Figure 6: Transcriptional control of BAT development (modified from Kajimura et al., 2010).
PRDM16-C/EBPβ complexes induce the expression of PPARγ and PGC-1α in myoblastic precursors and preadipocytes. PRDM16 coactives PPARγ and PGC-1α, which drives the brown fat differentiation program.

1.6. Role of mitogen-activated protein kinase (MAPK) signaling in adipocyte differentiation

Mitogen-activated protein kinases (MAPKs) like the extracellular signaling-regulated kinase 1/2 (ERK1/2) and p38 are activated by a large variety of stimuli. One of their major functions is to connect cell surface receptors to transcriptional factors in the nucleus. MAPKs are serine/threonine kinases, regulated by phosphorylation cascades, organized in specific modules. MAPKs are phosphorylated by MAPK kinases (MAPKKs) like MEK, which in turn are phosphorylated by MAPKK kinases (MAPKKKs) like cRaf (Bost et al., 2005a). The components of the different pathways upstream of MAPKKKs are many and diverse. The MAPKs ERK1/2 and p38, which play important roles in adipogenic differentiation, can be activated for example by cRaf/MEK and Rac-1 activation, respectively (Bost et al., 2005a).
MAPK pathways are involved in a wide variety of cellular functions. A huge panel of different stimuli are capable to activate MAPKs. ERK is preferentially activated by mitogens such as serum or growth factors and, accordingly, this pathway is an important regulator of cell cycle and cell proliferation (Bost et al., 2005a). Because of the essential role in cell proliferation and the fact that adipogenic stimuli, such as insulin, activate ERK, the role of this pathway in adipogenesis has been intensively investigated in 3T3-L1 preadipocytes during the last decades (Bost et al., 2005a). It has been demonstrated that the function of ERK in adipogenesis has to be timely regulated: in early stages, ERK has to be activated for the

early proliferative step of differentiation (Sale et al., 1995), while it has to be shut-off later to avoid PPARγ phosphorylation, which decreases its transcriptional activity and inhibits adipogenesis (Camp and Tafuri, 1997; Hu et al., 1996) (Figure7). Moreover, ERK activity was shown to be necessary for the expression of the crucial adipogenic regulators C/EBPα, β and δ as well as PPARγ (Bost et al., 2005a) and ERK phosphorylation of C/EBPβ increases its transcriptional activity (Hu et al., 2001; Trautwein et al., 1993).

p38, like ERK, also seems to be required during the early stages of adipogenic differentiation (Figure 7), although opposing roles for adipogenesis have been described depending on the stage of differentiation (Bost et al., 2005a).

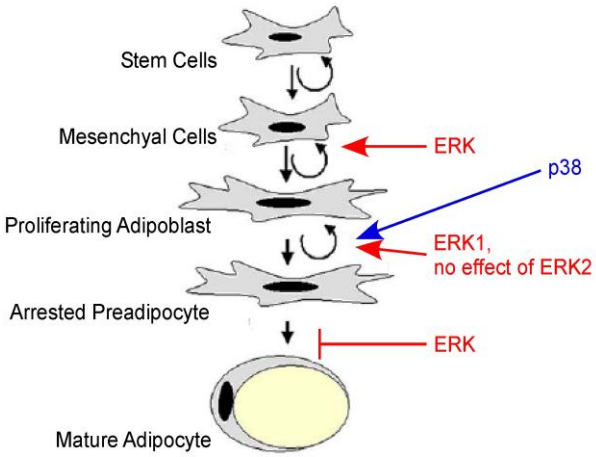

Figure 7: Involvement of the MAPKs at the various steps of adipogenesis (modified from Bost et al., 2005a).

The influence of the MAPKs ERK1/2 and p38 at different stages of adipogenic differentiation is shown. MAPK pathways are able to regulate adipogenesis at each step of the process.

1.7. Aim of the PhD thesis

Previous studies demonstrated that the NO/cGMP signaling cascade positively regulates BAT differentiation via PKGI (Haas et al., 2009; Nisoli et al., 2003). VASP is one of the major substrates of PKG (Butt et al., 1994). Up to now, the function of VASP in stem cell differentiation and brown fat development was unknown. Therefore, the aim of this study was to investigate the role of VASP in brown fat cell differentiation and function.
Hence, the following questions were raised:

1) Does VASP ablation influence brown adipocyte differentiation and function *in vitro*?
2) Which signaling cascades are involved in these processes?
3) Does VASP deletion affect BAT differentiation and function *in vivo*?

In order to determine the role of VASP in brown fat cell differentiation *in vitro*, VASP knock out ($VASP^{-/-}$) mice were used (Aszodi et al., 1999) to establish brown adipocyte cell lines, which were further modified by lentiviral expression of target proteins. To investigate the role of VASP *in vivo*, the consequences of VASP deletion in BAT of $VASP^{-/-}$ mice were analyzed.

2. Materials and Methods

2.1. Common Chemicals

All chemicals used in this study were purchased from the following companies if not otherwise stated: Calbiochem (Darmstadt), Carl Roth GmbH (Karlsruhe), Merck (Darmstadt), Sarstedt (Nümbrecht), Sigma-Aldrich (München), VWR (Darmstadt). Water was purified and distilled using an EASYpure UV/UF system (WeteA, Wilhelm Werner GmbH, Leverkusen).

2.2. Animals

2.2.1. Animal housing and breeding

Mice used in this study were maintained and bred in the animal facility of the Institute of Pharmacology and Toxicology, University of Bonn, Bonn. They were maintained on a daily cycle of 12 hours light (0600 to 1800) and 12 hours darkness (1800 to 0600) at 24 ± 1°C and were allowed free access to chow (standard rodent diet) and water. Mice were separated by sex and marked with ear tags at the age of 4 weeks after birth. $VASP^{-/-}$ mice (background C57BL/6N) (Aszodi et al., 1999) were kept in the heterozygous state and were bred at the age of 8 weeks.

2.2.2. Cold exposure experiments

The analysis of the influence of VASP deletion on BAT *in vivo* was performed using littermatched male mice at the age of 4 – 5 weeks. Mice were fasted for 3 - 12 hours (specified below) at 24 ± 1°C (room temperature, RT) with free access to water but without access to chow to exclude the possibility of different feeding states. Afterwards, mice were exposed to RT or 4 ± 1°C, respectively, for additional 3 hours without access to chow. Subsequently, mice were sacrificed and dissected.

Fasting conditions	
Subsequent experiment	**Fasting period at RT**
Histological analysis (H/E staining)	12 hours
RQ-PCR	3 hours
Measurement of TG content	3 hours
Measurement of mitochondrial respiration	3 hours
Measurement of lipolysis	3 hours
Preparation of total protein lysates	3 hours

2.3. Histological analysis

2.3.1. Materials

Eosin G, Merck (Cat.No. 1.09844)
Mayers hemalaun, Merck (Cat.No. 1.09249)
Roti®-Histokitt, Carl Roth GmbH (Cat. No. 6638.1)

2.3.2. Equipment

Camera, LEICA DFC425 C, Leica Microsystems GmbH, Wetzlar
Fluorescence microscope, LEICA DMI4000 B, Leica Microsystems GmbH, Wetzlar
Microtome, HM335E, Microm, Walldorf
Software, Leica Application Suite V3, Leica Microsystems GmbH, Wetzlar

2.3.3. Preparation of paraffin sections

Paraffin embedding is a common method to cut rather thin sections of a variety of tissues. Paraformaldehyde (PFA) was used for fixation as it cross-links proteins while retaining their antigenicity.

In order to prepare paraffin sections from BAT, mice were sacrificed and dissected. Interscapular BAT was removed, transferred to PFA fixative (4% PFA in PBS) and incubated at 4°C for 45 minutes. Afterwards tissue samples were dehydrated by successive incubations in ethanol of ascending concentrations (50%, 70%, 90%, 95%, 100%) for 1 hour each at RT. Subsequently, samples were incubated in xylol 3 times for 10 minutes at RT and placed in paraffin 3 times for 1 hour at 60°C. Tissue samples were embedded with fluid paraffin (60°C)

and paraffin blocks were stored at RT. 4 µm thick sections of the embedded BAT were cut using a microtome (Microm). Slides were dried at RT and stored at 4°C.

Phosphate-buffered saline (PBS)

NaCl	137 mM
Na_2HPO_4	8 mM
KH_2PO_4	1.4 mM
KCl	2.7 mM

dissolved in H_2O and adjusted to pH 7.4 with HCl

PFA fixative

PFA	4%

dissolved in PBS, pH 7.4, boiled for 1 minute and cooled on ice

2.3.4. Hematoxylin/Eosin (H/E) staining

H/E staining is a widely used technique to visualize numerous tissue structures. Cell nuclei are staining in blue by hematoxylin whereas the cytoplasm and connective tissue appear in a variety of pink nuances, caused by the eosin staining.

H/E stainings were performed at RT. Paraffin sections were incubated for 2 minutes in xylol (deparaffinization), then in ethanol of descending concentrations (100%, 95%, 90%, 70%, 50%) and finally in PBS (rehydration) 2 minutes each. Afterwards, slides were treated with hematoxylin (Mayers hemalaun, Merck) for 1 minute, washed in water, stained with eosin (Eosin G, Merck) for 1 minute and again washed in water. Sections were dehydrated in ethanol of ascending concentrations (50%, 70%, 90%, 95%, 100%) and xylol for 2 minutes each and mounted with Roti®-Histokitt (Carl Roth GmbH). Images were taken using a LEICA DMI4000 B microscope (Leica Microsystems GmbH) equipped with a LEICA DFC425 C camera (Leica Microsystems GmbH).

2.4. Cell culture methods

2.4.1. Materials

5 ml / 10 ml / 25 ml pipette, Sarstedt (Cat. No. 86.1253.001, 86.1254.001, 86.1685.001)
6-well / 12-well plate, Sarstedt (Cat. No. 86.1836.001, 83.1839.001)

100 mm dish, Sarstedt (Cat. No. 83.1802.001)

15 ml / 50 ml Falcon tube, Sarstedt (Cat. No. 62.554.001, 62.548.004)

1H-[1,2,4]oxadiazolo[4,3-a]quinoxalin-1-one (ODQ), Sigma-Aldrich (Cat. No. O-3636)

8- (4- Chlorophenylthio)guanosine- 3', 5'- cyclic monophosphate (8-pCPT-cGMP), Biolog, Bremen (Cat. No. C009-10E)

Collagenase II, Worthington, Lakewood, USA (Cat. No. CLS2)

Cryogenic vials, Sarstedt (Cat. No. 72.379.992)

Dexamethasone, Sigma-Aldrich (Cat.No. D-4902)

Dulbecco's modified Eagle's medium (DMEM) Glutamax I + 4500 mg/l Glucose, Gibco, Karlsruhe (Cat. No. 61965059)

Foetal bovine serum (FBS), Biochrom AG, Berlin (Cat. No. S0115)

Insulin, Sigma-Aldrich (Cat. No. I-9278)

Isobutylmethylxanthine (IBMX), Sigma-Aldrich (Cat. No. I-5879)

Nylon meshes, Millipore, Schwalbach (Cat. No. NY3002500 and NY1H00010)

PD184161, Biomol GmbH, Hamburg (Cat. No. 10012431)

Penicillin/Streptomycin (P/S), Biochrom AG, Berlin (Cat. No. A2213)

Sterile filter 0.22 µm, VWR (Cat. No. 514-0061)

Triiodothyronine-Na, Sigma-Aldrich (Cat. No. T-6397)

Trypan blue 0.4% solution, Sigma-Aldrich (Cat. No. T-8154)

Trypsin-ethylene diamine tetraacetic acid (EDTA) 0.05%, Invitrogen, Berlin (Cat. No. 25300-096)

2.4.2. Equipment

Camera, LEICA DFC425 C, Leica Microsystems GmbH, Wetzlar

Centrifuge, Biofuge Primo, Heraeus, Hanau

Incubator, HeraCell 150, Heraeus, Hanau

Laminar air flow, HeraSafe, Heraeus, Hanau

Microscope, LEICA DMIL, Leica Microsystems GmbH, Wetzlar

Neubauer counting chamber, Labomedic, Gießen

QuantityOne® Software, BioRad, München

Software, Leica Application Suite V3, Leica Microsystems GmbH, Wetzlar

2.4.3. Isolation and culture of primary BAT-MSCs

BAT-MSCs were isolated from interscapular brown fat of newborn litter-matched wild type (wt) and VASP$^{-/-}$ mice (Haas et al., 2009) (Figure 8). Interscapular BAT was resected and transferred to collagenase digestion buffer. After incubation in a shaking water bath for 30 minutes at 37°C, tissue remnants were removed by filtration through a 100 µm nylon mesh (Millipore). Afterwards the cell suspension was placed on ice for 30 minutes. The resulting infranatant, which contained the MSC fraction, was filtered through a 30 µm nylon mesh (Millipore) and centrifuged at 700 g for 10 minutes. The cell pellet was resuspended in dissection medium. Cells were counted with trypan blue (1:1) (Sigma-Aldrich) in a Neubauer counting chamber (Labomedic) and 5.7 x 10^5 cells per well were seeded on 6-well plates and incubated at 37°C and 5% CO_2.

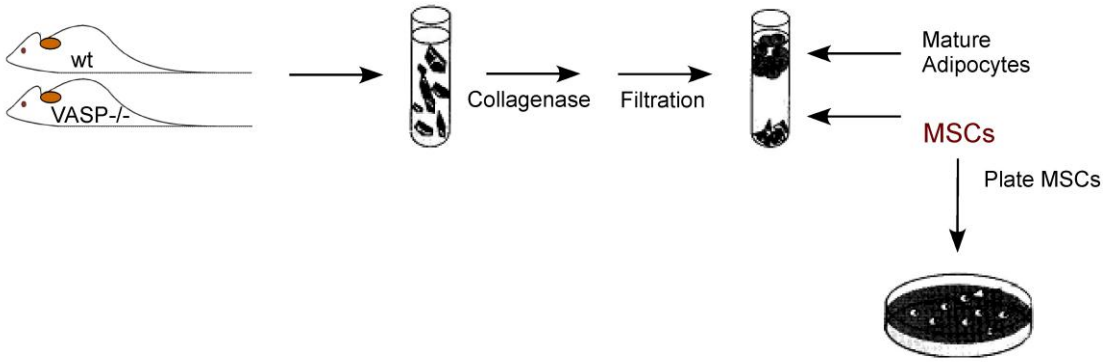

Figure 8: Isolation of BAT-MSCs from interscapular BAT of newborn mice.
BAT-MSCs were isolated from interscapular BAT of newborn wt and VASP$^{-/-}$ littermates and collagenase digested. BAT-MSCs were separated from mature brown adipocytes and seeded on 6-well plates.

Collagenase digestion buffer

NaCl	123 mM
KCl	5 mM
$CaCl_2$	1.3 mM
Glucose	5 mM
HEPES	100 mM

dissolved in H_2O, adjusted to pH 7.4, sterile filtered and stored at 4°C

The following substances were added freshly before use:

Bovine serum albumin (BSA)	1.5%
Collagenase II	0.2%

sterile filtered and stored at 4°C

Dissection medium

DMEM Glutamax I + 4500 mg/l Glucose	
FBS	10%
P/S	1%
Insulin	4 nM
Triiodothyronine-Na	4 nM
HEPES	10 mM
Sodium ascorbate	25 µg/ml

2.4.4. Immortalization of primary BAT-MSCs

Primary BAT-MSCs (passage 0) were immortalized 24 hours after isolation by infection (2.4.7.) with a lentivirus expressing the Simian Virus 40 (SV40) large T-antigen under control of the phosphoglycerate kinase (PGK) promoter. Immortalized cells were expanded in growth medium at 37°C and 5% CO_2 and were not used beyond passage 5.

Growth medium

DMEM Glutamax I + 4500 mg/l Glucose	
FBS	10%
P/S	1%

2.4.5. Cell culture and trypsinization of cells

Cells were maintained in growth medium at 37°C and 5% CO_2 as described above (2.4.4.). In order to detach cells from the well plate, cells were washed in prewarmed PBS (37°C) and detached by incubation with trypsin-EDTA (Invitrogen) for approximately 5 minutes at 37°C. Detached cells were resuspended in growth medium.

To store cells for longer periods of time, cells were trypsinized and resuspended in prewarmed (37°C) growth medium. Cell suspensions were centrifuged for 5 minutes at 200 g. Cell pellets were resuspended in growth medium, mixed with freezing medium in a ratio of 1:1 to achieve a final dimethyl sulfoxide (DMSO) concentration of 10% and transferred to cryogenic vials (Sarstedt). Cryogenic vials were incubated on ice for 15 minutes and were finally stored at -80°C. After 24 hours cryo-cultures were transferred to liquid nitrogen (-196°C).

Freezing medium

Growth medium	
DMSO	20%

In order to thaw cryo-preserved cells, cryo-cultures were quickly placed in a water bath at 37°C. Afterwards cells were transferred to prewarmed (37°C) growth medium (approximately 10 times the volume of the cryo-culture) and centrifuged for 5 minutes at 200 g. Cell pellets were resuspended in growth medium and seeded on well plates.

2.4.6. Adipogenic differentiation of immortalized BAT-MSCs

To differentiate immortalized BAT-MSCs into mature brown adipocytes, 1.8 x 10^5 cells/well were seeded on 6-well plates or 0.9 x 10^5 cells/well on 12-well plates (day -4) in growth medium and after 48 hours the medium was changed to differentiation medium (day -2). Adipogenesis was induced by treating confluent cultures (day 0) with induction medium for 48 hours. After this induction phase, cells were maintained in differentiation medium (day 2), which was replenished every second day until day 7 or 8, when the cells had differentiated into brown adipocytes (Figure 11).

Differentiation medium (DM)

DMEM Glutamax I + 4500 mg/l Glucose	
FBS	10%
P/S	1%
Insulin	20 nM
Triiodothyronine-Na	1 nM

Induction medium (IM)

Differentiation medium	
Dexamethasone	1 µM
IBMX	0.5 mM

The following substances were included into the media as indicated:

PKG activation: 8-pCPT-cGMP (Biolog)

sGC inhibition: ODQ (Sigma-Aldrich)

MEK inhibition: PD184161 (Biomol GmbH)

2.4.7. Infection of cells with lentiviral vectors

The day before infection, 1.8 x 10^5 cells/well were seeded in 6-well plates and maintained over night as described (2.4.5.). Approximately 24 hours later, 800 µl growth medium containing 0.5 – 10 µl of the virus solution (corresponding to a amount of viral reverse transcriptase of 200 ng/well of a 6-well plate) were added to the cells. The next day, the medium was removed and growth medium was added. Cells were incubated over night. Afterwards, the infected cells were subjected to further experiments.

2.4.8. Analysis of cell attachment and cell spreading

In order to perform *in vitro* attachment assays, 1.8 x 10^5 cells/well were seeded in 6-well plates and allowed to attach for 2 hours. Afterwards, brightfield micrographs were taken using a LEICA DMIL microscope (Leica Microsystems GmbH), equipped with a LEICA DFC425 C camera (Leica Microsystems GmbH), and the attached cells were counted.

Cell spreading was analyzed by measuring the surface area, covered by single cells. Therefore, 1.8 x 10^5 cells/well were seeded in 6-well plates. After 24 hours, brightfield images were taken and the cell surface area was determined using QuantityOne® Software (BioRad).

2.5. Biochemical methods

2.5.1. Materials

8- Bromoadenosine- 3', 5'- cyclic monophosphate (8-Br-cAMP), Biolog, Bremen (Cat. No. B 007-100)

8- (4- Chlorophenylthio)guanosine- 3', 5'- cyclic monophosphate (8-pCPT-cGMP), Biolog, Bremen (Cat. No. C009-10E)

Acrylamide, Rotiphorese®Gel 30 (37.5:1), Carl Roth GmbH (Cat. No. 3029.1)

BSA (essential fatty acid free), Sigma-Aldrich (Cat. No. A-7030)

Cell scraper, Labomedic, Gießen (Cat. No. 2015217)

Chemiluminescence films, Hyperfilm®, Amersham Biosciences, Buckinghamshire, UK (Cat. No. 28906837)

Coomassie dye, Coomassie brilliant blue, Merck (Cat. No. 1.15444.0025)

Diethylamine NONOate sodium salt hydrate (DEA-NO), Sigma-Aldrich (Cat. No. D-184)

Direct cyclic AMP Enzyme Immunoassay Kit, Assay Designs, Ann Arbor, USA (Cat. No. 900-067)

Direct cyclic GMP Enzyme Immunoassay Kit, Assay Designs, Ann Arbor, USA (Cat. No. 900-014)

DMEM, liquid (4.5 g/L D-glucose), Gibco, Karlsruhe (Cat. No. 21063029)

Dual-Luciferase® Reporter Assay System, Promega, Mannheim (Cat. No. E1910)

Enhanced chemiluminescence (ECL) reagent, ECL, Amersham Biosciences, Buckinghamshire, UK (Cat. No. 1059250/243)

Entwicklerkonzentrat T-Matic, ADEFO-CHEMIE GmbH, Dietzenbach (Cat. No. 00034)

Fixierkonzentrat T-Matic, ADEFO-CHEMIE GmbH, Dietzenbach (Cat. No. 00091)

Free Glycerol Reagent, Sigma-Aldrich (Cat. No. F-6428)

Glutathione-sepharose beads, Glutathione sepharose 4 fast flow, Amersham Biosciences, Buckinghamshire, UK (Cat. No. 17-5132-01)

Glycerol Standard Solution, Sigma-Aldrich (Cat. No. G-7793)

L-(-)-Norepinephrine bitartate salt monohydrate (NE), Sigma-Aldrich (Cat. No. A-9512)

Natriuretic Peptide, C-Type (CNP), Sigma-Aldrich (Cat. No. N-8768)

Oil RedO, Sigma-Aldrich (Cat. No. O-0625)

pRL-TK Vector, Pomega, Mannheim (Cat. No. E2241)

Protease inhibitor cocktail, Complete® EDTA-free, Roche, Mannheim (Cat. No. 11873580)

Protein standard, Precision plus All Blue Standard, BioRad, München (Cat. No. 161-0373)

Polyvinylidenfluoride (PVDF) membranes, Immobilon®P 0.45µm, Millipore, Schwalbach (Cat. No. IPVH 00010)

Streptavidin-agarose beads, Sigma-Aldrich (Cat. No. S-1638)

Transfection reagent, Lipofectamine 2000, Invitrogen, Karlsruhe (Cat. No. 11668019)

Triglyceride Reagent, Sigma-Aldrich (Cat. No. T-2449)

The following antibodies were used:

Name of the antigene	**Manufacturer**	**Cat. No.**	**Dilution**
β3-AR	Santa Cruz, Santa Cruz, USA	sc-1473	1:1000
aP2	Santa Cruz, Santa Cruz, USA	sc-18661	1:1000
Akt	Cell Signaling, Danvers, USA	9272	1:1000
Akt pSer473	Cell Signaling, Danvers, USA	4058	1:1000
C/EBPα	Santa Cruz, Santa Cruz, USA	sc-61	1:1000

cRaf	Santa Cruz, Santa Cruz, USA	sc-227	1:1000
cRaf pSer338	Cell Signaling, Danvers, USA	9427	1:1000
Cytc	BD Biosciences, Franklin Lakes, USA	556433	1:1000
ERK1/2	Cell Signaling, Danvers, USA	9102	1:1000
ERK1/2 pThr202/Tyr204	Cell Signaling, Danvers, USA	9101	1:1000
goat-HRP	Chemicon (Millipore, Schwalbach)	AP309P	1:5000
HSL	Cell Signaling, Danvers, USA	4107	1:1000
HSL pSer660	Cell Signaling, Danvers, USA	4126	1:1000
mouse-HRP	Dianova, Hamburg	115-035-146	1:10000
p38	Cell Signaling, Danvers, USA	9212	1:1000
p38 pThr180/Tyr182	Cell Signaling, Danvers, USA	9215	1:1000
PAK	Santa Cruz, Santa Cruz, USA	sc-882	1:1000
PAK1 pThr423/ PAK2 pThr402	Cell Signaling, Danvers, USA	2601	1:1000
PKAα/β/γ cat	Santa Cruz, Santa Cruz, USA	sc-28892	1:1000
PPARγ	Santa Cruz, Santa Cruz, USA	sc-7273	1:1000
rabbit-HRP	Cell Signaling, Danvers, USA	7074	1:5000
Rac-1	BD Biosciences, Franklin Lakes, USA	610650	1:2500
RhoA	Santa Cruz, Santa Cruz, USA	sc-418	1:1000
RhoA pSer188	Santa Cruz, Santa Cruz, USA	sc-32954	1:1000
sGCα1	Santa Cruz, Santa Cruz, USA	sc-23801	1:1000
sGCα2	Santa Cruz, Santa Cruz, USA	sc-20954	1:1000
sGCβ1	Santa Cruz, Santa Cruz, USA	sc-20955	1:1000
Tubulin	Dianova, Hamburg	DLN-09992	1:1000
UCP-1	Santa Cruz, Santa Cruz, USA	sc-6529	1:500
VASP	Santa Cruz, Santa Cruz, USA	sc-1950	1:1000
VASP pSer239	nanoTools, Teningen	0047-100/ VASP-16C2	1:1000

2.5.2. Equipment

Centrifuge, 5415R, Eppendorf Hamburg
Centrifuge, Sigma 8k with 12510-H rotor, Sartorius, Göttingen
Disperser, Ultra-turrax®, T8, IKA, Staufen
Electrophoresis/blotting system, Mini Trans Blot System, BioRad, München
Film processor, CP100, Agfa, Köln
Luminometer, Lumat LB 9507, EG&G BERTHOLD, Bad Wildbad
Micro plate reader, SUNRISE-BASIC TECAN, Tecan, Grödig, Austria
Thermomixer, 5350, Eppendorf, Hamburg
Power supply, Consort E835, Peqlab, Erlangen
Photometer, Biophotometer, Eppendorf, Hamburg

2.5.3. Preparation of total protein lysates from adherent cells and tissue

Cells were washed with ice cold PBS. 200 µl of 4°C cold lysis buffer (radioimmunoprecipitation (RIPA)-buffer) were added to each well of a 6-well plate or 100 µl to each well of a 12-well plate. Cells were scraped with a cell scraper and lysates were centrifuged at 15000 g for 10 minutes at 4°C. The protein concentration of the supernatant was determined using the Bradford protein assay (2.5.4.). After adjusting the protein concentration, the appropriate amount of 3 x Laemmli buffer (Laemmli, 1970) was added and samples were incubated at 97°C for 5 minutes, except sample for detection of β3-ARs, which were incubated at 37°C for 10 minutes. Samples were either frozen at -20°C or directly subjected to SDS-PAGE (2.5.6.).

Lysis buffer (RIPA-buffer)

TrisHCl	10 mM	pH 7.4
NaCl	150 mM	
NP-40	1%	
Desoxy-cholic acid-Na	1%	
Sodium dodecyl sulphate (SDS)	0.1%	
sterile filtered and stored at 4°C		
before use the following substances were added		
Complete® EDTA-free	40 µl/ml	
NaF	10 mM	

Na_3VO_4	1 mM	

3 x Laemmli buffer

TrisHCl	125 mM	pH 6.8
Glycerol	20%	
SDS	17%	
Bromphenol blue	0.015%	
dissolved in H_2O and stored at -20°C		
before use the following substance was added		
β-mercaptoethanol	5%	

For preparation of total protein lysates from tissue, mice were sacrificed and BAT or other tissues were resected and either snap-frozen in liquid nitrogen for longer storage or directly processed. Therefore, 500 µl lysis buffer (RIPA-buffer) were added to the BAT or to about 30 – 40 mg of other tissues. Tissue samples were disrupted using an Ultra-turrax® (IKA). Proteins were isolated as described above.

2.5.4. Quantification of protein concentrations using the Bradford protein assay

The Bradford protein assay is based on the Coomassie brilliant blue G-250 dye, which specifically interacts with certain amino acid residues (Bradford, 1976). It is a colorimetric protein assay based on an absorbance shift of the dye, caused by binding to amino acids. The protein content was determined using a BSA standard ranging series. 2 µl of protein lysates were diluted in 98 µl 0.15 M NaCl solution. After addition of 1 ml Coomassie solution, samples were incubated for 2 minutes and the absorbance was measured at 595 nm.

Coomassie solution

Coomassie brilliant blue G-250	0.01%
EtOH	5%
Phosphoric acid	8.5%
dissolved in H_2O and stored at 4°C, protected from light	

2.5.5. Immunoprecipitation of Rac-1-GTP and Rho-GTP

Cells grown on 100 mm dishes were washed with 4°C cold PBS and 500 µl immunoprecipitation buffer were added. Cells were scraped with a cell scraper and centrifuged at 15000 g at 4°C for 10 minutes. The protein concentration of the supernatant was determined using the Bradford method (2.5.4.) and 500 µg of total protein were used for the immunoprecipitation assays. First, the Rho-GTP immunoprecipitation assay was accomplished. Therefore, lysates were incubated with glutathione S-transferase (GST)-rhotekin (provided by B. Haas) and glutathione-sepharose beads (Amersham Biosciences) for 1 hour at 4°C to capture GTP-bound Rho. The beads were collected by centrifugation for 1 minute at 7200 g and 4°C. Subsequently, the supernatant was used for the Rac-1-GTP immunoprecipitation assay. For this purpose, cell lysates were incubated with a biotinylated peptide, consisting of the Rac/Cdc42 binding motif of p21-actived kinase (PAK-CRIB) (provided by R. Faessler), and streptavidin-agarose beads (Sigma) for 30 minutes at 4°C to capture GTP-bound Rac. For both assays, the beads were washed 3 times with immunoprecipitation buffer, collected by centrifugation at 7200 g for 1 minute, boiled in 3 x Laemmli buffer (2.5.3.) at 97°C for 5 minutes and subjected to Western blot analysis using antibodies against Rac-1 (BD Biosciences) and RhoA (Santa Cruz). Total protein lysates (5% of input) were analyzed in parallel as loading controls.

Immunoprecipitation buffer

TrisHCl	50 mM	pH 7.4
NaCl	200 mM	
$MgCl_2$	5 mM	
NP-40	1%	
Glycerol	10%	
dissolved in H_2O and stored at 4°C		
before use the following substances were added		
Complete® EDTA-free	40 µl/ml	
NaF	1 mM	
Na_3VO_4	1 mM	

2.5.6. One-dimensional SDS-polyacrylamide-gelelectrophoresis (SDS-PAGE)

SDS-PAGE, performed under denaturating conditions, is the most widely used method to separate proteins. Proteins are solubilized by boiling in the presence of SDS and β-mercaptoethanol to give negative charge and to reduce disulfide bonds, respectively, and are separated electrophoretically.

To perform discontinuous gel electrophoresis, proteins first pass through a stacking gel to become concentrated and then pass through the separating gel to be separated according to molecular size under denaturating conditions. SDS-PAGE was performed in SDS-PAGE running buffer at 100V at RT using the Mini Trans Blot System (BioRad).

Stacking gel (5 ml)	**5%**	
H_2O	3.4 ml	
Rotiphorese®Gel 30	0.83 ml	
1.0 M TrisHCl	0.63 ml	pH 6.8
10% SDS	0.04 ml	
20% ammonium persulfate (APS)	0.02 ml	
N, N, N', N'-Tetramethylethylene-diamine (TEMED)	8 µl	

Separating gel (10 ml)	**8%**	**10%**	**12%**	
H_2O	4.6 ml	4.0 ml	3.3 ml	
Rotiphorese®Gel 30	2.7 ml	3.3 ml	4.0 ml	
1.5 M TrisHCl	2.5 ml	2.5 ml	2.5 ml	pH 8.8
10% SDS	0.1 ml	0.1 ml	0.1 ml	
APS	0.05 ml	0.05 ml	0.05 ml	
TEMED	6 µl	4 µl	4 µl	

10 x SDS-PAGE running buffer	
Tris	250 mM
Glycine	2 M
SDS	0.1%
dissolved in H_2O and stored at RT	

2.5.7. Western blotting and immunodetection

Western blot analysis is a method to detect specific proteins by polyclonal or monoclonal antibodies. First, proteins are separated by SDS-PAGE and then electrically transferred onto a PVDF membrane. Proteins on the membrane can be visualized by immunodetection reagents. After separating the proteins by SDS-PAGE (2.5.6.), a transfer construction was assembled using a methanol activated and transfer buffer equilibrated PVDF membrane. Proteins were electrically transferred under different conditions depending on their size.

Protein size	**Voltage**	**Current**	**Time**	**Temperature**
15 – 30 kDa	100 V	250 mA	1 hour	4°C
30 – 50 kDa	100 V	275 mA	1 hour	4°C
50 – 75 kDa	100 V	300 mA	1 hour	4°C
75 – 250 kDa	100 V	300 mA	1 – 1.5 hours	RT

After disassembling the transfer construction, membranes were incubated in methanol for 30 seconds and dried for at least 30 minutes at RT. After drying, membranes were incubated in methanol for 30 seconds and blocked in blocking buffer I or II for 1 hour at RT. Blocked membranes were washed 3 times in Tris-buffered saline (TBS) supplemented with 1% Tween-20 (TBST) and incubated with the primary antibody at 4°C over night in blocking buffer according to the manufacturer's instructions. After 3 washes with TBST, the membranes were incubated with a horseradish peroxidise (HRP)-coupled secondary antibody for 1 hour at RT in blocking buffer according to the manufacturer's instructions. Finally, the membranes were washed 3 times in TBST and subjected to chemiluminescence based detection using ECL reagent and chemiluminescence films (Amersham Biosciences). Films were finally developed in an automatic film processor (CP-100, Agfa).

Transfer buffer

10 x SDS-PAGE running buffer	10%
Methanol	20%
dissolved in H_2O and stored at RT	

10 x TBS

Tris	100 mM

NaCl 1.4 M

dissolved in H_2O, adjusted to pH 8.0 with HCl and stored at RT

TBST

10 x TBS 10%

Tween-20 0.1%

dissolved in H_2O and stored at RT, protected from light

Blocking buffer I

Skimmed milk powder 5%

dissolved in TBST and stored at 4°C

Blocking buffer II

BSA 5%

dissolved in TBST and stored at 4°C

2.5.8. Oil RedO staining of differentiated adipocytes

Oil RedO is a dye, used for staining of lipids in tissues and cells. Lipid droplets, stained by accumulated Oil RedO, appear in a red color.

Differentiated brown adipocytes (day 7) were washed with PBS, fixed in 4% PFA in PBS for 15 minutes at RT and washed 3 times with PBS. Afterwards, the cells were incubated with Oil RedO working solution for 4 hours at RT and, finally, cells were washed 3 times with PBS.

Oil RedO stock solution (5 mg/ml Oil RedO)

Isopropyl alcohol (99%)

Oil RedO 0.5%

dissolved with a magnetic stir bar over night and stored at RT

Oil RedO working solution (3 mg/ml Oil RedO)

H_2O

Oil RedO stock solution 60%

mixed one day before use and filtered through a paper filter on the next day

2.5.9. Quantification of triglyceride (TG) accumulation in differentiated brown adipocytes and BAT

TGs are esters of fatty acids and glycerol. To determine TG accumulation in differentiated brown adipocytes and BAT, an assay was performed, based on coupled enzyme reactions resulting in an increase in the absorbance at 540 nm that is directly proportional to the glycerol concentration.

Free Glycerol Reagent and Triglyceride Reagent (Sigma-Aldrich) were used according to the manufacturer's instructions. In brief, differentiated adipocytes (day 7), grown in 6-well plates, were washed with PBS, 200 µl TG-Tx-lysis buffer were added and cells were immediately frozen at -80°C. After thawing on ice, cells were resuspended and centrifuged for 10 minutes at 15000 g at 4°C. Afterwards, 2 µl of the supernatant were used for protein content determination applying the Bradford method (2.5.4.). The remaining part of each sample was resuspended, added to 1 ml of the TG assay reagent, incubated at 37°C for 5 minutes and centrifuged for 2 minutes at 15000 g at RT. Afterwards the absorbance was measured at 540 nm. A glycerol standard (Glycerol Standard Solution; Sigma-Aldrich) was used to calculate glycerol concentrations according to the manufacturer's instructions.

For determination of TG content from BAT, mice were sacrificed, BAT was resected and snap-frozen in liquid nitrogen. For the assay, 200 µl TG-Tx-lysis buffer were added to the BAT and the tissue was disrupted using an Ultra-turrax® (IKA). Afterwards, suspensions were centrifuged for 10 minutes at 15000 g at 4°C. 2 µl of the supernatant were used for protein content determination applying the Bradford method (2.5.4.). The remaining part of each sample was processed as described above.

TG-Tx-lysis buffer

NaCl	150 mM	
Tris-HCl	10 mM	pH 8.0
Triton-X 100	0.05%	
sterile filtered and stored at 4°C		
before use the following substance was added		
Complete® EDTA-free	40 µl/ml	

TG assay reagent

Free Glycerol Reagent	80%
Triglyceride Reagent	20%

2.5.10. Determination of cGMP and cAMP concentrations in adherent cells

To measure cGMP and cAMP concentrations in adherent cells, commercially available enzyme immunoassay kits were used (Assay Designs). The used kits were competitive immunoassays for the quantitative determination of cGMP and cAMP in samples treated with 0.1 M HCl. Therefore, polyclonal antibodies to cGMP and cAMP were applied to competitively bind to cGMP/cAMP in the standards or samples. An enzymatic reaction of alkaline phosphatase with its substrate was used for detection in a microplate reader (Tecan) at 405 nm. The measured optical density was used to calculate the concentrations of cGMP and cAMP.

The assays were performed according to the manufacturer's instructions. In brief, for basal measurements cells, grown in 6-well plates, were directly subjected to the assay procedures. For stimulated conditions, cells were incubated with 10 µM DEA-NO or 0.5 µM CNP in differentiation medium for 3 or 10 minutes, respectively, at 37°C and 5% CO_2 prior to the assay. After washing with PBS, cells were lyzed by incubation with 200 µl 0.1 M HCl/well for 15 minutes at RT, scraped with a cell scraper and centrifuged at 600 g for 2 minutes. Supernatents were used to perform the enzyme immunoassays. The 2 hours acetylated versions of the assays were performed following the manufacturer's instructions. Concentrations of cGMP and cAMP were normalized to the protein content determined from reference wells using the Bradford protein assay (2.5.4.).

2.5.11. Measurement of lipolysis in differentiated brown adipocytes and BAT

Lipolysis is the process of TG hydrolysis into FFAs and glycerol. Lipolysis in adipocytes is controlled by lipolytic hormones such as catecholamines (Langin, 2010). Catecholamines stimulate lipolysis by binding to β-ARs resulting in an elevation of intracellular cAMP levels. This leads to a phosphorylation of HSL, a major lipase in adipocytes, which hydrolyzes TGs.

To measure the lipolytic activity in brown adipocytes under basal and stimulated conditions, differentiated adipocytes, grown in 12-well plates, were washed 3 times with prewarmed lipolysis medium (37°C) followed by a 2 hours incubation with 400 µl lipolysis medium/well (basal conditions) supplemented with 10 µM NE, 200 µM 8-Br-cAMP, 200 µM 8-pCPT-cGMP, 10 µM DEA-NO or 0.5 µM CNP (stimulated conditions) at 37°C and 5% CO_2.

Subsequently, 50 µl of the medium were used for determination of lipolytic activity by measuring the glycerol concentration. For this purpose, 750 µl of Free Glycerol Reagent (Sigma) were added to the 50 µl of medium, the samples were incubated at 37°C for 5 minutes and the absorbance was measured at 540 nm. A glycerol standard (Glycerol Standard Solution; Sigma-Aldrich) was used to calculate glycerol concentrations. The glycerol release was normalized to the protein content of the samples. Therefore, the remaining lipolysis medium was removed from the cells, total cell lysates were prepared as described above (2.5.3.) and protein concentration was determined using the Bradford protein assay (2.5.4.).
To determine the lipolytic activity of BAT, mice were sacrificed and BAT was resected, weighed and chopped into small pieces. The chopped tissue was transferred to a 12-well plate, containing 1 ml lipolysis medium per well, and incubated for 2 hours at 37°C and 5% CO_2. Afterwards, 50 µl of the lipolysis medium were used for determination of lipolytic activity by measuring the glycerol concentration as described above. The glycerol release was normalized to the wet weight of the tissue.

Lipolysis medium

DMEM, liquid (4.5 g/L D-glucose) (Gibco)	
P/S	1%
BSA, essential fatty acid free (Sigma-Aldrich)	2%

2.5.12. Luciferase reporter assay

In research, luciferases are commonly used as reporters to assess the activity of promoters in cells, which are transfected with constructs containing the luciferase gene under control of the promoter of interest. In the luciferase reaction, light is emitted, when the enzyme acts on the appropriate luciferin substrate.
Cells were transiently co-transfected on day -2 with firefly and Renilla luciferase expression vectors at a ratio of 1:1 using Lipofectamine 2000 (Invitrogen) according to the manufacturer's instructions. Lipofectamine 2000 is a cationic lipid formulation that offers high transfection efficiencies and protein expression levels in a variety of cell lines. Luciferase reporter assays were performed in preadipocytes (day 0 without addition of differentiation medium on day -2), on day 0 and on day 2 using the Dual-Luciferase® Reporter Assay System (Promega) according to the assay protocol. In these assays the

activities of firefly and Renilla luciferases are measured sequentially from a single sample by adding different substrates. Cell lysates were prepared following the instructions for passive lysis. The activity of the firefly luciferase was normalized to the corresponding Renilla activity value for each sample.

2.6. Molecular biological methods

2.6.1. Materials

100 mm dish, Sarstedt (Cat. No. 83.1802.001)
Ethidium bromide 10 mg/ml, Carl Roth GmbH (Cat. No. 2218.1)
Gel extraction kit, QIAquick Gel Extraction Kit, QIAGEN, Hilden (Cat. No. 28704)
NucleoBond® PC 500 EF Kit, MACHERY-Nagel, Düren (Cat. No. 740550)
NucleoBond® PC 500 Kit, MACHERY-Nagel, Düren (Cat. No. 740574.25)
NovaBlue Singles™ Competent Cells, Merck (Cat. No. 70181)
PeqGOLD TriFast®, Peqlab, Erlangen (Cat. No. 30-2020)
Platinum® Taq Polymerase High Fidelity, Invitrogen, Karlsruhe (Cat. No. 11304-011)
Proteinase K, Roche, Mannheim (Cat. No. 03115828)
Restriction enzymes, New England Biolabs (NEB), Schwalbach
Roti® Phenol/C/I, Carl Roth GmbH (Cat. No. A156.2)
T4 DNA ligase, Invitrogen, Karlsruhe (Cat. No. 15224-041)
TaqCORE Kit, Qbiogen, Montreal, Canada (Cat. No. EPTQK109)
The Original TA Cloning® Kit (pCR®2.1 TOPO), Invitrogen, Karlsruhe (Cat. No. 45-0046)
Transcriptor First Strand Synthesis Kit, Roche, Mannheim (Cat. No. 4896866)

2.6.2. Equipment

Autoclave, Varioklav 135 T, Faust, Meckenheim
Casting platforms, EmbiTech, San Diego, USA
Electrophoresis chamber, Peqlab, Erlangen
Incubator, Certomat IS, Sartorius, Göttingen
Microwave, Severin, Sundern
Real-time PCR machine, Mx3000P Multiplex Quantitative PCR System, STRATAGENE (Agilent Technologies, Santa Clara, USA)
Thermocycler, T1, Biometra, Göttingen
Thermomixer, 5350, Eppendorf, Hamburg

UV light transilluminator, GelDoc®XR, BioRad, München
QuantityOne® Software, BioRad, München

2.6.3. Phenol/Chloroform extraction of tail DNA

For genotyping, a small biopsy of the mouse tail was digested in 500 µl proteinase K buffer at 55°C and 800 rpm in a thermomixer (Eppendorf) over night. Afterwards, 500 µl phenol/chloroform/isoamyl alcohol (25:24:1, Roti® Phenol/C/I, Carl Roth GmbH) were added, samples were mixed, incubated at RT for 5 minutes and centrifuged for 10 minutes at 15000 g. The upper phase was taken and added to 500 µl chloroform, mixed and centrifuged again for 10 minutes at 15000 g. The upper phase was taken and DNA was precipitated by addition of 800 µl isopropyl alcohol and inverting the samples. The white DNA precipitates were washed in 70% ethanol and pelleted by centrifugation at 15000 g for 1 minute. Pellets were air-dried and dissolved in 50 – 100 µl H_2O at 50°C over night.

Proteinase K buffer		
Tris-HCl	100 mM	pH 7.6
NaCl	200 mM	
EDTA	5 mM	
SDS	0.2 %	
dissolved in H_2O and stored at RT		
before use the following component was added		
Proteinase K	0.1 mg/ml	

2.6.4. Bacteriological tools

NovaBlue Singles™ Competent Cells (Merck) were cultured in lysogeny broth (LB) rich medium (LB+ medium). Media were prepared and autoclaved for 20 minutes at 120°C. Antibiotics were added after cooling to temperatures below 50°C.
For transformation of competent bacteria according to the manufacturer's instructions, bacteria were thawn on ice, DNA was added and incubated on ice for 5 minutes. Afterwards, bacteria were placed in a water bath at 42°C for 30 seconds (heat shock) and placed on ice again for 2 minutes. 150 µl prewarmed (37°C) LB+ medium were added and bacteria were incubated for 1 hour at 37°C shaking at 225 rpm. Bacteria were plated on LB+ plates with the appropriate antibiotics and incubated over night at 37°C.

LB+ medium

NaCl	0.5%
Peptone	1%
Yeast extract	0.5%
Glucose	0.1%

dissolved in H_2O, adjusted to pH 7.5, autoclaved and stored at 4°C

LB+ plates

LB+ medium

Agar-agar	1.5%

autoclaved, poured into 100 mm Petri dishes and stored at 4°C

Additives

Ampicillin	50 µg/ml
Kanamycin	25 µg/ml

In order to prepare plasmid DNA from bacterial cultures, two different protocols were applied. For the first one, the mini preparation, bacterial colonies were inoculated with 5 ml LB+ medium containing the appropriate antibiotics over night at 37°C and shaking at 225 rpm. To isolate plasmid DNA, a protocol from Sambrook and Russel for alkaline lysis was used. This method allows a rapid DNA isolation with a sufficient degree of purity for subsequent restriction digests and sequencing.

For the second method, the maxi preparation, bacterial colonies were inoculated with 200 ml LB+ medium containing the appropriate antibiotics over night at 37°C and shaking at 225 rpm. The next day, cultures were centrifuged at 5000 rpm for 20 minutes at 4°C. Plasmid DNA was isolated using the NucleoBond® PC 500 Kit (MACHERY-Nagel) or for endotoxin-free DNA preparation (for virus preparation) using the NucleoBond® PC 500 EF Kit (MACHERY-Nagel). Preparations were performed according to the manufacturer's instructions.

2.6.5. Enzymatic manipulation of DNA

Restriction enzymes are molecular tools for the cleavage of DNA at specific sites. They are divided into 3 groups: type I enzymes, which cut DNA randomly far from their recognition site, type II enzymes, which cut DNA within or close to their specific binding sites, and type III enzymes, which cleave DNA outside the recognition sequence. Type II restriction enzymes are widely used as molecular tools.

All restriction enzymes used in this study were purchased from New England Biolabs (NEB), Schwalbach). Digestion was performed according to the manufacturer's instructions using the buffers supplied with the enzymes by NEB. In general the following reaction conditions were used:

DNA digestion

DNA	1 – 4 µg
10 x buffer	10%
10 x BSA (optional, depending on the restriction enzyme)	10%
Restriction enzyme	5 – 20 units

filled up to 30 µl with H_2O, incubated for 1 – 2 hours or over night at 37°C

For DNA ligation, the generation of phosphodiester bonds, the following protocol was used:

DNA ligation

DNA (target vector)	20 – 50 ng
DNA (insert)	60 – 150 ng
5 x ligation buffer (Invitrogen)	20%
T4 DNA ligase (Invitrogen)	2.5 units

filled up to 20 µl with H_2O and incubated over night at 14 °C

2 µl of the ligation products were used for transformation of competent bacteria (2.6.4.).

2.6.6. Agarose gel electrophoresis

Agarose gel electrophoresis is used to separate, identify and purify DNA fragments. For gel preparation, the appropriate amount (0.7 – 2%) of agarose was added to Tris-acetic acid-

EDTA (TAE) buffer and boiled in a microwave (Severin). 800 ng/ml ethidium bromide (Carl Roth GmbH) were added and the solution was poured into casting platforms (EmbiTech), allowed to harden at RT and placed in an electrophoresis chamber (Peqlab) containing TAE buffer. For electrophoretic separation, 6 x loading buffer was added to the DNA and samples were loaded on the agarose gel. Electrophoresis was performed at 80 – 120 V at RT. DNA bands were visualized using a UV light transilluminator (GelDoc®XR, BioRad) at 366 nm using QuantityOne® Software (BioRad).

50 x TAE buffer

Tris	2 M
Acetic acid	5.71%
Na_2-EDTA	50 mM
dissolved in H_2O and stored at RT	

6 x loading buffer

50 x TAE	2%
Ficoll Typ 400	18%
EDTA	0.12 mM
Bromphenol blue	0.15%
Xylencyanol FF	0.15%
dissolved in H_2O and stored at -20°C	

Extraction of DNA fragments was performed using the QIAquick Gel Extraction Kit (QIAGEN) according to the manufacturer's instructions.

2.6.7. Generation of lentiviral expression constructs

Lentiviral expression constructs were used to stably express proteins of interest. The constructs were derived from the pRRL.SIN-18 vector, containing sequences of the human immune deficiency virus-1 (HIV-1) and the transgene of interest. The pRRL.SIN-18 vector

system contains no wildtype copies of the HIV-long terminal repeats (LTRs): the 5'-LTR is chimeric and contains an enhancer and promoter of the respiratory syncital virus (RSV) instead of the U3-region of the wildtype HIV (RRL). The U3-region in the 3'-LTR was nearly completely deleted. Therefore, both LTRs are transcriptionally inactivated (self-inactivating (SIN) vector) (Dull et al., 1998). The original virus plasmids were provided by Inder Verma (The Salk Institute for Biological Studies, Laboratory of Genetics, La Jolla, CA, USA).

Lentiviral plasmids

Plasmid	**Backbone**	**Promoter**	**Transgene**	**Provided by**
LV-cntr	pRRL.SIN18	----------	----------	A. Pfeifer
LV-RacL61	pRRL.SIN18	CMV	RacL61	B. Haas
LV-RacN17	pRRL.SIN18	CMV	RacN17	B. Haas
LV-sGCβ1	pRRL.SIN18	PGK	sGCβ1	self-generated
LV-sicntr	Hplm	H1	sicntr	A. Hofmann
LV-siERK1	Hplm	H1	siERK1	A. Hofmann
LV-VASP	pRRL.SIN18	CMV	VASP	R. Hermann

Expression vectors

Vector	**Resistance**	**Source**
CMVpRRL.SIN18	Ampicillin	A. Pfeifer / I. Verma
Hplm-H1	Ampicillin	A. Pfeifer / I. Verma
PGKpRRL.SIN18	Ampicillin	A. Pfeifer / I. Verma

The LV-sGCβ1 construct was generated by ligating (2.6.5.) the sGCβ1 complementary DNA (cDNA) into the AgeI and SalI restriction sites of the vector PGKpRRL.SIN18. The sGCβ1 cDNA containing a 5' AgeI recognition site was generated from isolated RNA (2.6.9.) by reverse transcription (2.6.9.) using oligo-dT primers followed by a PCR (2.6.10.) using the following primers:

Forward Primer: 5’ – ATACCGGTGCCACCATGTACGGTTTCGTGAACCAT – 3’
AgeI site

Reverse Primer: 5’ – ACTCAGTTTTCATCCTCCTCATTTG – 3’

The cDNA fragment was ligated into the pCR®2.1-TOPO® vector (Invitrogen) using The Original TA Cloning® Kit (Invitrogen) according to the manufacturer’s instructions. The AgeI recognition site of the cDNA fragment and the SalI recognition site of the pCR®2.1-TOPO® vector were used to retrieve the cDNA fragment from the vector and ligate it into the PGKpRRL.SIN18 expression vector. Insertion was checked by Acc56I (NEB) digestion (2.6.5.).
Preparation of the lentivirus (LV) was accomplished by the lentiviral vector platform of our institute (Institute of Pharmacology and Toxicology, University of Bonn, Bonn).

2.6.8. Generation of constructs for luciferase reporter assays

In order to perform luciferase reporter assays, constructs are used, which contain the luciferase gene under control of the promoter of interest. To generate a plasmid carrying the firefly luciferase under control of the sGCβ1 promoter, a 1.4 kb fragment of the sGCβ1 5’-flanking region was cloned into the KpnI and BglII sites of the firefly luciferase expressing vector pGL3-basic. The pGL3-basic vector lacks eukaryotic promoter and enhancer sequences and was also used as negative control. The pRL-TK vector (Promega) served as an internal control expressing Renilla luciferase under control of the herpes simplex virus thymidine kinase (TK) promoter.
The 1.4 kb fragment of the sGCβ1 5’-flanking region was generated from genomic DNA by PCR (2.6.10) using the following primers, which contain a KpnI and BglII recognition site, respectively:

Forward Primer: 5’ – TATGGTACCAAGAGGGAAGGAGAAAGGG – 3’
KpnI site

Reverse Primer: 5’ – ACCAGATCTCAGCTTCCAGGCAAGAGTA – 3’
BglII site

The resulting fragment was ligated into the pCR®2.1-TOPO® vector (Invitrogen) using The Original TA Cloning® Kit (Invitrogen) according to the manufacturer’s instructions. The KpnI and BglII recognition sites of the DNA fragment were used to retrieve the fragment

from the vector and ligate it into the pGL3-basic luciferase vector. Insertion was checked by NcoI (NEB) digestion (2.6.5.).

2.6.9. Isolation of RNA from adipocytes and BAT and reverse transcription of the RNA

Total RNA from cultured cells and BAT was isolated using the TriFast® reagent (Peqlab) according to the manufacturer's instructions. For real-time PCR analysis (2.6.10.) 0.5 µg RNA were reverse transcribed into cDNA using the Transcriptor First Strand Synthesis Kit (Roche) and random hexamer primers according to the manufacturer's instructions. For cloning, RNA was reverse transcribed into cDNA using oligo-dT primers.

2.6.10. Polymerase chain reaction (PCR)

PCR is a widely used method to amplify DNA fragments (Saiki et al., 1988). To perform PCRs, 3 different nucleic acid segments are required: the DNA template, a forward primer and a reverse primer. Moreover, a DNA polymerase (Taq polymerase) and deoxynucleotide triphosphates (dNTPs) are needed. The amplification of DNA fragments occurs in 3 different steps: denaturation at 95°C, annealing of the primers to the DNA template at 52 - 65°C (depending on the primers) and DNA synthesis at 72°C.
The following specific primer combinations were used for genotyping VASP mice:

Primers for genotyping PCRs

Name	**Primer sequence**
mVE10f	5' – ACCTGTGAGAAGACCCTGGGAG – 3'
mVE11r	5' – CTGCTTCACCCTCTCCAAGTCG – 3'
mVE13r2	5' – GAACAAGAGAAGGTGAGACCC – 3'
Neof1	5' – TTCTATCGCCTTCTTGACGAG – 3'

PCR reactions for genotyping were performed using genomic tail DNA (2.6.3.) and the TaqCORE kit (Qbiogen).

Genotyping PCR

Isolated tail DNA	1 µl
Primer 1 (10 pmol/µl)	1.25 µl

Primer 2 (10 pmol/µl)	1.25 µl
dNTPs (1.25 mM each)	4 µl
10 x PCR buffer with $MgCl_2$	2.5 µl
Taq polymerase	0.25 µl
H_2O	14.75 µl

The following PCR program was used for genotyping:

PCR program for genotyping

Step	**Time [seconds]**	**Temperature [°C]**
1	120	94
2	30	94
3	30	65 (-1°C per cycle)
4	35	72
steps 2 – 4 were repeated 10 times		
5	30	94
6	30	55
7	35	72
steps 5 – 7 were repeated 35 times		
8	600	72
9	∞	4

Quantitative real-time (RQ) PCRs were performed according to the SYBR Green method. SYBR Green I is a dye, which intercalates into double-stranded DNA, thereby producing a fluorenscence signal. The intensity of the signal is proportional to the amount of double-stranded DNA present in the reaction. Therefore, the intensity increases with each cycle of the PCR as the amount of the product increases. Thus, monitoring PCRs in real time is possible using this method.

SYBR Green RQ-PCRs were accomplished using the LightCycler® SYBR Green I Master mix (Roche) on a Mx3000P Multiplex Quantitative PCR System (STRATAGENE; 96-well format) using the following specific primer combinations:

Primers for RQ-PCRs

Name	**Sequence**
β3-AR forward	5’ – ATCTTCTCTCTGTGCTGGCTGCCCT – 3’
β3-AR reverse	5’ – CATCGGTTCTGGAGCGTTGGAGAGT – 3’
GLUT-4 forward	5’ – GCTGAGCTGAAGGATGAGAAACGGA – 3’
GLUT-4 reverse	5’ – CAACATACTGGAAACCCATGCCGAC – 3’
HPRT forward	5’ – ACATTGTGGCCCTCTGTGTGCTCA – 3’
HPRT reverse	5’ – CTGGCAACATCAACAGGACTCCTCGT – 3’
HSL forward	5’ – CTACGGGAAGGACAGGACAGCAAGG – 3’
HSL reverse	5’ – GAGGCTCAGCAGACGAGAGGGAGAA – 3’
PGC-1α forward	5’ – GCACACACCGCAATTCTCCCTTGTA – 3’
PGC-1α reverse	5’ – ACGCTGTCCCATGAGGTATTGACCA – 3’
Plin forward	5’ – CTCTGGGAAGCATCGAGAAGGTGGT – 3’
Plin reverse	5’ – CCTTCAGGGCATCGGATAGGGACAT – 3’
UCP-1 forward	5’ – GGTGAACCCGACAACTTCCGAAGTG – 3’
UCP-1 reverse	5’ – GGGTCGTCCCTTTCCAAAGTGTTGA – 3’

SYBR Green RQ-PCR

cDNA	3 µl
Primer 1 (5 pmol/µl)	1.25 µl
Primer 2 (5 pmol/µl)	1.25 µl
2 x SYBR Green I Master mix	4 µl

SYBR Green RQ-PCR program

Step	**Time [seconds]**	**Temperature [°C]**	
1	600	95	
2	10	95	
3	15	72	
4	90	72	
5	1	82	single acquisition

steps 2 – 5 were repeated 40 times			
melting curve:			
6	1	95	
7	15	65	
8	-	95	20 acquisitions per °C from 65°C to 95°C

Relative quantification of mRNA levels was performed based on the crossing point (CP) values of the amplification curves using the ΔΔCT method. Hypoxanthine-guanine-phosphoribosyltransferase (HPRT) served as an internal control.

To generate the lentiviral expression construct LV-sGCβ1 and the luciferase construct containing the sGCβ1 promoter, PCR was used to amplify the sGCβ1 cDNA and a 1.4 kb fragment of the sGCβ1 5'-flanking region (sGCβ1 promoter) from cDNA and genomic DNA, respectively, using specific primer combinations (2.6.7. and 2.6.8.) and the Platinum® Taq Polymerase High Fidelity (Invitrogen).

Cloning PCR

DNA / cDNA	1 µl
Primer 1 (10 pmol/µl)	2 µl
Primer 2 (10 pmol/µl)	2 µl
dNTPs (1.25 mM each)	1 µl
$MgSO_4$	2 µl
10 x PCR buffer	5 µl
Platinum® Taq DNA Polymerase HF	0.25 µl
H_2O	14.75 µl

Cloning PCR programm

Step	**Time [seconds]**	**Temperature [°C]**
1	60	94
2	30	94
3	30	60 (-1°C per cycle)
4	60 / 1kb amplicon	68
steps 2 – 4 were repeated 10 times		

5	30	94
6	30	55
7	60 / 1kb amplicon	68
steps 5 – 7 were repeated 35 times		
8	120	68
9	∞	4

2.7. Measurement of mitochondrial respiration

2.7.1. Materials

Adenosine 5′-diphosphate monopotassium salt dihydrate (ADP), Sigma-Aldrich (Cat. No. A-5285)
Digitonin, Sigma-Aldrich (Cat. No. R-8875)
Oligomycin, Sigma-Aldrich (Cat. No. O-4876)

2.7.2. Equipment

Oxygraph-2k, Oroborus Instruments, Insbruck, Austria
Software, DatLab Version 4.2.0.73, Oroborus Instruments, Insbruck, Austria

2.7.3. Measurements of mitochondrial respiration in cultured adipocytes and BAT

Analysis of mitochondrial function is central for the study of energy metabolism and thermogenic activity in brown fat cells. However, important properties of mitochondria differ *in vivo* and *in vitro*. To study mitochondrial function in BAT and in cultured brown adipocytes, a protocol for the *in situ* analysis of functional mitochondria in selectively permeabilized cells using digitonin, without the isolation of organelles, was applied (Kuznetsov et al., 2008).
For measurement of mitochondrial respiration in cultered adipocytes, differentiated cells (day 7), grown in 6-well plates, were washed 3 times with PBS. 200 µl of storage solution were added to each well. Cells were scraped with a cell scraped and stored on ice. To analyze mitochondrial respiration in tissue, mice were sacrificed, BAT was removed, weighed and dissected using scissors and microsurgery forceps. The dissected tissue was transferred to 200 µl storage solution and stored on ice. The duration of storage time was kept to a minimum.

Measurements of mitochondrial respiration were performed at 30°C in measurement solution using an oxygraph (Oxygraph-2k, Oroborus Instruments) and DatLab software (Oroborus Instruments, Insbruck). To measure endogenous respiration, the storage solution, containing cells or dissected tissue, was transferred to the measurement chamber of the oxygraph. The chamber contained 2 ml measurement solution, supplemented with 5 mM $MgCl_2$, equilibrated with atmospheric oxygen and prewarmed to 30°C. Respiration rates were measured, when a steady state was reached.

Additionally, the maximal mitochondrial oxygen consumption in permeabilized cells and tissue under maximal substrate availability conditions as well as the UCP-1-dependent fraction were determined. Therefore, a substrate/inhibitor titration protocol was applied. The following substances were successively added to the chamber using Hamilton syringes to the indicated final concentrations in the stated order. Each substance was added after reaching a steady state of the respiration rate.

Substance	**Final concentration**	**Function**
Digitonin	25 µg/ml	Permeabilization
Glutamate/Malate	10 mM each	Substrate
Succinate	10 mM	Substrate
ADP	2 mM	Substrate
Oligomycin	10 µg/ml	Inhibitor

The maximal mitochondrial respiration was determined after addition of ADP. The UCP-1-dependent respiration was measured after addition of the ATP-synthase inhibitor oligomycin.

To mimic cold exposure *in vitro,* differentiated brown adipocytes were pretreated with 1 mM 8-Br-cAMP for 24 hours prior to the measurements.

The obtained respiration rates were normalized to the wet weight of the tissue which was used or to the protein content, determined by the Bradford method (2.5.4.) from reference wells.

Storage solution	
4-Morpholineethanesulfonic acid	49 mM
KH_2PO_4	3 mM
Taurine	20 mM
Dithiothreitol	0.5 mM
Imidazole	20 mM

$MgCl_2$	9.5 mM
ATP	5.26 mM
Creatine phosphate	15 mM
K_2Ca-ethylene glycol tetraacetic acid (EGTA)	1.878 mM
K_2-EGTA	8.122 mM

dissolved in H_2O, adjusted to pH 7.1 with KOH and stored at -20°C

Measurement solution

KH_2PO_4	10 mM
KCl	60 mM
Tris	60 mM
Mannitol	110 mM
Na-EDTA	0.5 mM

dissolved in H_2O, adjusted to pH 7.4 with KOH or HCl and stored at 4°C

2.8. Statistical analysis

All values are presented as means ± standard error of the mean (SEM). The Student's t-test was performed to compare two groups. p values < 0.05 were considered as statistically significant. Statistical differences among more than two groups were determined by ANOVA (analysis of variance) and subsequent Bonferroni multiple comparison post-tests.

3. Results

3.1. Role of VASP in brown adipocyte differentiation and function

3.1.1. Expression of VASP in BAT and brown preadipocytes

Adipocytes orginate from MSCs. MSCs are multipotent adult stem cells, which can give rise to a variety of lineages including, for example, osteoblasts, chondrocytes, myocytes, endothelial cells and adipocytes depending on the *in vitro* cell culture conditions (Guilak et al., 2004; Hattori et al., 2004; Safford et al., 2004; Zuk et al., 2002). MSCs differentiate into preadipocytes, which give rise to white or brown adipocytes.

To study the role of VASP in brown adipocyte differentiation, BAT derived MSCs (BAT-MSCs) and preadipocytes were isolated from interscapular brown fat pads of newborn wt and VASP$^{-/-}$ littermates (Aszodi et al., 1999) by collagenase digestion, filtration and subsequent fractionation into mature adipocytes and the stroma-vascular fraction that contains BAT-MSCs (Haas et al., 2009; Nechad, 1983). The cells of the stroma-vascular fraction were immortalized by transduction with a lentiviral vector expressing the SV40 large T-antigen.

The focal adhesion protein VASP is expressed in a variety of tissues including BAT (Figure 9A) and is a major substrate for PKGI phosphorylation in a broad range of tissues (Krause et al., 2003; Reinhard et al., 2001). Western blot analysis revealed that VASP is highly expressed in BAT-MSCs and phosphorylated by PKGI as assessed by stimulation of PKGI activity using 8-pCPT-cGMP (Figure 9B).

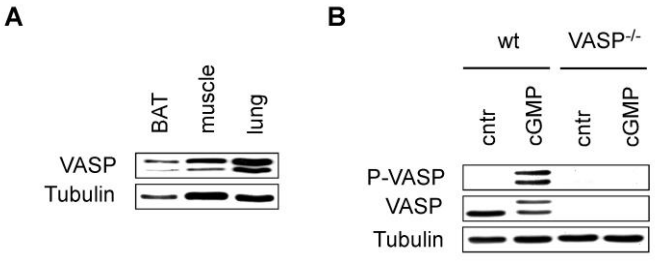

Figure 9: Expression of VASP in BAT and BAT-MSCs.
(A) Western blot analysis of VASP expression in BAT, skeletal muscle and lung from newborn wt mice. **(B)** Western blot analysis of VASP expression and phosphorylation by PKGI in wt and VASP$^{-/-}$ BAT MSCs, treated with or without (control, cntr) 100 µM 8-pCPT-cGMP (cGMP) for 30 minutes. Phosphorylated VASP (P-VASP) was detected using a phosphorylation-specific antibody, which detects PKG-specific phosphorylation of VASP at Ser235.

3.1.2. Analysis of cell spreading in VASP$^{-/-}$ preadipocytes

Ena/VASP proteins are activators of actin dynamics and play pivotal roles in cell motility and determination of cell shape (Krause et al., 2003). Moreover, it has been shown that cell shape regulates the adipogenic-osteogenic switch in human mesenchymal stem cell (hMSC) lineage commitment (McBeath et al., 2004). Previous studies using mouse embryonic fibroblasts (MEFs) revealed that VASP$^{-/-}$ MEFs are highly spread compared to wt cells (Garcia Arguinzonis et al., 2002). Therefore, the attachment and spreading behavior of wt and VASP$^{-/-}$ preadipocytes was studied. BAT-MSCs exhibited a fibroblast-like morphology (Figure 10B). Compared to wt cells, VASP$^{-/-}$ preadipocytes attached significantly slower to the surface of the well plate (Figure 10A), but once attached were highly spread. VASP$^{-/-}$ cells covered a 1.79 ± 0.12 fold larger surface area compared to wt cells (Figure 10B). (Data regarding cell attachment and cell spreading were generated in collaboration with and by Michaela-Rosemarie Hermann during her master thesis under my supervision.)

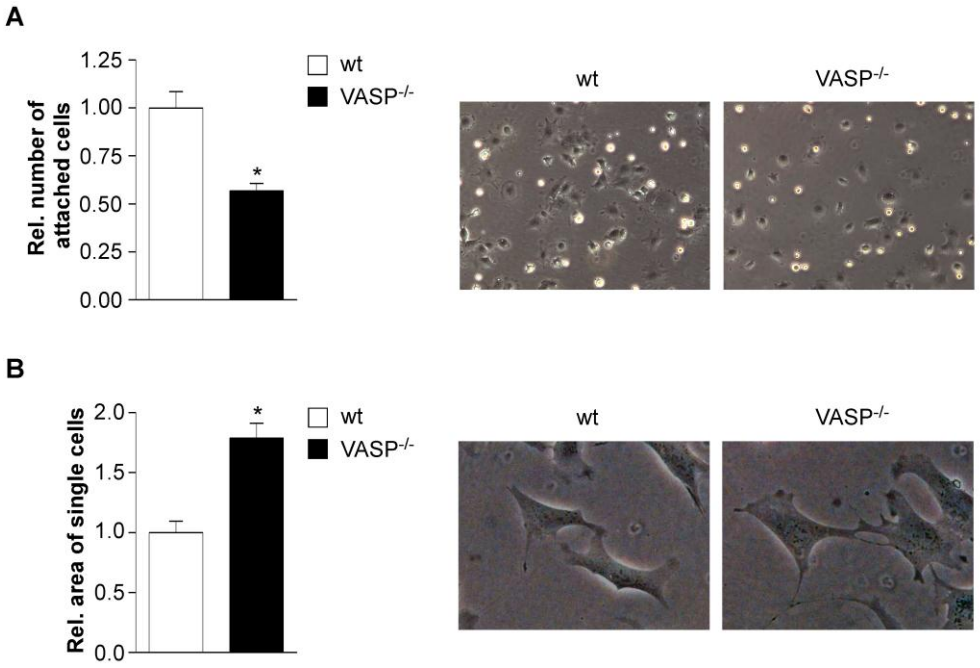

Figure 10: VASP$^{-/-}$ cells showed a decreased attachment and increased spreading ability.
(A) Attachment analysis of wt and VASP$^{-/-}$ BAT-MSCs. Relative (Rel.) number of attached cells within the first 2 hours after seeding (left). Data are represented as means of 3 independent experiments ± SEM; * $p < 0.05$. Exemplary brightfield micrographs of attached BAT-MSCs 2 hours after seeding (right). **(B)** Spreading ability of wt and VASP$^{-/-}$ cells. The mean area of wt cells (n = 192) from 3 independent experiments was set as 1. The relative area of n = 163 VASP$^{-/-}$ cells was determined 24 hours after seeding (left). Data are represented as means ± SEM; * $p < 0.05$. Exemplary brightfield micrographs of spread BAT-MSCs 24 hours after seeding (right).

3.1.3. Influence of VASP ablation on lipid accumulation and adipogenic marker expression

To investigate the role of VASP in brown adipogenic differentiation, BAT-MSCs were subjected to a certain differentiation protocol applying a defined combination of adipogenic substances (Figure 11A). After 11-12 days of differentiation, VASP$^{-/-}$ cells exhibited a markedly increased accumulation of lipid droplets as assessed by Oil RedO staining (Figure 11B). Cellular triglyceride (TG) content in VASP$^{-/-}$ adipocytes was 2.38 ± 0.33 fold increased compared to wt cells (Figure 11C).

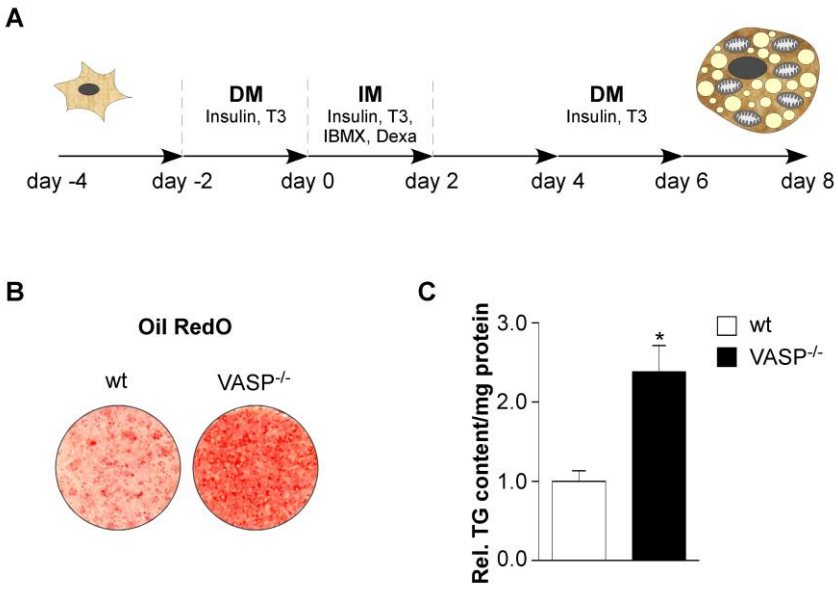

Figure 11: VASP ablation resulted in an increased lipid accumulation in brown adipocytes.
(A) Protocol of adipogenic differentiation of BAT-MSCs. Different media (DM, differentiation medium; IM, induction medium; IBMX, 3-isobutyl-1-methylxanthine; T3, triiodothyronine; Dexa, dexamethasone) were used at the indicated stages of adipogenic differentiation (day -4 to day 8). **(B)** Oil RedO staining of differentiated wt and VASP$^{-/-}$ brown adipocytes on day 8. **(C)** Quantitative measurement of lipid accumulation in differentiated wt and VASP$^{-/-}$ brown adipocytes on day 8 (n = 6 independent experiments). TG content was normalized to the protein content of the samples. Data are given as means ± SEM; * $p < 0.05$.

To further analyze the effect of VASP ablation on brown adipogenic differentiation, the expression of adipogenic markers in wt and VASP$^{-/-}$ adipocytes was investigated by Western blot analysis. Compared to wt brown adipocytes, VASP$^{-/-}$ cells showed a significantly increased expression of the CCAAT/enhancer-binding protein α (C/EBPα) as well as the peroxisome proliferator-activated receptor γ (PPARγ), which in turn stimulate the expression of downstream adipogenic genes (Rosen et al., 2000). Moreover, the expression of the late adipocyte marker fatty acid-binding protein 4 (aP2) was also enhanced (Figure 12A).

Additionally, RQ-PCR expression analysis of a panel of adipocyte markers including perilipin (Plin), glucose transporter type 4 (GLUT-4), hormone-sensitive lipase (HSL) and the β3-adrenergic receptor (β3-AR) was performed. VASP ablation caused an increase in the mRNA levels of Plin (5.48 ± 0.46 fold), GLUT-4 (2.29 ± 0.19 fold), HSL (3.52 ± 0.40 fold) and β3-AR (3.07 ± 0.51) (Figure 12B).

These data indicate that brown adipogenic differentiation is enhanced in the absence of VASP.

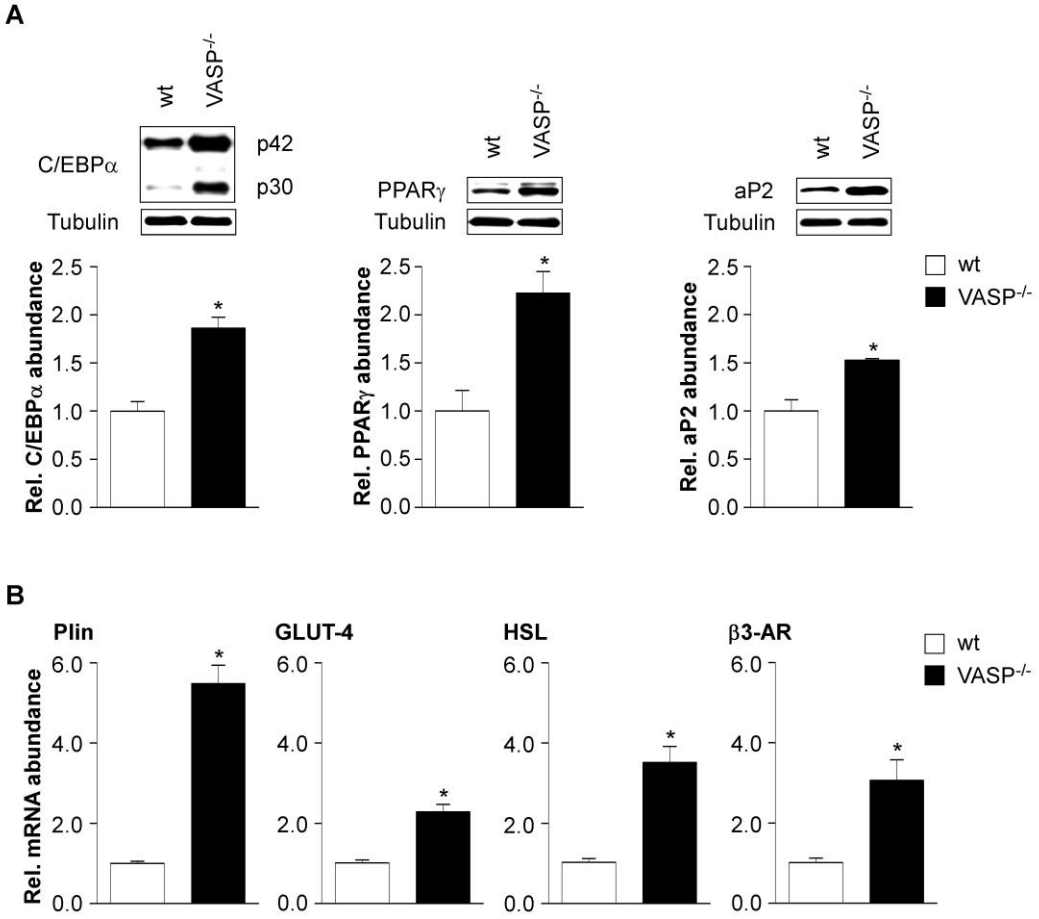

Figure 12: Expression of adipogenic markers in wt and VASP$^{-/-}$ brown adipocytes.

(A) Western blot analysis of C/EBPα, PPARγ and aP2 expression in differentiated wt and VASP$^{-/-}$ brown adipocytes on day 7 (upper panels). Densitometric analysis of the marker protein amount normalized to tubulin ($n \geq 3$ independent experiments) (lower panels). Data are represented as means ± SEM; * $p < 0.05$. **(B)** RQ-PCR analysis of adipogenic marker expression. Quantification of Plin, GLUT-4, HSL and β3-AR expression was performed in differentiated brown adipocytes on day 7 ($n = 3$ independent experiments). HPRT was used as an internal control and data are represented as fold changes with means ± SEM; * $p < 0.05$.

3.1.4. Mitochondrial function in VASP$^{-/-}$ adipocytes

Brown adipocyte differentiation is characterized by a multiplication and functional activation of mitochondria (Cannon and Nedergaard, 1996). The thermogenic activity of brown adipocytes requires the uncoupling protein-1 (UCP-1), which uncouples the proton gradient across the inner mitochondrial membrane from ATP synthesis (Cannon and Nedergaard, 2004). To study the expression of the thermogenic program in VASP$^{-/-}$ cells, the expression of UCP-1 and the PPARγ-coactivator-1α (PGC-1α), which activates UCP-1 transcription, as well as Cytochrome c (Cytc), which is an essential component of the electron transport chain in mitochondria, were analyzed. Compared to wt cells, VASP$^{-/-}$ adipocytes showed an elevated expression of all three mitochondrial markers (Figure 13A and B) indicating an enhanced development of the thermogenic program in the absence of VASP.

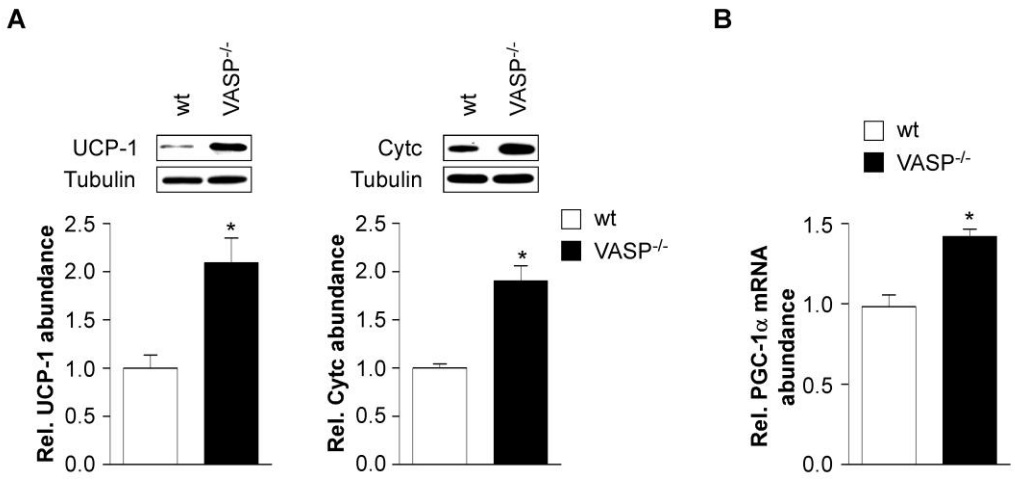

Figure 13: Increased expression of mitochondrial markers in the absence of VASP.
(A) Western blot analysis of UCP-1 and Cytc expression in differentiated wt and VASP$^{-/-}$ brown adipocytes on day 7 (upper panels). Densitometric analysis of the marker protein amount normalized to tubulin ($n \geq 3$ independent experiments) (lower panels). Data are represented as means ± SEM; * $p < 0.05$. **(B)** RQ-PCR quantification of PGC-1α expression, performed in differentiated brown adipocytes on day 7 ($n = 3$ independent experiments). HPRT was used as an internal control and data are represented as fold changes with means ± SEM; * $p < 0.05$.

Furthermore, mitochondrial function in wt and VASP$^{-/-}$ cells was investigated using an oxygraph (measurement protocol: Figure 14A). Endogenous mitochondrial respiration under basal conditions and after stimulation of cold-induced thermogenesis was measured in differentiated brown adipocytes. Cold-induced thermogenesis *in vivo* is mediated by a process involving β3-adrenergic stimulation resulting in increased cAMP levels. Therefore,

endogenous mitochondrial respiration was determined with and without pretreatment of differentiated brown adipocytes with 8-Br-cAMP for 24 hours to mimic cold exposure. $VASP^{-/-}$ cells showed a significantly increased endogenous respiration (5.21 ± 0.21 nmol O_2/min/mg protein; 2.68 ± 0.11 fold increase) compared to wt adipocytes (1.94 ± 0.20 nmol O_2/min/mg protein). After treatment with 8-Br-cAMP, the oxygen consumption was increased 2.05 ± 0.23 fold in wt cells (3.99 ± 0.45 nmol O_2/min/mg protein), whereas $VASP^{-/-}$ cells exhibited a 4.61 ± 0.22 fold increase (8.96 ± 0.42 nmol O_2/min/mg protein) compared to non-treated wt adipocytes (Figure 14B).

Additionally, the maximal mitochondrial oxygen consumption in permeabilized cells under maximal substrate availability conditions as well as the UCP-1-dependent fraction were determined. To measure maximal respiration, ADP was added, whereas the UCP-1-dependent respiration was determined after addition of the ATP-synthase inhibitor oligomycin. The maximal mitochondrial respiration in permeabilized cells was significantly increased in $VASP^{-/-}$ cells (1.83 ± 0.13 fold). cAMP pretreatment stimulated the maximal respiration by 1.54 ± 0.12 fold in wt cells, whereas pretreated $VASP^{-/-}$ cells showed a 2.67 ± 0.25 fold increase (Figure 14C). Taken together, basal as well as cAMP-induced and UCP-1-dependent mitochondrial respiration were significantly increased in $VASP^{-/-}$ cells.

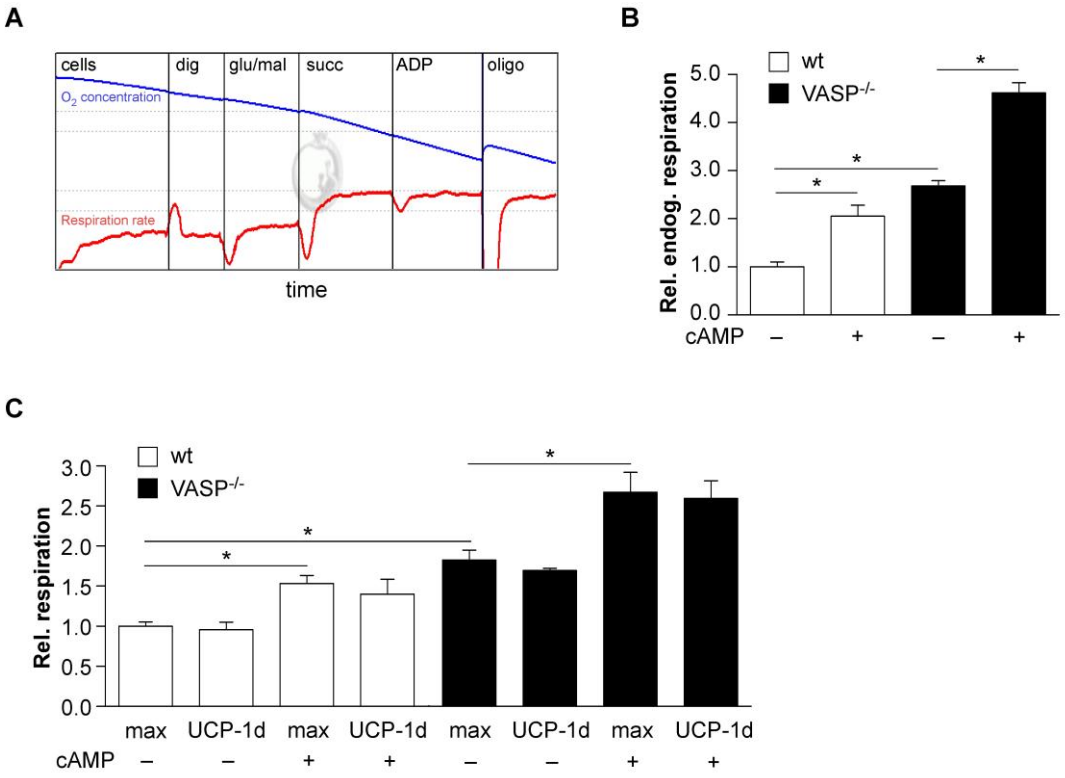

Figure 14: VASP$^{-/-}$ brown adipocytes showed an increased mitochondrial respiration.
(A) Representative oxygraph trace of VASP$^{-/-}$ brown adipocytes on day 7 showing the measurement protocol. Cells were permeabilized using digitonin (25 µg/ml; dig). Afterwards the substrates glutamate/malate (10 mM each; glu/mal) and succinate (10 mM; succ) were added. The maximal mitochondrial respiration capacity was achieved by stimulation with ADP (2 mM). The ATP synthase inhibitor oligomycin (10 µg/ml; oligo) was applied to identify the uncoupled/UCP-1-dependent fraction of total respiration. **(B)** Endogenous mitochondrial respiration under basal conditions and after pretreatment with 1 mM 8-Br-cAMP (cAMP) for 24 hours as indicated (n = 3 independent experiments). Data were obtained after the addition of cells to the oxygraph chamber and reaching a steady state. Data are represented as means ± SEM; * $p < 0.05$. **(C)** Maximal mitochondrial respiration (max) in permeabilized adipocytes after addition of glu/mal, succ and ADP as well as the UCP-1-dependent fraction (UCP-1d), determined after addition of oligomycin (n = 3 independent experiments). Measurements were performed under basal conditions and after pretreatment of the cells with 1 mM 8-Br-cAMP (cAMP) for 24 hours as indicated. Data are represented as means ± SEM; * $p < 0.05$.

3.1.5. Lipolytic activity in VASP$^{-/-}$ adipocytes

The enzymatic hydrolysis of stored TGs in adipocytes is an exquisitely regulated process. In both WAT and BAT, lipolysis is rapidly enhanced by lipolytic hormones such as catecholamines (Langin, 2010). In BAT, catecholamine stimulated lipolysis provides fatty acids for heat production (Robidoux et al., 2004). Catecholamines like norepinephrine (NE) stimulate lipolysis by binding to β-adrenergic receptors resulting in an elevation of intracellular cAMP levels and therefore, activation of PKA. PKA activation leads to the phosphorylation of HSL, a major lipase in adipocytes that hydrolyzes TGs.

To investigate the effect of VASP ablation on brown adipocyte lipolysis, glycerol release was measured under basal as well as stimulated conditions by incubating differentiated brown adipocytes with 8-Br-cAMP and NE. Under basal conditions, lipolytic activity in VASP$^{-/-}$ adipocytes was 2.44 ± 0.21 fold increased compared to wt cells. In both wt and VASP$^{-/-}$ cells, lipolysis was stimulated by 8-Br-cAMP and NE, but the effect was much more pronounced in the absence of VASP (Figure 15A). Moreover, VASP$^{-/-}$ cells expressed higher amounts of PKA (Figure 15B), β3-AR (Figure 15C) and HSL (Figure 15D). Additionally, HSL phosphorylation and therefore, activation was markedly increased in VASP$^{-/-}$ adipocytes under basal and stimulated conditions (Figure 15D).

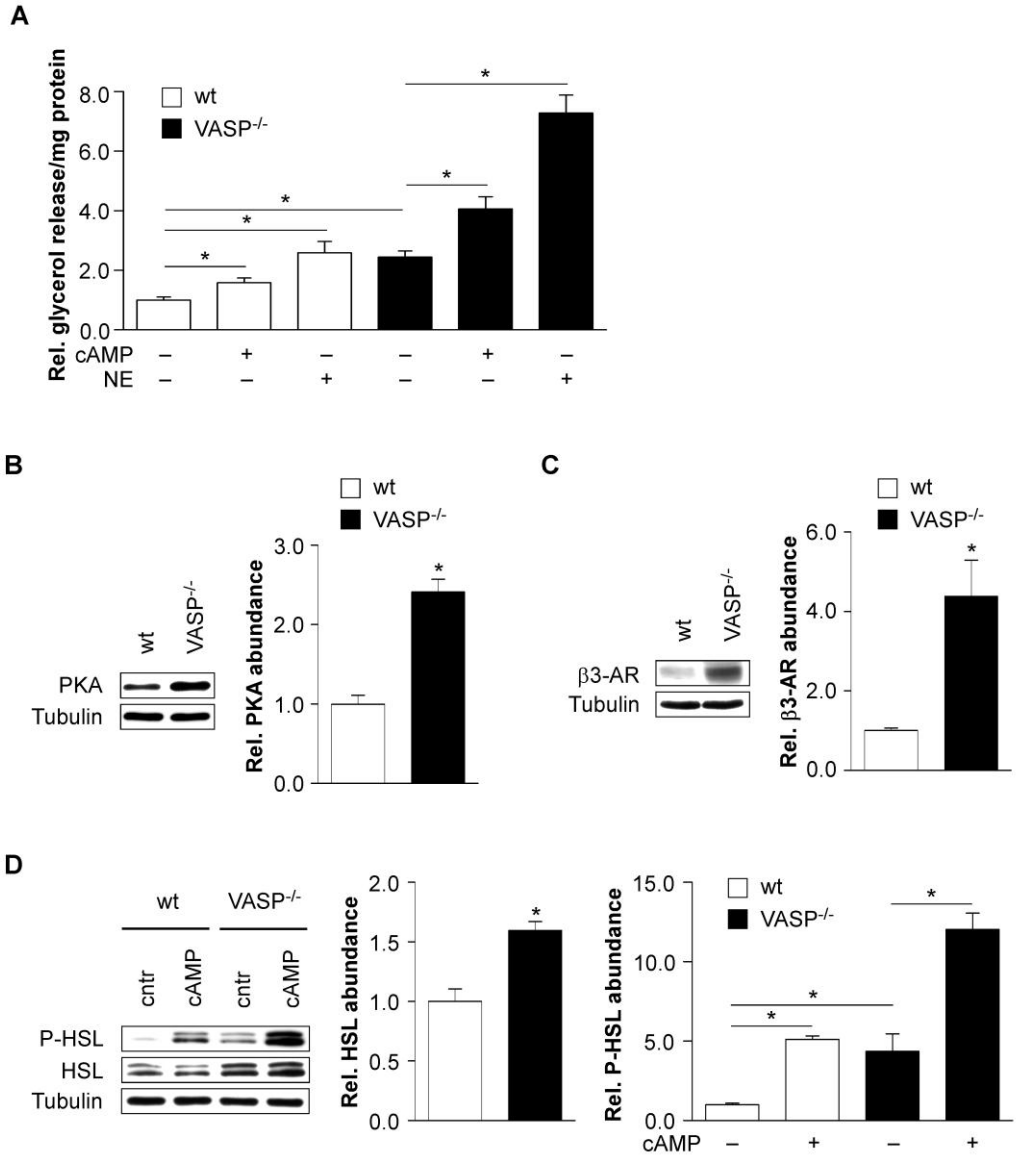

Figure 15: Lipolytic activity was increased in the absence of VASP.

(A) Lipolytic activity of wt and VASP$^{-/-}$ adipocytes on day 7. Glycerol release was measured under basal and stimulated conditions. Lipolysis was stimulated by incubation with 200 µM 8-Br-cAMP (cAMP) and 10 µM NE

for 2 hours. Data are represented as means ± SEM; * $p < 0.05$. **(B)** Western blot analysis of PKA expression in differentiated wt and VASP$^{-/-}$ brown adipocytes on day 7 using an antibody, which detects all catalytic subunits of PKA (left). Densitometric analysis of the protein amount normalized to tubulin (n = 3 independent experiments) (right). Data are represented as means ± SEM; * $p < 0.05$. **(C)** Western blot analysis of β3-AR expression in differentiated wt and VASP$^{-/-}$ brown adipocytes on day 7 (left). Densitometric analysis of the protein amount normalized to tubulin (n = 3 independent experiments) (right). Data are represented as means ± SEM; * $p < 0.05$. **(D)** Western blot analysis of the amounts of total HSL and phosphorylated HSL (P-HSL) with and without (control; cntr) application of 200 µM 8-Br-cAMP (cAMP) for 2 hours using a phosphorylation-specific antibody (Ser660) (left). Densitometric analysis of the total HSL protein amount (middle) and P-HSL abundance (right) normalized to tubulin (n = 3 independent experiments). Data are represented as means ± SEM.

In human white adipocytes, lipolysis is also regulated by natriuretic peptides (NPs), which elevate intracellular cGMP levels. This effect is mediated by PKG, which phosphorylates HSL (Langin, 2010; Sengenes et al., 2003). However, it was published that this regulation of white adipocyte lipolysis is primate-specific and does not occur in rodents (Sengenes et al., 2003). Because there is no data on cGMP-dependent lipolysis in murine brown adipocytes, it was investigated, whether 8-pCPT-cGMP and cGMP-elevating substances like the NO donor and sGC activator DEA-NO and the C-type natriuretic peptide (CNP) are capable of stimulating lipolysis and HSL phosphorylation in brown adipocytes from wt and VASP$^{-/-}$ mice. CNP activates the particulate GC-B. CNP was used because our previous studies revealed that brown adipocytes express only the GC-B form of the NP receptor and not the GC-A form (Haas et al., 2009). 8-pCPT-cGMP as well as DEA-NO and CNP were not able to stimulate lipolysis in murine brown adipocytes (Figure 16A). Moreover, in contrast to PKA, PKGI expression was not altered in differentiated VASP$^{-/-}$ cells compared to wt adipocytes (Figure 16B). Previous studies have shown that PKGI is the only PKG isoform being expressed in brown (pre)adipocytes (Haas et al., 2009). Analysis of HSL phosphorylation revealed that 8-pCPT-cGMP in contrast to 8-Br-cAMP did not stimulate the phosphorylation of HSL in murine brown adipocytes (Figure 16C).

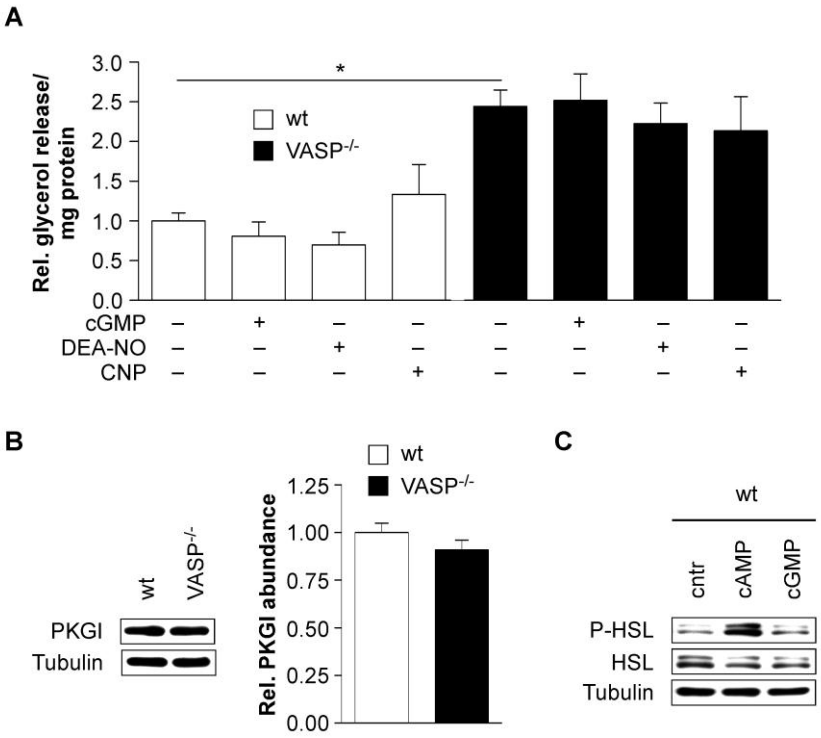

Figure 16: Brown fat cell lipolysis was not stimulated by 8-pCPT-cGMP and cGMP-elevating substances. **(A)** Lipolytic activity of wt and VASP$^{-/-}$ adipocytes on day 7. Glycerol release was measured under basal conditions and after application of 200 µM 8-pCPT-cGMP (cGMP), 10 µM DEA-NO or 0.5 µM CNP for 2 hours. Data are represented as means ± SEM; * $p < 0.05$. **(B)** Western blot analysis of PKGI expression in differentiated wt and VASP$^{-/-}$ brown adipocytes on day 7 (left). Densitometric analysis of the protein amount normalized to tubulin (n = 3 independent experiments) (right). Data are represented as means ± SEM; * $p < 0.05$. **(C)** Western blot analysis of the amount of phosphorylated HSL (P-HSL) with and without (cntr) application of 200 µM 8-Br-cAMP (cAMP) and 200 µM 8-pCTP-cGMP (cGMP), respectively, for 2 hours using a phosphorylation-specific antibody (Ser660) .

3.1.6. Rescue of the VASP$^{-/-}$ phenotype by lentiviral restoration of VASP expression

To verify that the lack of VASP was responsible for the observed phenotype in VASP$^{-/-}$ cells, wt and VASP$^{-/-}$ cells were infected with a lentivirus (LV) expressing full-length VASP (LV-VASP) under control of the cytomegalo virus (CMV) promoter (Figure 17A and B). Additionally, a control (cntr) vector without promoter and transgene (LV-cntr) was used (Figure 17A). Whereas restoration of VASP in VASP$^{-/-}$ cells rescued the knockout phenotype as assessed by Oil RedO staining (Figure 17C) and determination of TG content (Figure 17D), transduction with the control virus did not affect adipogenic differentiation in both genotypes. Rescue of VASP expression significantly reduced TG content to levels similar to those found in wt cells (1.33 ± 0.06 fold higher). Transduction with LV-cntr did not significantly affect TG levels (Figure 17D).

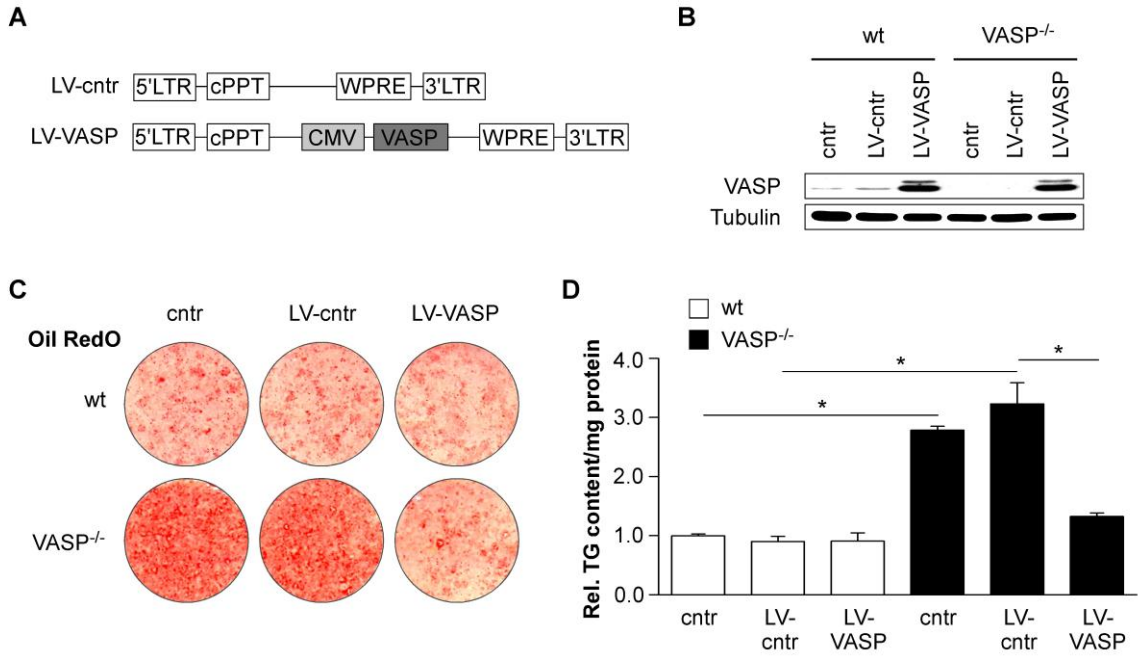

Figure 17: Restoration of VASP in VASP$^{-/-}$ cells rescued the knockout phenotype.
(A) Linear map of the lentiviral vectors used for restoration of VASP in VASP$^{-/-}$ cells. The LV-cntr vector without promoter and transgene was used as a control virus. Restoration of VASP was achieved by using the LV-VASP construct expressing VASP under control of the CMV promoter. LTR, long terminal repeat; cPPT, central polypurine tract; WPRE, posttranscriptional regulatory element of the woodchuck hepatitis virus. **(B)** Western blot analysis of VASP expression in wt and VASP$^{-/-}$ cells, non-infected (cntr) or transduced with LV-cntr or LV-VASP as indicated. **(C)** Oil RedO staining of non-infected and LV-cntr or LV-VASP infected wt and VASP$^{-/-}$ adipocytes on day 7. **(D)** Relative TG content in differentiated wt and VASP$^{-/-}$ cells, non-transduced, LV-cntr or LV-VASP transduced (n = 3 independent experiments). TG content was normalized to the protein content of the samples. Data are given as means ± SEM; * $p < 0.05$.

3.2. Influence of VASP ablation on cGMP signaling in brown preadipocytes

3.2.1. Analysis of cGMP concentration and PKGI expression in VASP$^{-/-}$ cells

Previous studies on signaling pathways in brown fat cells have demonstrated that cGMP enhances adipogenic differentiation by PKGI activation (Haas et al., 2009). Because VASP is a major substrate of PKGI (Butt et al., 1994), cGMP signaling in wt and VASP$^{-/-}$ cells was investigated. As expected, treatment of wt cells with 8-pCPT-cGMP resulted in a markedly increased differentiation as assessed by Oil RedO staining (Figure 18A). Interestingly, cGMP treated wt cells exhibited a phenotype quite similar to the VASP$^{-/-}$ phenotype, which was characterized by an elevated lipid droplet accumulation (Figure 18A). These results raised the question, whether cGMP concentration and cGMP signaling might be altered in VASP$^{-/-}$ cells. To address this issue, cGMP content was measured in wt and VASP$^{-/-}$ cells at different stages

of differentiation. Compared to wt cells, VASP$^{-/-}$ cells showed a significant increase in cGMP content in preadipocytes as well as on day 0 and day 2 (Figure 18B). Moreover, the expression of PKGI was also increased in preadipocytes and day 0 cells (Figure 18C).

As VASP is not only a substrate of PKGI but also a substrate of PKA (Butt et al., 1994) and because cAMP is known to stimulate adipogenic differentiation (Nedergaard et al., 1995), cAMP levels in wt and VASP$^{-/-}$ cells were also determined. cAMP concentrations in both genotypes did not significantly differ at different stages of differentiation (Figure 18D).

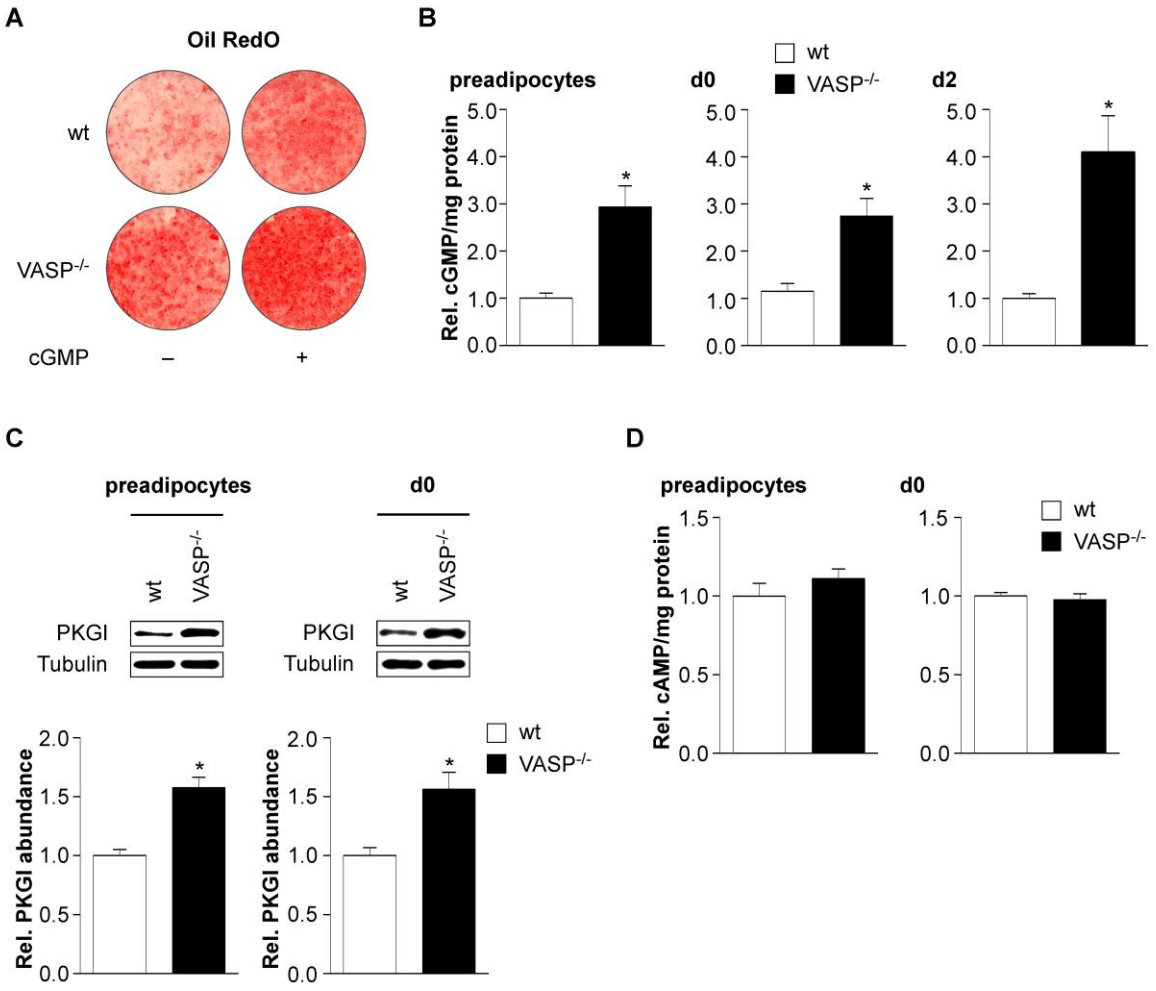

Figure 18: cGMP levels and PKGI expression, but not cAMP levels and PKA expression, were markedly increased in VASP$^{-/-}$ cells.

(A) Oil RedO staining of differentiated wt and VASP$^{-/-}$ brown adipocytes (day 7) after treatment with 200 µM 8-pCPT-cGMP (cGMP) during the whole differentiation process. cGMP was added to the medium every second day. **(B)** Relative cGMP content of wt and VASP$^{-/-}$ cells at different stages of differentiation: preadipocytes, day 0 (d0) and day 2 (d2) ($n \geq 3$ independent experiments). Data are represented as means ± SEM; * $p < 0.05$. **(C)** Western blot analysis of PKGI expression in wt and VASP$^{-/-}$ preadipocytes and d0 cells (upper panels). Densitometric analysis of PKGI protein amount normalized to tubulin ($n = 3$ independent experiments; lower panels). Data are represented as means ± SEM; * $p < 0.05$. **(D)** Relative cAMP content of wt and VASP$^{-/-}$ cells

at different stages of differentiation (preadipocytes, d0; n ≥ 3 independent experiments). Data are represented as means ± SEM; * p < 0.05.

3.2.2. Influence of VASP ablation on sGCβ1 expression

Given the fact that cGMP levels in cells are regulated by different cGMP-producing and cyclic nucleotide-hydrolyzing enzymes, there might be several reasons for elevated cGMP concentrations in VASP$^{-/-}$ cells. Taken into account that increased cGMP levels in VASP$^{-/-}$ cells were measured not only in preadipocytes and on day 0 but also on day 2 (4.08 ± 0.79 fold increase) (Figure 18B), which is 2 days after addition of induction medium containing the non-specific PDE inhibitor IBMX, it was suggested that the observed differences in cGMP levels should not be due to changes in PDE expression or activity in VASP$^{-/-}$ cells. Therefore, further investigations focussed on cGMP-synthesizing enzymes, which are either the NO-sensitive sGCs (Koesling et al., 2004) or the natriuretic peptide activated pGCs (Garbers et al., 2006). For that reason, wt and VASP$^{-/-}$ cells were preincubated with the NO donor and sGC activator DEA-NO or with CNP, which actives the particulate GC-B. Notably, DEA-NO treated wt cells showed a 56.45 ± 14.05 fold increase in cGMP content (1.816 ± 0.452 pmol cGMP/mg protein), whereas VASP$^{-/-}$ cells exhibited a markedly higher increase of 133.78 ± 12.30 fold (4.303 ± 0.396 pmol cGMP/mg protein) compared to non-treated wt preadipocytes (0.032 ± 0.005 pmol cGMP/mg protein) (Figure 19A). These results suggested an elevated sGC expression in VASP$^{-/-}$ cells. In contrast, CNP caused a lower increase of cGMP content in VASP$^{-/-}$ cells (95.18 ± 7.52 fold) compared to wt preadipocytes (118.19 ± 14.10 fold) indicating a decreased GC-B expression in VASP$^{-/-}$ (Figure 19A). Therefore, an altered expression of sGC was suspected to cause the observed differences in cGMP levels.

Mammalian sGCs are heterodimeric enzymes consisting of two subunits, termed sGCα and sGCβ, which form the functional heterodimers sGCα1β1 and sGCα2β1 (Friebe and Koesling, 2003). Interestingly, an elevated expression of the sGCβ1 subunit, but not the sGCα2 subunit, was detected in VASP$^{-/-}$ preadipocytes as well as in cells on day 0 and day 2 (Figure 19B). The sGCα1 subunit was not detected in brown preadipocytes and adipocytes suggesting that the sGCα2β1 heterodimer is the only isoform, which is present in these cells. Thus, it was hypothesized that an increase in sGCβ1 expression alone might be sufficient to elevate cGMP levels in VASP$^{-/-}$ cells. In this scenario, the sGCα2 subunit would have a higher availability in brown preadipocytes, whereas the sGCβ1 subunit would limit the amount of catalytically active heterodimeric enzyme in the cell. To prove this hypothesis, wt cells were infected with a lentivirus expressing sGCβ1 (LV-sGCβ1) under control of the PGK promoter without

altering the expression of the sGCα2 subunit (Figure 19C). Interestingly, overexpression of sGCβ1 alone resulted in a 4.50 ± 0.66 fold elevated cGMP content in LV-sGCβ1 infected wt cells (0.132 ± 0.019 pmol cGMP/mg protein) compared to control transduced cells (0.030 ± 0.003 pmol cGMP/mg protein) on day 0 (Figure 19D).

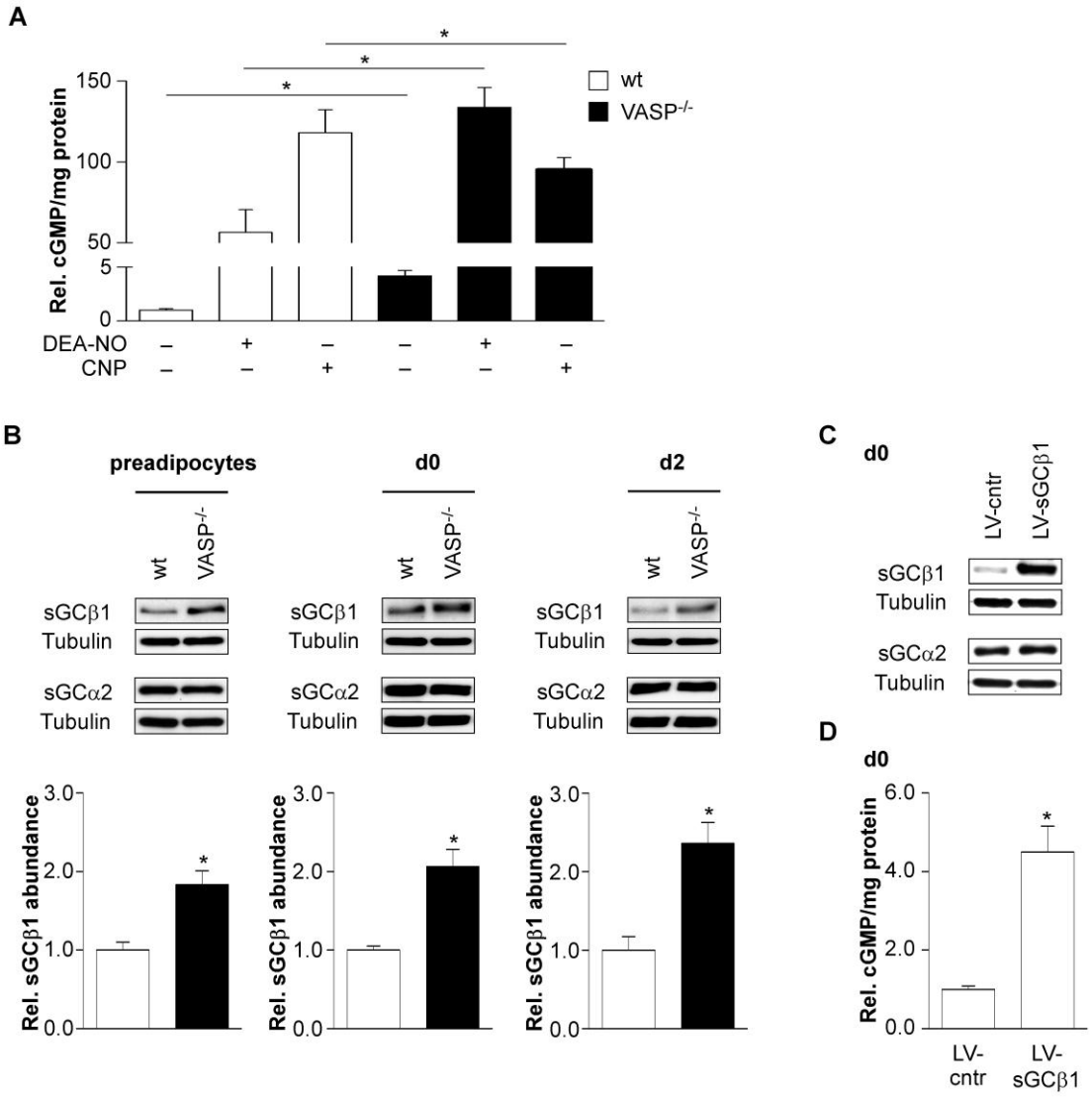

Figure 19: Increased expression of sGCβ1 in the absence of VASP.

(A) Relative cGMP content of wt and VASP$^{-/-}$ cells on day 0 after treatment with 10 µM DEA-NO for 3 minutes and 0.5 µM CNP for 10 minutes, respectively (n ≥ 3 independent experiments). Data are represented as means ± SEM; * $p < 0.05$. **(B)** Western blot analysis of sGCβ1 and sGCα2 expression in wt and VASP$^{-/-}$ cells at different stages of differentiation (preadipocytes, d0, d2; upper panels). Densitometric analysis of sGCβ1 protein amount normalized to tubulin (n = 3 independent experiments; lower panels). Data are represented as means ± SEM; * $p < 0.05$. **(C)** Western blot analysis of sGCα2 and sGCβ1 expression in wt cells on day 0, which were infected with LV-sGCβ1 or LV-cntr. **(D)** Relative cGMP content of wt cells transduced with LV-sGCβ1 or LV-cntr (n = 3 independent experiments). Data are represented as means ± SEM; * $p < 0.05$.

3.2.3. Rescue of the VASP$^{-/-}$ phenotype by inhibition of sGC

To verify that the observed phenotype in VASP$^{-/-}$ cells was indeed attributed to an increased amount of catalytically active sGC, the highly selective sGC inhibitor ODQ was applied. Treatment of wt and VASP$^{-/-}$ cells with ODQ during the differentiation process led to a decreased differentiation as assessed by Oil RedO staining (Figure 20A) and TG measurement (Figure 20B) as well as Western blot analysis of mitochondrial and adipogenic marker expression (Figure 20C). Interestingly, ODQ treatment could completely rescue the VASP$^{-/-}$ phenotype.

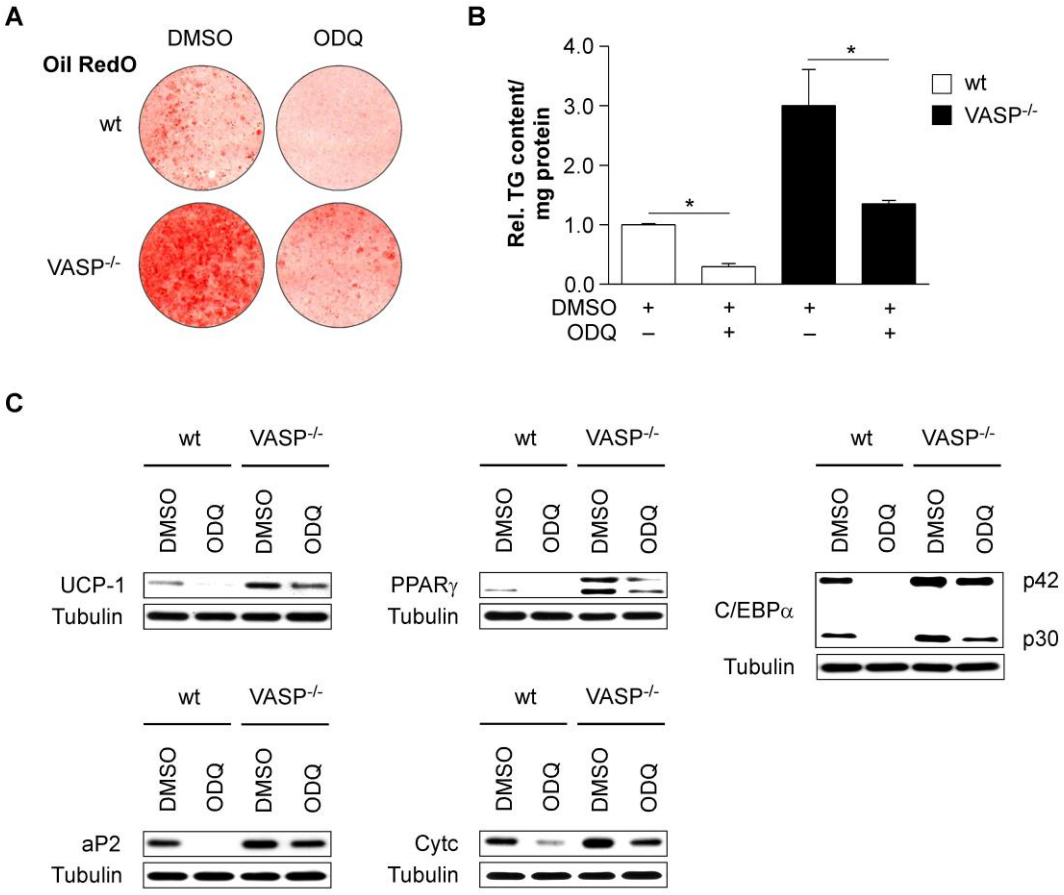

Figure 20: Rescue of the VASP$^{-/-}$ phenotype by inhibition of sGC using ODQ.
(A) Oil RedO staining of wt and VASP$^{-/-}$ cells on day 7 after treatment with 30 µM ODQ or vehicle (DMSO) during differentiation. ODQ was added, when the medium was replenished every second day. **(B)** TG content of differentiated wt and VASP$^{-/-}$ brown adipocytes on day 7 after treatment with ODQ during differentiation as indicated (n = 3 independent experiments). Data are represented as means ± SEM; * $p < 0.05$. **(C)** Western blot analysis of the fat cell markers C/EBPα, PPARγ and aP2 as well as the mitochondrial markers UCP-1 and Cytc in differentiated wt and VASP$^{-/-}$ brown adipocytes (day 7) after treatment with ODQ and vehicle, respectively.

3.2.4. Analysis of sGCβ1 promoter activity in VASP$^{-/-}$ cells

To investigate, whether the increased expression of sGCβ1 in VASP$^{-/-}$ cells is a result of enhanced promoter activity or increased mRNA stability, luciferase reporter assays were performed using a luciferase construct carrying 1.4 kb of the sGCβ1 5'-flanking region, which was shown to represent the sGCβ1 promoter (Sharina et al., 2000). The activity of the sGCβ1 promoter was increased in VASP$^{-/-}$ preadipocytes as well as in day 0 and day 2 cells (Figure 21A), which coincides with the elevated sGCβ1 protein levels in VASP$^{-/-}$ cells (Figure 19B). Because sGCβ1 expression is also controlled at the post-transcriptional level by the mRNA-binding protein human-antigen R (HuR) (Kloss et al., 2005), RQ-PCR analysis of HuR expression was performed, which revealed similar HuR expression in wt and VASP$^{-/-}$ preadipocytes (Figure 21B).

These data indicate that VASP$^{-/-}$ cells possess elevated amounts of sGCβ1 due to increased expression rather than increased mRNA stability.

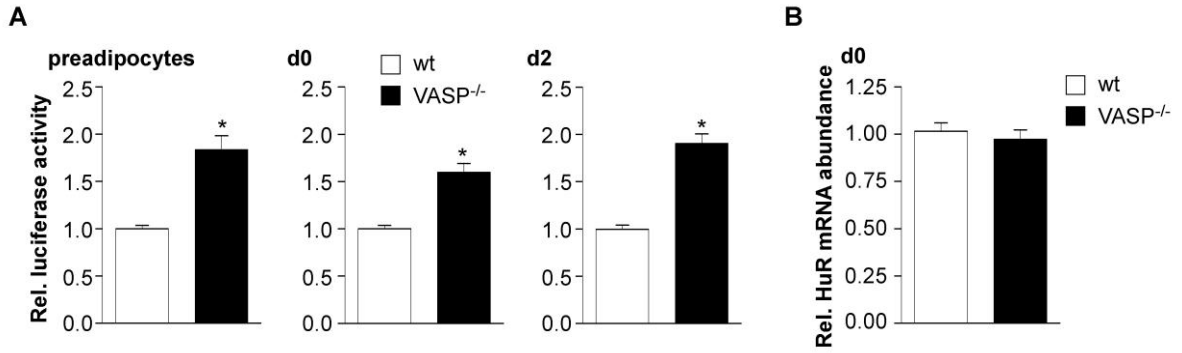

Figure 21: VASP$^{-/-}$ cells possessed an increased sGCβ1 promoter activity.
(A) Activity of the sGCβ1 promoter in wt and VASP$^{-/-}$ cells at different stages of differentiation. Luciferase reporter assays were accomplished with d0 and d2 cells as well as preadipocytes ($n \geq 3$ independent experiments). Data are represented as means ± SEM; * $p < 0.05$. **(B)** Abundance of HuR mRNA in wt and VASP$^{-/-}$ cells on day 0 as analyzed by RQ-PCR ($n = 3$ independent experiments). Data are represented as means ± SEM; * $p < 0.05$.

3.2.5. Rescue of altered cGMP signaling in VASP$^{-/-}$ cells by lentiviral restoration of VASP expression

To demonstrate that the observed alterations in cGMP signaling in VASP$^{-/-}$ cells were due to the loss of VASP, rescue experiments were performed using LV-VASP to restore VASP expression in knockout cells (see also Figure 17A and B). Indeed, VASP$^{-/-}$ cells transduced with LV-VASP possessed a significant reduction of cGMP content. Restoration of VASP reduced the cGMP concentration in VASP$^{-/-}$ cells to levels similar to those found in non-

infected wt cells (0.95 ± 0.19 fold compared to wt), whereas transduction with LV-cntr did not significantly affect cGMP levels (Figure 22A). Moreover, the expression of sGCβ1 was also rescued by restoration of VASP in VASP$^{-/-}$ cells as assessed by Western blot analysis (Figure 22B).

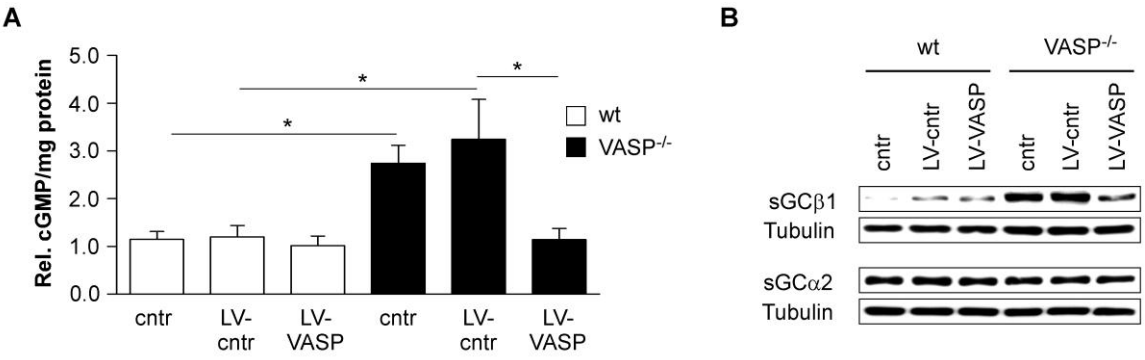

Figure 22: Rescue of increased cGMP content and elevated sGCβ1 expression in VASP$^{-/-}$ cells by restoration of VASP expression.

(A) Relative cGMP content of non-infected, LV-cntr and LV-VASP infected wt and VASP$^{-/-}$ cells on day 0 (n = 3 independent experiments). Data are represented as means ± SEM; * $p < 0.05$. **(B)** Western blot analysis of sGCβ1 and sGCα2 expression in wt and VASP$^{-/-}$ brown preadipocytes (day 0) rescued with LV-VASP.

3.3. Effects of VASP deficiency on Rho/ROCK and insulin signaling in brown preadipocytes

3.3.1. Analysis of RhoA activity in VASP$^{-/-}$ cells

VASP$^{-/-}$ cells displayed increased levels of cGMP compared to wt cells. It has previously been shown that cGMP exerts a positive effect on brown adipocyte differentiation via PKGI mediated inhibition of the RhoA/ROCK signaling cascade (Haas et al., 2009). Previous studies demonstrated that the activity of the small GTPase RhoA is negatively regulated by PKGI in brown adipocytes. PKGI phosphorylates RhoA at Ser188, thereby inhibiting its activation (Haas et al., 2009). As VASP$^{-/-}$ ablation resulted in an increased cGMP content, which would lead to an increased PKGI activity, RhoA phosphorylation at Ser188 was determined using a phosphorylation-specific antibody. Moreover, levels of active RhoA (RhoA-GTP) were measured using glutathione S-transferase (GST)-rhotekin immuno-precipitation assays. Compared to wt cells, RhoA phosphorylation at Ser188 was significantly increased in VASP$^{-/-}$ cells (Figure 23A). Correspondingly, VASP$^{-/-}$ cell exhibited reduced levels of RhoA-GTP (Figure 23B) indicating a reduced RhoA activity, which was shown to enhance adipogenic differentiation (Haas et al., 2009).

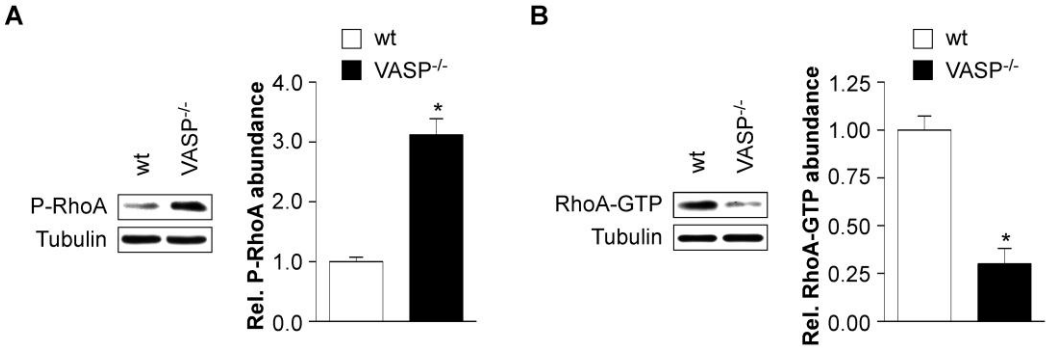

Figure 23: VASP$^{-/-}$ cells showed a decreased RhoA activity.
(A) Western blot analysis of RhoA phosphorylation at Ser188 (P-RhoA) in wt and VASP$^{-/-}$ preadipocytes (left). Densitometric analysis of P-RhoA abundance normalized to tubulin (n = 3 independent experiments) (right). Data are represented as means ± SEM; * $p < 0.05$. **(B)** Western blot analysis of GST-rhotekin immunoprecipitations of activated RhoA (RhoA-GTP) in wt and VASP$^{-/-}$ preadipocytes (left). Densitometric analysis of RhoA-GTP protein amount normalized to tubulin (n = 3 independent experiments) (right). Data are represented as means ± SEM; * $p < 0.05$.

3.3.2. Influence of VASP ablation on insulin signaling

The RhoA/ROCK pathway inhibits insulin signaling (Haas et al., 2009). Given a decreased RhoA activity in VASP$^{-/-}$ cells, the activity of Akt/Proteinkinase B, an important downstream target of the insulin signaling cascade (White and Kahn, 1994), was analyzed using a phosphorylation-specific antibody. Compared to wt cells, VASP$^{-/-}$ cells displayed a markedly increased amount of activated Akt (Figure 24) indicating enhanced insulin signaling in the absence of VASP.

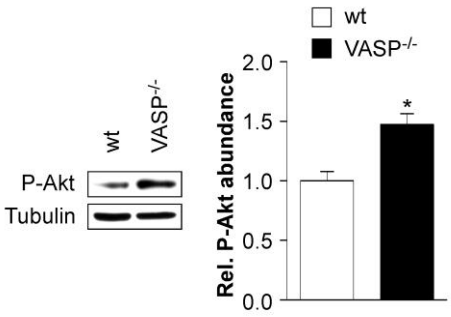

Figure 24: VASP ablation resulted in an increased Akt activation.
Western blot analysis of Akt phosphorylation at Ser473 (P-Akt) in wt and VASP$^{-/-}$ preadipocytes (left). Densitometric analysis of the amount of P-Akt normalized to tubulin (n = 3 independent experiments) (right). Data are represented as means ± SEM; * $p < 0.05$.

Taken together, increased cellular cGMP levels in the absence of VASP exerted an inhibitory effect on RhoA/ROCK signaling, thereby releasing the inhibition of the RhoA/ROCK cascade on insulin signaling.

3.4. Influence of VASP ablation on MAPK signaling

3.4.1. Analysis of Rac-1/PAK/MAPK signaling in VASP$^{-/-}$ cells

To clearify the mechanism, by which VASP ablation caused an increased adipogenic differentiation as well as an enhanced expression of sGCβ1 and increased cGMP levels in VASP$^{-/-}$ cells, downstream targets of VASP became the focus of interest. As already shown in Figure 10, VASP$^{-/-}$ preadipocytes, compared to wt cells, are highly spread. Previous studies have demonstrated that cell shape regulates lineage commitment in hMSCs (McBeath et al., 2004) and the small Rho-GTPase Rac-1 and its effector, the p21-activated kinase (PAK), are key regulators of cell spreading (Bishop and Hall, 2000; Kiosses et al., 1999; Price et al., 1998). Therefore, the activities of Rac-1 and PAK were investigated in VASP$^{-/-}$ and wt cells. Furthermore, also the activity of downstream targets of Rac-1 and PAK, namely cRaf and the MAPKs ERK1/2 and p38, was examined. The MAPK p38 was shown to be a central regulator of cAMP-dependent transcription of the UCP-1 gene (Cao et al., 2004) and it was demonstrated that the activation of the MEK/ERK signaling cascade promotes adipogenesis by enhancing PPARγ and C/EBPα gene expression during the differentiation of 3T3-L1 preadipocytes (Prusty et al., 2002).

Rac activation was determined by performing Rac immunoprecipitation assays. Immunoblots using the biotinylated Rac/Cdc42 binding (CRIB) motif of PAK to affinity precipitate activated Rac (GTP-Rac) revealed 1.28 ± 0.04 fold increased levels of GTP-Rac-1 in VASP$^{-/-}$ cells compared to wt cells on day -2 (Figure 25A and B). Moreover, Western blot analysis using phosphorylation-specific antibodies against PAK and the MAPKs of the downstream signaling cascade demonstrated a significantly increased abundance of activated PAK (P-PAK; 1.32 ± 0.08 fold), cRaf (P-cRaf; 1.38 ± 0.11 fold), ERK1/2 (P-ERK1/2; 1.46 ± 0.09 fold) and p38 (P-p38; 1.21 ± 0.02 fold) in VASP$^{-/-}$ cells on day -2 (Figure 25A and B). Statistically significant differences between wt and VASP$^{-/-}$ cells during later stages of differentiation (day 0 – day 7) were not observed.

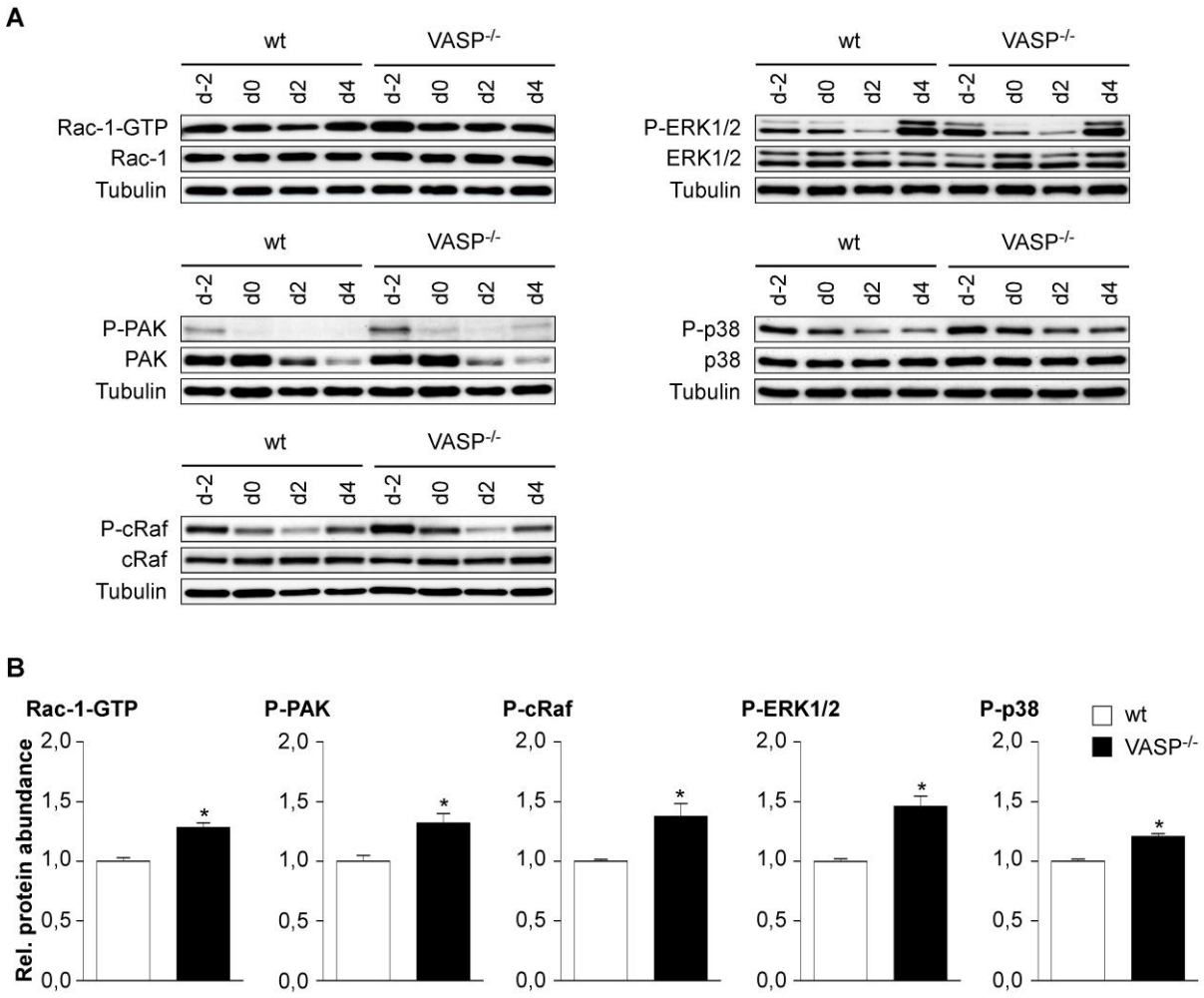

Figure 25: Increased Rac-1/PAK/MAPK signaling in VASP$^{-/-}$ preadipocytes.
(A) Western blot analysis of different components of the Rac-1/PAK/cRaf/ERK and p38 signaling cascades and their activation state (Rac-1-GTP, P-PAK, P-cRaf, P-ERK1/2, P-p38) using immunoprecipitation assays (Rac-1-GTP) and phosphorylation-specific antibodies in wt and VASP$^{-/-}$ preadipocytes at different stages of differentiation (day -2 to day 4; d-2, d0, d2, d4). **(B)** Densitometric analysis of Rac-1-GTP (immunoblot of biotinylated PAK-CRIB immunoprecipitation) and phosphorylated PAK (P-PAK), cRaf (P-cRaf), ERK1/2 (P-ERK1/2) and p38 (P-p38) on d-2 normalized to tubulin ($n \geq 3$ independent experiments). Data are represented as means ± SEM; * $p < 0.05$.

3.4.2. Consequences of modulation of Rac-1 signaling for sGCβ1 promoter activity in brown preadipocytes

The increased Rac-1/PAK/MAPK signaling and the enhanced sGCβ1 promoter activity and protein expression in VASP$^{-/-}$ preadipocytes raised the question, whether there is any correlation between these two observations. Therefore, Rac-1 mutants were used to enhance Rac-1 signaling in wt cells or suppress Rac-1 signaling in VASP$^{-/-}$ cells. Interestingly, lentiviral expression of the constitutively active mutant RacL61 (LV-RacL61) increased sGCβ1 promoter activity in wt cells by 31.6 ± 0.4 % compared to control vector infected (LV-

cntr) cells (Figure 26). Moreover, expression of the dominant negative mutant RacN17 (LV-RacN17) in VASP$^{-/-}$ cells decreased sGCβ1 promoter activity to levels similar to those found in LV-cntr infected wt cells (1.13 ± 0.10 fold higher) (Figure 26).

These data indicate that Rac-1 activity positively regulates sGCβ1 promoter activity. Therefore, increased Rac-1 activity in the absence of VASP can account for increased sGCβ1 expression and cGMP signaling in VASP$^{-/-}$ preadipocytes.

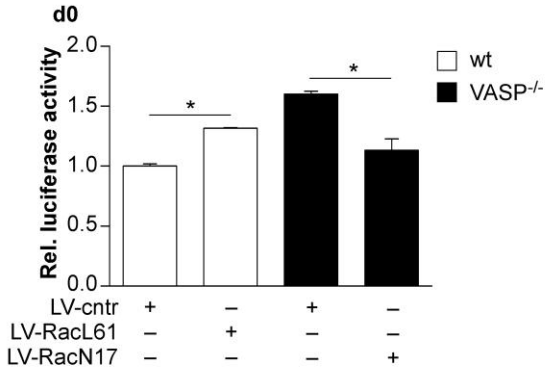

Figure 26: Modulation of Rac-1 signaling altered the activity of the sGCβ1 promoter in wt and VASP$^{-/-}$ cells.

Activity of the sGCβ1 promoter in LV-RacL61 infected wt cells and LV-RacN17 infected VASP$^{-/-}$ cells as well as LV-cntr transduced cells. Luciferase reporter assays were performed using d0 cells (n = 3 independent experiments). Data are represented as means ± SEM; * $p < 0.05$.

3.4.3. Role of the ERK1/2 activity in brown adipogenic differentiation

VASP$^{-/-}$ preadipocytes (day -2) exhibited an increased ERK1/2 activity. Previous studies using 3T3-L1 cells revealed that ERK has to be activated for the early proliferative step of white adipogenic differentiation (Sale et al., 1995). During later stages of differentiation ERK1/2 has to be shut-off to avoid PPARγ phosphorylation, which decreases its transcriptional activity and inhibits white adipogenesis (Camp and Tafuri, 1997; Hu et al., 1996). To investigate, whether the increased ERK1/2 activity in VASP$^{-/-}$ preadipocytes could serve as an additional explanation for the enhanced differentiation apart from the increased cGMP and insulin signaling, ERK1/2 activity was reduced in VASP$^{-/-}$ cells during early stages of differentiation (from day -3 to day 0) using the MEK inhibitor PD184161 (Figure 27A) and adipogenic differentiation was monitored. Interestingly, treatment with PD184161 was sufficient to rescue the knockout phenotype. Application of the MEK inhibitor for 3 days during early stages of differentiation resulted in a reduced lipid accumulation (Figure 27B)

and decreased adipogenic marker expression (Figure 27C) in differentiated VASP$^{-/-}$ adipocytes.

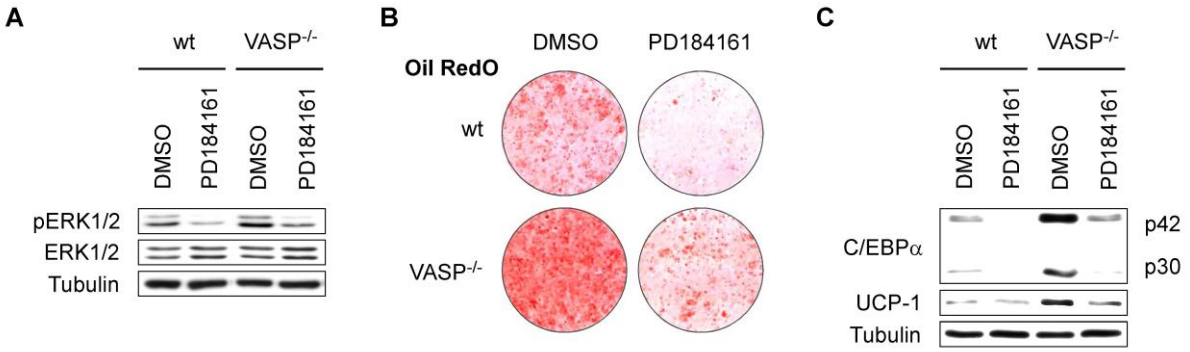

Figure 27: Inhibition of ERK1/2 activity by the MEK inhibitor PD184161 reduced adipogenic differentiation and rescued the VASP$^{-/-}$ phenotype.

(A) Western blot analysis of ERK1/2 activity (P-ERK1/2) in wt and VASP$^{-/-}$ preadipocytes incubated with 5 µM PD184161 or vehicle (DMSO) for 24 hours using a phosphorylation-specific antibody against ERK1/2. **(B)** Oil RedO staining of differentiated wt and VASP$^{-/-}$ cells, incubated with the MEK inhibitor PD184161 (5 µM) or vehicle from day -3 to day 0 (preadipocytes). **(C)** Western blot analysis of C/EBPα and UCP-1 expression in differentiated wt and VASP$^{-/-}$ brown adipocytes incubated with 5 µM PD184161 or vehicle from day -3 to day 0.

Moreover, the reduction of ERK1 expression and consequently, ERK1 activity in VASP$^{-/-}$ cells (Figure 28A) using a lentivirus carrying a small interfering ribonucleic acid (siRNA) against ERK1 (LV-siERK1) also reversed the VASP$^{-/-}$ phenotype and decreased lipid accumulation (Figure 28B) as well as adipogenic marker expression (Figure 28C) to levels similar to those found in wt cells infected with a lentivirus expressing a control siRNA (LV-sicntr).

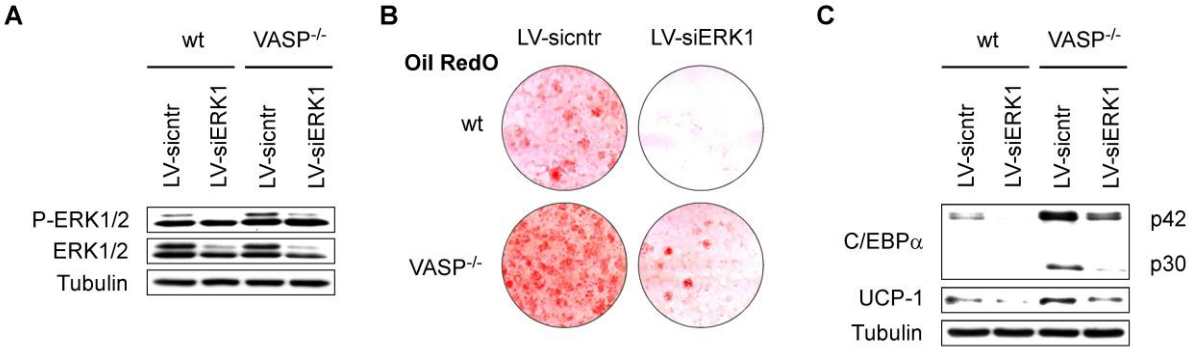

Figure 28: Inhibition of ERK1 expression by a siRNA against ERK1 reduced adipogenic differentiation and rescued the VASP$^{-/-}$ phenotype.

(A) Western blot analysis of ERK1/2 expression and phosphorylation in wt and VASP$^{-/-}$ preadipocytes 24 hours after transduction with a lentivirus expressing a siRNA against ERK1 (LV-siERK1) or a control siRNA (scrambled; LV-sicntr), respectively. **(B)** Oil RedO staining of differentiated wt and VASP$^{-/-}$ cells, infected with

LV-sicntr and LV-siERK1, respectively. **(C)** Western blot analysis of C/EBPα and UCP-1 expression in differentiated wt and VASP$^{-/-}$ brown adipocytes, transduced with LV-sicntr and LV-siERK1, respectively.

These data show that the observed phenotype in VASP$^{-/-}$ cells resulted from increased cGMP production due to an enhanced activation of Rac-1, which activates sGCβ1 expression. Elevated cGMP levels released the RhoA-mediated inhibition of insulin signaling by PKGI, which together with increased activity of the Rac-1 downstream effectors PAK, cRaf, ERK1/2 and p38 promoted brown adipogenesis.

3.5. Effects of VASP ablation on BAT morphology and function *in vivo*

3.5.1. Analysis of BAT morphology and adipogenic marker expression in VASP$^{-/-}$ mice

To investigate the role of VASP in BAT *in vivo*, male mice at the age of 4 - 5 weeks were used. BAT was resected from wt and VASP$^{-/-}$ littermates and compared in terms of tissue morphology as well as expression of brown adipogenic and mitochondrial markers. H/E stainings of paraffin sections revealed a similar appearance of BAT from wt and VASP$^{-/-}$ mice (Figure 29A). Furthermore, Western blot analysis of UCP-1, PGC-1α and Cytc expression yielded no statistically significant differences between both genotypes (Figure 29B).

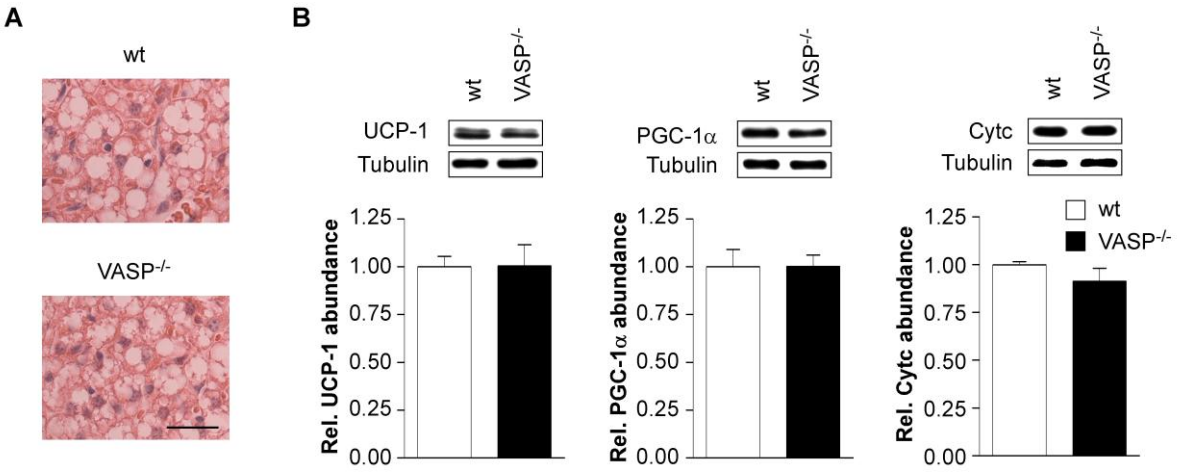

Figure 29: BAT from VASP$^{-/-}$ mice resembled tissue from wt mice in terms of morphology and marker expression.

(A) H/E staining of BAT, resected from 4 weeks old wt and VASP$^{-/-}$ male littermates; scale bar, 25µm. **(B)** Western blot analysis of UCP-1, PGC-1α and Cytc expression in BAT, resected from 4 - 5 weeks old wt and VASP$^{-/-}$ male littermates (upper panels). Densitometric analysis of the marker protein amount normalized to tubulin (n = 8 mice per genotype) (lower panels). Data are represented as means ± SEM; * $p < 0.05$.

3.5.2. Influence of VASP ablation on BAT morphology and function after activation of BAT thermogenesis by cold exposure

As the functional significance of BAT in mammals is the generation of heat by non-shivering thermogenesis as a defense against cold (Cannon and Nedergaard, 2004), the influence of VASP ablation on BAT morphology and function under cold exposure conditions was studied. Therefore, male littermatched mice at the age of 4 - 5 weeks were exposed to room temperature (RT) or 4°C, respectively, for 3 hours. To ensure a comparable feeding status, mice were fasted for 3 – 12 hours prior to (2.2.2.) and during RT and cold exposure.
In wt mice, cold exposure resulted in a reduction in the number and size of BAT lipid droplets (Figure 30A) as well as a decreased TG content (Figure 30B). However, this reduction was markedly enhanced in VASP$^{-/-}$ mice (Figure 30A and B).

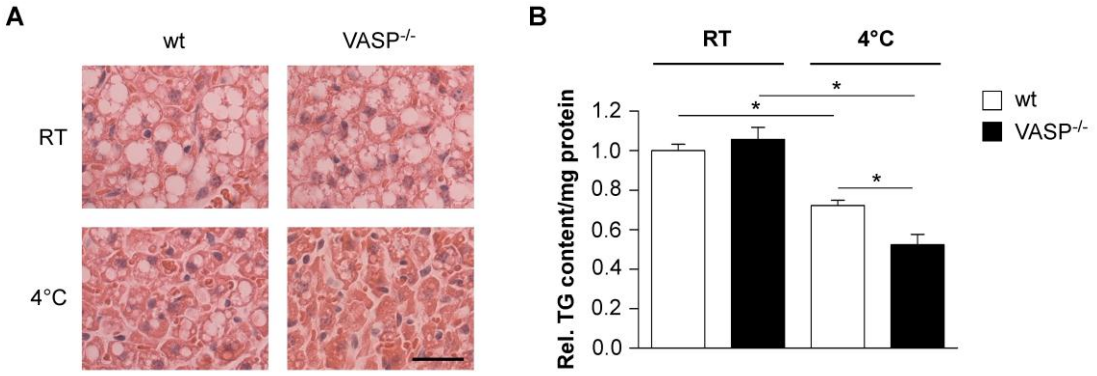

Figure 30: Cold exposure resulted in a markedly enhanced reduction of stored lipids in BAT from VASP$^{-/-}$ compared to wt mice.
(A) H/E staining of BAT, resected from 4 weeks old wt and VASP$^{-/-}$ male littermates, exposed to RT and 4°C, respectively; scale bar, 25µm. **(B)** TG content of BAT from 4 - 5 weeks old wt and VASP$^{-/-}$ mice, exposed to RT or 4°C, respectively (n = 5 mice per group). TG content was normalized to the protein content of the samples. Data are represented as mean ± SEM; * $p < 0.05$.

This increased reduction in lipid content in BAT from VASP$^{-/-}$ mice was reflected by a significantly enhanced mobilization of stored lipids in VASP$^{-/-}$ mice as assessed by measuring the lipolytic activity of the tissue (Figure 31A). Additionally, BAT from VASP$^{-/-}$ mice displayed an increased mitochondrial respiration after cold exposure (Figure 31B) indicating an enhanced metabolization of free fatty acids, released from intracellular TG stores by lipolysis. Interestingly, mitochondrial respiration in VASP$^{-/-}$ BAT was already enhanced under RT conditions (Figure 31B).

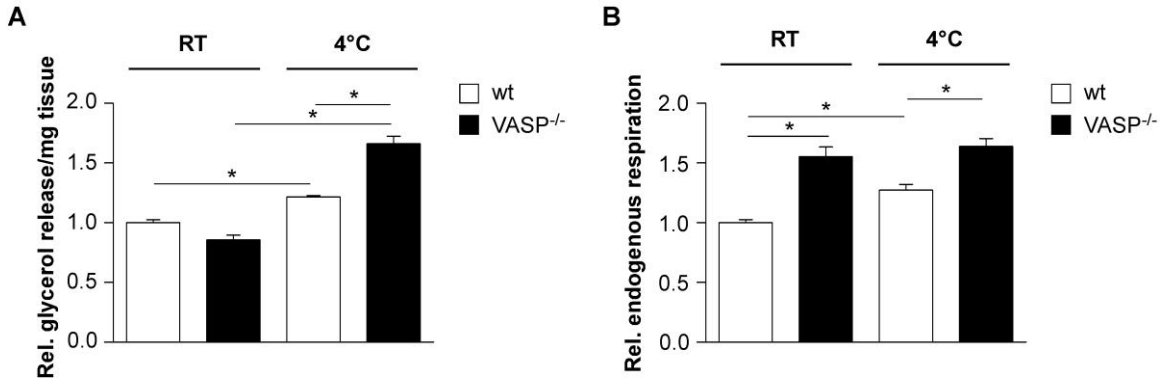

Figure 31: VASP ablation resulted in an increased lipolysis and mitochondrial respiration in BAT after cold exposure.

(A) Lipolytic activity of BAT from RT and 4°C exposed, 4 – 5 weeks old wt and VASP$^{-/-}$ male mice (littermates; n = 4 mice per group). Glycerol release was measured from resected and chopped brown fat pads and normalized to the wet weight of the tissue. Data are represented as means ± SEM; * $p < 0.05$. **(B)** Endogenous mitochondrial respiration in BAT from 4 – 5 weeks old, RT and 4°C exposed wt and VASP$^{-/-}$ male mice (n = 5 mice per group). Data are represented as means ± SEM; * $p < 0.05$.

Taken together, these results indicate an enhanced susceptibility of BAT from VASP$^{-/-}$ mice for being activated by cold, which leads to an increased thermogenesis in response to cold. To further substantiate this hypothesis, the induction of UCP-1 and PGC-1α gene expression by cold was determined in both genotypes using RQ-PCR analysis. In support of the previous results, cold exposure resulted in a markedly increased induction of the expression of both markers (Figure 32A and B).

To test, whether the enhanced activation of BAT thermogenesis in response to cold in VASP$^{-/-}$ mice is due to a difference in the expression of β3-ARs, which was observed in the *in vitro* cell cultures, Western blot analysis of β3-AR expression was accomplished. Compared to BAT from wt mice, VASP$^{-/-}$ BAT displayed a 1.21 ± 0.04 fold increase in β3-AR expression (Figure 32C), which can facilitate an enhance response to cold.

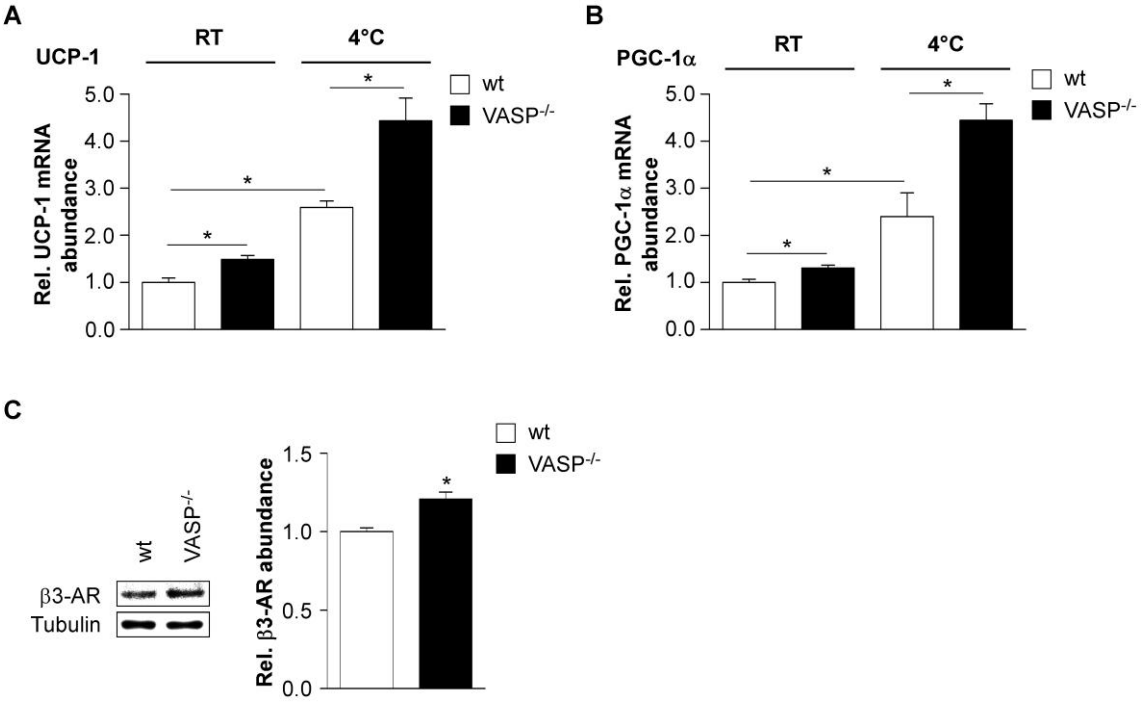

Figure 32: BAT from VASP$^{-/-}$ mice showed an increased susceptibility for activation by cold.
(A) Abundance of UCP-1 mRNA in BAT, resected from wt and VASP$^{-/-}$ mice, exposed to RT and 4°C, respectively, as analyzed by RQ-PCR (n = 4 mice per group). Data are represented as means ± SEM; * $p < 0.05$. **(B)** Abundance of PGC-1α mRNA in BAT, resected from wt and VASP$^{-/-}$ littermates, exposed to RT and 4°C, respectively, as analyzed by RQ-PCR (n = 4 mice per group). Data are represented as means ± SEM; * $p < 0.05$. **(C)** Western blot analysis of β3-AR expression in BAT from 4 - 5 weeks old wt and VASP$^{-/-}$ mice (left). Densitometric analysis of the β3-AR protein amount normalized to tubulin (n = 8 mice per genotype) (right). Data are represented as means + SEM; * $p < 0.05$.

Interestingly, VASP$^{-/-}$ mice also displayed a decreased body weight (Figure 33), which could be due to the differences in endogenous mitochondrial respiration, which were already detected in VASP$^{-/-}$ BAT under RT conditions (Figure 31B).

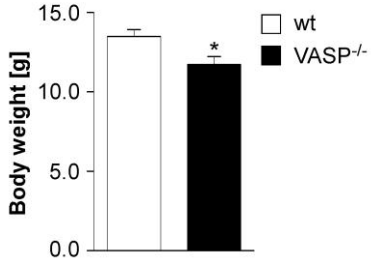

Figure 33: VASP$^{-/-}$ mice displayed a reduced body weight.
Body weight of 4 weeks old male wt and VASP$^{-/-}$ mice (n = 22 mice per genotype). Data are represented as means ± SEM; * $p < 0.05$.

Taken together, in line with the *in vitro* results, BAT of VASP$^{-/-}$ mice displayed an enhanced response to stimulation by cold as indicated by increased lipolysis and mitochondrial respiration. These phenomena were likely due to elevated β3-AR expression, which is also consistent with the results obtained from cultured VASP$^{-/-}$ cells.

4. Discussion

4.1. Role of cGMP/PKG signaling in brown adipogenic differentiation

The role of the cAMP/PKA signaling pathway as a major regulator of BAT thermogenesis is well characterized. The cAMP signaling cascade is activated by the sympathetic nervous system. Catecholamines stimulate β3-ARs resulting in an elevation of intracellular cAMP levels that activates PKA (Cannon and Nedergaard, 2004). PKA activation in BAT induces lipolysis (Cannon and Nedergaard, 2004) and UCP-1 expression, which is essential for the thermogenic function of BAT (Cao et al., 2004).

In addition, recent studies indicated that the NO/cGMP signaling cascade also plays an important role in BAT. NO was identified as a key regulator of BAT mitochondrial biogenesis through activation of cGMP-dependent mechanisms (Nisoli et al., 2003; Nisoli et al., 1998). Previous studies demonstrated that the NO/cGMP signaling cascade positively regulates BAT differentiation via PKGI (Haas et al., 2009). PKGI was shown to play a key role in BAT differentiation and function and was identified as an essential permissive factor of insulin signaling in BAT. Loss of PKGI results in the abrogation of cGMP signaling as well as insulin resistance and ultimately the suppression of BAT differentiation and function (Haas et al., 2009).

PKGs are serine/threonine kinases that mediate cGMP effects via phosphorylation of their substrates (Pfeifer et al., 1999). Several proteins have been identified as targets of PKGI phosphorylation including the small GTPase Rho (Sawada et al., 2001) and the IP_3 receptor-associated cGMP kinase substrate (IRAG) (Schlossmann et al., 2000). Moreover, the focal adhesion protein VASP is one of the major substrates of PKGI (Butt et al., 1994).

VASP is an actin binding protein (Huttelmaier et al., 1999) that was initially isolated from human platelets (Halbrugge and Walter, 1989). However, it is ubiquitously expressed with highest concentrations in platelets, lung, spleen, the gastrointestinal tract and blood vessels (Aszodi et al., 1999; Gambaryan et al., 2001).

VASP regulates cell motility in a variety of cells (Anderson et al., 2003; Bear et al., 2000; Garcia Arguinzonis et al., 2002; Goh et al., 2002) and is associated with highly dynamic membrane structures, focal adhesions and cell-cell-contacts in various cell types (Reinhard et al., 1992). Although VASP has been extensively studied in the context of the actin cytoskeleton, platelet aggregation and neural development, up to now, its role in adipose tissue and the differentiation of adipocytes is unknown. So far, only the influence of RhoA as an important target for PKG phosphorylation on BAT differentiation has been investigated.

RhoA phosphorylation by PKGI leads to an inhibition of ROCK. This inhibition of ROCK activity results in an increase in insulin signaling and enhancement of brown adipocyte differentiation. Therefore, PKGI positively regulates BAT differentiation by releasing the inhibition of RhoA on insulin signaling (Haas et al., 2009). Given the fact that besides RhoA VASP is a major substrate of PKG (Butt et al., 1994), the following scenarios for the influence of VASP on brown fat cell differentiation could be envisioned:

1) VASP is involved in the positive effect of PKGI on brown fat cell differentiation and mediates at least parts of this effect in parallel to the identified inhibition of RhoA/ROCK signaling (Haas et al., 2009). In this case, VASP ablation would result in a decreased adipogenic differentiation resembling the PKG knockout phenotype.
2) VASP does not play a role in brown adipogenic differentiation leading to an unaltered phenotype in VASP$^{-/-}$ cells and BAT.
3) VASP plays an unexpected role in BAT resulting in an increased adipogenic differentiation in the absence of VASP.

4.2. Loss of VASP results in an increased brown adipogenic differentiation and function

In contrast to the suppression of brown adipogenic differentiation in the absence of PKGI, ablation of VASP resulted in a markedly increased accumulation of lipids and expression of brown adipogenic markers. This phenotype was unexpected because VASP is one of the major substrates of PKGI (Butt et al., 1994). In addition, VASP$^{-/-}$ cells exhibited a highly spread phenotype compared to wt cells. Interestingly, it has previously been shown that cell shape regulates lineage commitment in hMSCs (McBeath et al., 2004). According to these studies, a highly spread phenotype should be associated with a decreased adipogenic differentiation. However, VASP$^{-/-}$ cells showed an increased TG accumulation and adipogenic marker expression.

Surprisingly, recent studies on PGC-1α-deficient cells revealed a differential regulation of brown fat cell differentiation (adipogenesis) and thermogenesis indicating two independent programs that drive mitochondrial biogenesis and adipogenesis in BAT (Uldry et al., 2006). Therefore, the development of the thermogenic program was also studied in VASP$^{-/-}$ adipocytes. Compared to wt cells, VASP$^{-/-}$ adipocytes showed a markedly increased expression of the thermogenic markers UCP-1 and PGC-1α. Correspondingly, analysis of

mature brown adipocyte function demonstrated an increased mitochondrial respiration and lipolytic activity due to an enhanced expression of all components of the β3-AR/cAMP/PKA/HSL signaling pathway, which regulates BAT thermogenesis (Cannon and Nedergaard, 2004). Taken together, these results show that the positive effect of VASP ablation is not confined to the induction of the adipogenic program but also entails an enhanced development of the thermogenic program.

Importantly, restoration of VASP in VASP$^{-/-}$ cells provided evidence that the observed phenotype was indeed attributed to the loss of VASP rather than representing a cell cultural artefact.

In addition, results presented in this thesis could show that in contrast to human white adipocytes and similar to rodent white adipocytes (Langin, 2010; Sengenes et al., 2003), lipolysis was not regulated by intracellular cGMP levels in murine brown fat cells. This is very likely due to the fact that in murine brown adipocytes, HSL phosphorylation was not stimulated by PKG activation. These findings indicate a differential role of cGMP in the regulation of brown fat cell function in different species.

4.3. Ablation of VASP enhances cGMP and insulin signaling

Investigating the mechanism underlying an increased brown adipogenic differentiation in VASP$^{-/-}$ cells, unravelled an enhanced cGMP signaling in the absence of VASP. Interestingly, VASP$^{-/-}$ cells exhibited increased cGMP levels whereas cAMP content was not altered. Intracellular cGMP levels are regulated by cGMP-producing as well as cyclic nucleotide-hydrolyzing enzymes (PDEs).

Analyzing the expression and activity of the NO/cGMP signaling cascade upstream of cGMP revealed that the elevated cGMP levels in VASP$^{-/-}$ cells were due to an increased expression of the cGMP producing enzyme sGC. The possibility that the observed elevated cGMP levels resulted from a decreased cGMP breakdown by PDEs rather than an increased cGMP generation is relatively unlikely for various reasons:

1) The expression of PDE5, which is the only cGMP-specific PDE, detected in brown (pre)adipocytes, was unaltered in VASP$^{-/-}$ cells (unpublished data).
2) Elevated cGMP levels were not only detected in preadipocytes but also 2 days after induction of adipogenic differentiation using a combination of different adipogenic substances including IBMX. IBMX is a non-specific PDE inhibitor. However,

differences in cGMP levels between wt and VASP$^{-/-}$ cells were still detectable after application of IBMX.

3) Treatment with the NO donor and sGC activator DEA-NO caused a markedly increased response (elevation of cGMP content) in VASP$^{-/-}$ cells compared to wt cells indicating an increased expression of sGC.
4) Inhibition of sGC by the selective inhibitor ODQ rescued the VASP$^{-/-}$ phenotype.

Thus, the observed increase in sGC expression is very likely the major reason for the enhanced cGMP signaling in VASP$^{-/-}$ cells. Interestingly, VASP$^{-/-}$ cells exhibited only an elevation of the promoter activity and protein amount of the sGCβ1 subunit.

Mammalian sGCs are heterodimers consisting of two different subunits, termed sGCα and sGCβ. Two different isoforms of the α subunit have been identified – sGCα1 and sGCα2 – giving rise to the following heterodimers: sGCα1β1 and sGCα2β1, which do not possess any differences in catalytic activity or substrate affinity (Friebe and Koesling, 2003). Except in brain, sGCα1 is the major occurring α subunit in a variety of tissues (Mergia et al., 2003). Surprisingly, sGCα1 was not detected in brown preadipocytes pointing to sGCα2β1 as the major heterodimer combination in these cells. However, VASP$^{-/-}$ cells displayed only an increase in sGCβ1 expression without any alterations of sGCα2 levels that was sufficient to increase intracellular cGMP levels as shown by lentiviral overexpression of sGCβ1. These results indicate that the sGCβ1 subunit represents the limiting factor in the assembly of catalytically active sGC heterodimers in brown preadipocytes whereas there seems to be a higher availability of sGCα2. It has previously been shown that both subunits can be regulated independently (Chen et al., 2000). Moreover, it was demonstrated that the sGC subunits do not only undergo heterodimerization but also form homodimers. These homodimeric complexes are catalytically inactive (Andreopoulos and Papapetropoulos, 2000). Evidence has been provided that upon coexpression of sGCα and sGCβ subunits, heterodimers are preferentially formed while homodimers are still detectable (Zabel et al., 1999). These observations suggest that brown preadipocytes could possess an excess expression of sGCα2, probably resulting in an increased formation of homodimers, with the sGCβ1 expression representing the limiting factor of the formation of catalytically active heterodimers. In this case an increase in sGCβ1 expression alone would indeed be sufficient to increase cellular cGMP levels like observed in VASP$^{-/-}$ cells.

Enhanced cGMP signaling in VASP$^{-/-}$ cells should lead to an activation of PKGI, which in turn should result in an increased phosphorylation of RhoA. Previous studies in smooth

muscle cells revealed that phosphorylation of RhoA at Ser188 by PKGI induces translocation from the membrane to the cytosol and thereby, inactivation of RhoA (Sawada et al., 2001). Analysis of RhoA phosphorylation and RhoA-GTP levels using rhotekin immunoprecipitation assays for the detection of active GTP-bound RhoA showed a decreased RhoA activity in $VASP^{-/-}$ cell verifying the activation of PKGI due to elevated cGMP levels in the absence of VASP. These results can account for the enhanced brown adipogenic differentiation in $VASP^{-/-}$ cells as previous studies in MEFs demonstrated that reduced RhoA activity favors adipogenesis whereas increased RhoA activity favors myogenesis (Sordella et al., 2003). Moreover, it was shown that dominant negative RhoA commits hMSCs to become adipocytes while constitutively active RhoA causes osteogenesis regardless of cell spreading (McBeath et al., 2004). In brown preadipocytes, RhoA/ROCK signaling has been shown to negatively regulate insulin signaling (Haas et al., 2009). In line with all these studies, increased cGMP levels and therefore, reduced RhoA activity in $VASP^{-/-}$ cells led to enhanced insulin signaling as indicated by an increased Akt activity.

Taken together, elevated cGMP levels in the absence of VASP exerted an inhibitory effect on RhoA/ROCK signaling thereby releasing the inhibition of the RhoA/ROCK cascade on insulin signaling. These findings are in line with the previously published positive influence of cGMP on brown adipogenic differentiation (Nisoli et al., 2003) via activation of PKGI (Haas et al., 2009) and can provide an explanation for the enhanced development of the adipogenic and thermogenic program in $VASP^{-/-}$ cells.

4.4. Loss of VASP causes an increased MAPK signaling in preadipocytes

The small Rho-GTPase Rac-1 and its effector PAK are key regulators of cell spreading (Bishop and Hall, 2000; Kiosses et al., 1999; Price et al., 1998). As $VASP^{-/-}$ cells exhibited a highly spread phenotype, Rac-1 and PAK activity in the absence of VASP were determined. Indeed, $VASP^{-/-}$ cells showed an increased amount of activated GTP-bound Rac-1 and phosphorylated PAK, but only in preadipocytes and not during later stages of differentiation. These results are consistent with the reported observations in $VASP^{-/-}$ MEFs (Garcia Arguinzonis et al., 2002).

PAK is implicated in a variety of cellular functions such as the activiation of MAPK pathways (Brown et al., 1996; Frost et al., 1996; Zhang et al., 1995), which have been demonstrated to play a role in white adipogenic differentiation (Bost et al., 2005a). PAK can activate the MAPK p38 (Zhang et al., 1995) and Raf leading to an activation of MEKs and subsequently

the MAPKs ERK1/2 (Maruta et al., 2003). Interestingly, analysis of cRaf, ERK1/2 and p38 activity revealed an increased activation of all these kinases in VASP$^{-/-}$ cells, but only in preadipocytes and not during later stages of differentiation, which is consistent with the previously mentioned observations regarding the activity of Rac-1 and PAK in VASP$^{-/-}$ preadipocytes.

Several studies have analyzed the role of MAPKs in white adipogenic differentiation. Although the available data are contradictory, there is one consensus scenario: ERKs are necessary for the initial proliferative step of adipogenic differentiation. Thereafter, the signal transduction pathway needs to be shut-off to proceed with adipocyte maturation (Bost et al., 2005a). This temporal regulation of ERK activity is probably also required in brown adipogenesis, as VASP$^{-/-}$ cells showed an increased activation of the Rac-1/PAK/cRaf/ERK1/2 signaling cascade exclusively in early stages of differentiation. Moreover, inhibition of ERK1/2 activity by the MEK inhibitor PD184161 during these early stages of differentiation rescued the VASP$^{-/-}$ phenotype. The observation that a permanent activation of the Raf/MEK/ERK signaling cascade by constitutively active Ras completely blocks brown adipogenesis (Murholm et al., 2010), further substantiates the hypothesis of the necessity of a timely regulated ERK activity during the differentiation of brown adipocytes. Interestingly, downregulation of ERK1 but not ERK2 in VASP$^{-/-}$ cells also rescued the knockout phenotype indicating that ERK1 but not ERK2 is essential for brown adipogenic differentiation. Data arising from the analysis of ERK1 knockout mice further reinforce distinct biological functions of ERK1 and ERK2 (Bost et al., 2005a). Preadipocytes isolated from these ERK1 knockout mice exhibit impaired adipogenesis and an inhibitor of the ERK pathway does not affect the residual adipogenesis of these cells suggesting that ERK2 is not implicated in adipocyte differentiation (Bost et al., 2005b).

Taken together, the increased adipogenic differentiation in VASP$^{-/-}$ cells – apart from the enhanced cGMP and insulin signaling – also seems to be attributed to an increased activation of the Rac-1/PAK/cRaf/ERK signaling pathway. This effect is very likely due to an enhancement or acceleration of the initial proliferative step of adipogenic differentiation and to an increased expression of the crucial adipogenic regulators PPARγ and C/EBPs by activated ERK, which was reported for white adipogenesis (Prusty et al., 2002). An enhanced ERK signaling in VASP$^{-/-}$ cells was not observed during later stages of differentiation.

Moreover, the increased activity of p38 exclusively in VASP$^{-/-}$ preadipocytes indicates also a timely regulated activity of p38 during brown adipogenic differentiation. Similar to ERK, the influence of p38 on white adipocyte differentiation has extensively been studied in 3T3-L1

cells. Similar to the ERK pathway, opposing roles are described for p38 in white adipogenesis. But although controversially discussed, a positive effect of p38 during early stages of differentiation in 3T3-L1 cells seems to be the commonly accepted consensus (Bost et al., 2005a). Furthermore, studies in brown adipocytes revealed that p38 activates as well as increases the expression of PGC-1α, which activates UCP-1 transcription and therefore, enhances the mitochondrial thermogenic capability (Cao et al., 2004).

In summary, the increased adipogenic differentiation in VASP$^{-/-}$ cells seems to be attributed to an increased activation of the Rac/PAK/cRaf/ERK and Rac/PAK/p38 signaling pathways in early stages of differentiation as well as to an enhanced cGMP and insulin signaling in the absence of VASP.

4.5. The role of VASP in BAT *in vivo*

The phenotype of VASP$^{-/-}$ mice is well characterized (Aszodi et al., 1999). VASP$^{-/-}$ mice are viable and fertile and were reported to have no obvious physical abnormalities. Agonist-induced smooth muscle contractility and cyclic nucleotide-dependent smooth muscle relaxation are not affected in intestinal and vascular smooth muscle of VASP$^{-/-}$ mice showing that VASP is not essential in the regulation of the smooth muscle tone. However, cAMP- and cGMP-mediated inhibition of platelet aggregation is significantly reduced (Aszodi et al., 1999).

VASP is expressed in a variety of tissues including BAT. But up to now the role of VASP in BAT was not investigated. Interestingly, the *in vivo* studies presented in this thesis revealed a reduced body weight in VASP$^{-/-}$ mice, which could be due to an increased endogenous mitochondrial respiration resulting in an increased energy expenditure. However, tissue histology and TG content were not altered in VASP$^{-/-}$ mice suggesting a potential compensation of elevated energy requirements of VASP$^{-/-}$ BAT by increased food intake or utilization of other energy stores like WAT.

In mammals, BAT is responsible for non-shivering thermogenesis as a defense against cold (Cannon and Nedergaard, 2004). Therefore, mice were exposed to cold to investigate the role of VASP in highly activated BAT. In response to cold activation, BAT of VASP$^{-/-}$ mice displayed a decreased lipid content as well as an increased lipolysis and endogenous respiration compared to wt tissue. These results indicate an enhanced thermogenesis resulting in an increased consumption of intracellular lipid stores. Moreover, the induction of UCP-1 and PGC-1α expression was markedly increased in VASP$^{-/-}$ mice after cold exposure poiting

to an enhanced activation of BAT. This is most likely due to an increased expression of β3-ARs, which mediate the cold response in BAT (Cannon and Nedergaard, 2004). The elevated β3-AR expression and endogenous respiration is in line with the observed effects of VASP ablation in the *in vitro* cell cultures.

Taken together, these results indicate an enhanced susceptibility of BAT from $VASP^{-/-}$ mice for activation by cold leading to an increased thermogenesis in response to cold.

4.6. A novel negative feedback loop for the regulation of cellular cGMP concentration via VASP and Rac-1

To investigate, whether there is any correlation between increased Rac-1/MAPK and enhanced cGMP signaling in $VASP^{-/-}$ cells, Rac activity was modulated using dominant negative and constitutively active Rac mutants. Interestingly, downregulation of Rac-1 activity in $VASP^{-/-}$ cells rescued the knockout phenotype, whereas activation of Rac-1 in wt cells mimicked the knockout phenotype regarding sGC expression. These findings link the regulation of Rac-1 activity by VASP to the control of cellular cGMP content. Taken together, the increased adipogenic differentiation in $VASP^{-/-}$ cells seems to be due to a Rac-1-mediated enhancement of MAPK signaling in early stages of differentiation and to a Rac-1-mediated increase in cGMP and subsequently insulin signaling (Figure 34).

In conclusion, this thesis reveals different signaling cascades and the crosstalk between these pathways, by which VASP regulates brown adipogenic differentiation and thermogenesis. Moreover, a novel signaling pathway was uncovered linking VASP and the control of cellular cGMP levels via Rac-1-dependent regulation of sGC expression (Figure 34). The VASP/Rac-1/sGC axis is independent from the previously described stimulation of transmembrane pGCs by Rac, which is mediated by direct activation via PAK (Guo et al., 2007), and constitutes a previously undescribed negative feedback loop for the regulation of cellular cGMP levels. However, the mechanism, by which Rac-1 activates the sGC promoter, still has to be investigated. Rac-1 activates a variety of downstream effector proteins including MAPKs (Bishop and Hall, 2000), which can regulate gene expression and could potentially be involved in the regulation of sGC promoter activity and sGC expression.

Given the positive role of NO/sGC/cGMP signaling in controlling energy balance (Haas et al., 2009; Nisoli et al., 2003; Nisoli et al., 2004) and the fact that obesity has reached pandemic dimensions with more than half a billion adults worldwide affected (Finucane et al.), the VASP/Rac/sGC pathway might be a potential target for novel therapeutic approaches directed

at cellular energy expenditure. Furthermore, VASP/Rac-1-mediated control of sGC expression and cGMP levels occurs also in other cell types (unpublished data) and could be a general mechanism for the control of cellular cGMP concentrations.

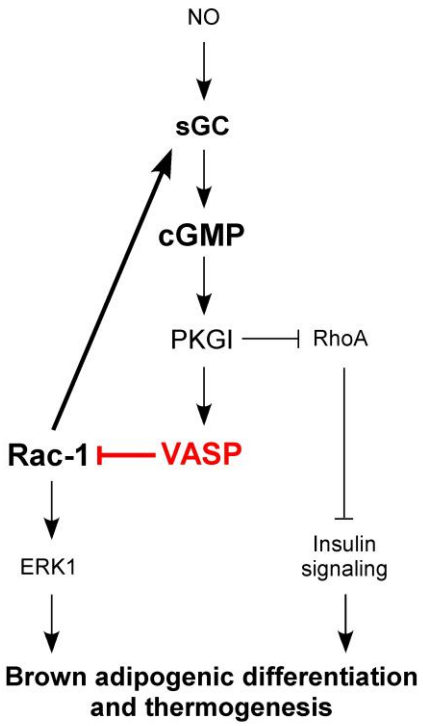

Figure 34: Scheme of the signaling pathways involved in the regulation of brown adipogenic differentiation and thermogenesis by VASP showing the novel feedback loop for the regulation of cellular cGMP concentrations.

Depicted is the crosstalk between VASP, Rac and MAPK signaling as well as the feedback loop, by which VASP regulates cGMP and insulin signaling via Rac-1.

5. Summary

BAT is a unique organ in mammals. It dissipates energy to produce heat as a defense against cold in neonates. Cold-induced thermogenesis is mediated via β3-adrenergic stimulation by the sympathetic nervous system resulting in increased cAMP levels. Recently, the NO/cGMP signaling cascade, which plays an important role in a variety of physiological processes such as smooth muscle relaxation (Hofmann et al., 2000; Lincoln, 1989), inhibition of platelet aggregation (Mellion et al., 1981; Schwarz et al., 2001) and modulation of synaptic transmission (Garthwaite et al., 1988; O'Dell et al., 1991; Zhuo and Hawkins, 1995), was identified as a key regulator of BAT differentiation and function (Haas et al., 2009; Nisoli et al., 2003).

cGMP exerts its influence on various cell functions via three different receptors: PDEs (Sonnenburg and Beavo, 1994), CNG channels (Biel et al., 1999) and PKGs (Pfeifer et al., 1999). Recently it has been shown that the positive effect of cGMP on BAT development is mediated via PKGI (Haas et al., 2009). These studies revealed that PKGI is an essential permissive factor for insulin signaling in BAT and ablation of PKGI results in the abrogation of cGMP signaling as well as insulin resistance and ultimately the suppression of BAT differentiation and function (Haas et al., 2009).

One of the major substrates of PKGI is VASP (Butt et al., 1994). Data presented in this study identify the role of VASP in brown adipogenic differentiation and function. Surprisingly, in contrast to the impairment of differentiation in the absence of PKGI, deletion of VASP promoted adipogenic differentiation. $VASP^{-/-}$ adipocytes exhibited an increased expression of adipogenic markers and lipid accumulation as well as an enhanced development of the brown fat-specific thermogenic program. Moreover, functional analysis revealed increased lipolysis and mitochondrial respiration in $VASP^{-/-}$ adipocytes.

Analysis of the mechanisms underlying the enhanced differentiation and function of $VASP^{-/-}$ brown adipocytes identified a novel feedback loop facilitating the regulation of cellular cGMP concentrations. This process was mediated by the small Rho-GTPase Rac. VASP ablation resulted in an increased activity of Rac-1, which positively regulated the expression of sGC. This enzyme is responsible for cellular cGMP production. Mechanistically, Rac-1 activated the sGC promoter resulting in an increased sGC expression and cGMP concentration in the absence of VASP. This novel VASP/Rac-1/cGMP signaling pathway constitutes a previously unknown negative feedback loop of the cGMP signaling cascade.

Interestingly, recent studies demonstrated that cGMP stimulates BAT differentiation and function via the enhancement of insulin signaling mediated by inhibition of the RhoA/ROCK signaling pathway (Haas et al., 2009). In line with these findings, $VASP^{-/-}$ cells exhibited a decreased RhoA activity, which led to an increased insulin signaling as a consequence of elevated cellular cGMP levels.

Moreover, VASP ablation resulted in an enhancement of Rac-1/PAK/cRaf/ERK1/2 and Rac-1/PAK/p38 signaling in preadipocytes, which in addition to increased cellular cGMP levels stimulated brown adipogenic differentiation.

In vivo, BAT of $VASP^{-/-}$ mice displayed an enhanced response to cold stimulation as indicated by an increased lipolysis and mitochondrial respiration due to an elevated β3-AR expression, which was consistent with the *in vitro* results in cultured $VASP^{-/-}$ cells. As β3-ARs mediate thermogenesis in BAT (Cannon and Nedergaard, 2004), increased receptor expression can account for an increased susceptibility for cold activation.

Taken together, these findings demonstrate an enhanced brown adipocyte differentiation and function in the absence of VASP. Moreover, a novel feedback loop was identified linking the focal adhesion protein VASP with the regulation of cellular cGMP levels via Rac, thereby controlling the cGMP signaling pathway and its downstream targets. Given the importance of the cGMP signaling cascade in a variety of physiological and pathophysiological processes, for example in the cardiovascular and nervous system, the VASP/Rac/sGC pathway might be a potential target for novel therapeutic approaches. One example could be the development of novel strategies directed against obesity, especially as not only newborns but also adult humans possess metabolically active BAT (Cypess et al., 2009; Nedergaard et al., 2007; van Marken Lichtenbelt et al., 2009; Virtanen et al., 2009).

6. Publications and Abstracts

6.1. Publications

Parts of the results of this thesis were compiled to a manuscript and submitted for publication (see below).

Jennissen K, Hermann M, Kunz WS, Fässler R, Pfeifer A (2011).
VASP controls cGMP production and adipocyte differentiation.
Submitted

Haas B, Mayer P*, **Jennissen K***, Scholz D, Diaz MB, Bloch W, Herzig S, Fässler R, Pfeifer A (2009).
Protein kinase G controls brown fat cell differentiation and mitochondrial biogenesis.
Sci Signal. 2009 Dec 1;2(99):ra78.

Karram K, Goebbels S, Schwab M, **Jennissen K**, Seifert G, Steinhäuser C, Nave KA, Trotter J (2008).
NG2-expressing cells in the nervous system revealed by the NG2-EYFP-knockin mouse.
Genesis. 2008 Dec;46(12):743-57.

* equally contributed

6.2. Abstracts

Jennissen K, Haas B, Kunz WS, Pfeifer A (2011).
cGMP and cAMP differentially regulate differentiation and function of brown adipocytes.
5th International Conference on cGMP – cGMP: Generators, Effectors and Therapeutic Implications, Halle, 2011.

Jennissen K, Haas B, Kunz WS, Pfeifer A (2011).
Differential regulation of differentiation and activation of brown adipocytes by cAMP and cGMP.
77th Annual Meeting of the German Society for Experimental and Clinical Pharmacology and Toxicology, Frankfurt, 2011.

Jennissen K, Haas B, Kipschull S, Mayer P, Pfeifer A (2010).
NO/cGMP regulates brown fat differentiation through protein kinase G.
ICO Procongress Meeting – Brown Adipose Tissue and Human Obesity, Stockholm, 2010.

Haas B, **Jennissen K**, Mayer P, Pfeifer A (2010).
Protein kinase G regulates mitochondrial biogenesis and differentiation of brown adipocytes via inhibition of the RhoA/ROCK pathway.
16th World Congress of Basic and Clinical Pharmacology (WorldPharma2010), Copenhagen, 2010.

Jennissen K, Hermann M, Haas B, Pfeifer A (2009).
Role of Vasodilator-Stimulated Phosphoprotein (VASP) in mesenchymal stem cell differentiation.
Internation Symposium, DFG Research Training Group (GRK677), Bonn, 2009.

Jennissen K, Seifert G, Steinhäuser C (2007).
Functional and molecular heterogeneity of 'complex' glial cells in the hippocampus.
7th Göttingen Meeting of the German Neuroscience Society, Göttingen, 2007.

7. References

Anderson, S.I., Behrendt, B., Machesky, L.M., Insall, R.H., and Nash, G.B. (2003). Linked regulation of motility and integrin function in activated migrating neutrophils revealed by interference in remodelling of the cytoskeleton. Cell Motil Cytoskeleton *54*, 135-146.

Andreopoulos, S., and Papapetropoulos, A. (2000). Molecular aspects of soluble guanylyl cyclase regulation. Gen Pharmacol *34*, 147-157.

Aszodi, A., Pfeifer, A., Ahmad, M., Glauner, M., Zhou, X.H., Ny, L., Andersson, K.E., Kehrel, B., Offermanns, S., and Fassler, R. (1999). The vasodilator-stimulated phosphoprotein (VASP) is involved in cGMP- and cAMP-mediated inhibition of agonist-induced platelet aggregation, but is dispensable for smooth muscle function. EMBO J *18*, 37-48.

Bachmann, C., Fischer, L., Walter, U., and Reinhard, M. (1999). The EVH2 domain of the vasodilator-stimulated phosphoprotein mediates tetramerization, F-actin binding, and actin bundle formation. J Biol Chem *274*, 23549-23557.

Baksh, D., Song, L., and Tuan, R.S. (2004). Adult mesenchymal stem cells: characterization, differentiation, and application in cell and gene therapy. J Cell Mol Med *8*, 301-316.

Bear, J.E., Loureiro, J.J., Libova, I., Fassler, R., Wehland, J., and Gertler, F.B. (2000). Negative regulation of fibroblast motility by Ena/VASP proteins. Cell *101*, 717-728.

Bear, J.E., Svitkina, T.M., Krause, M., Schafer, D.A., Loureiro, J.J., Strasser, G.A., Maly, I.V., Chaga, O.Y., Cooper, J.A., Borisy, G.G., *et al.* (2002). Antagonism between Ena/VASP proteins and actin filament capping regulates fibroblast motility. Cell *109*, 509-521.

Bieback, K., Kern, S., Kluter, H., and Eichler, H. (2004). Critical parameters for the isolation of mesenchymal stem cells from umbilical cord blood. Stem Cells *22*, 625-634.

Biel, M., Zong, X., Ludwig, A., Sautter, A., and Hofmann, F. (1999). Structure and function of cyclic nucleotide-gated channels. Rev Physiol Biochem Pharmacol *135*, 151-171.

Bishop, A.L., and Hall, A. (2000). Rho GTPases and their effector proteins. Biochem J *348 Pt 2*, 241-255.

Bost, F., Aouadi, M., Caron, L., and Binetruy, B. (2005a). The role of MAPKs in adipocyte differentiation and obesity. Biochimie *87*, 51-56.

Bost, F., Aouadi, M., Caron, L., Even, P., Belmonte, N., Prot, M., Dani, C., Hofman, P., Pages, G., Pouyssegur, J., *et al.* (2005b). The extracellular signal-regulated kinase isoform ERK1 is specifically required for in vitro and in vivo adipogenesis. Diabetes *54*, 402-411.

Bradford, M.M. (1976). A rapid and sensitive method for the quantitation of microgram quantities of protein utilizing the principle of protein-dye binding. Anal Biochem *72*, 248-254.

Brown, J.L., Stowers, L., Baer, M., Trejo, J., Coughlin, S., and Chant, J. (1996). Human Ste20 homologue hPAK1 links GTPases to the JNK MAP kinase pathway. Curr Biol *6*, 598-605.

Butt, E., Abel, K., Krieger, M., Palm, D., Hoppe, V., Hoppe, J., and Walter, U. (1994). cAMP- and cGMP-dependent protein kinase phosphorylation sites of the focal adhesion vasodilator-stimulated phosphoprotein (VASP) in vitro and in intact human platelets. J Biol Chem *269*, 14509-14517.

Camp, H.S., and Tafuri, S.R. (1997). Regulation of peroxisome proliferator-activated receptor gamma activity by mitogen-activated protein kinase. J Biol Chem *272*, 10811-10816.

Campagnoli, C., Roberts, I.A., Kumar, S., Bennett, P.R., Bellantuono, I., and Fisk, N.M. (2001). Identification of mesenchymal stem/progenitor cells in human first-trimester fetal blood, liver, and bone marrow. Blood *98*, 2396-2402.

Cannon, B., and Nedergaard, J. (1996). Adrenergic regulation of brown adipocyte differentiation. Biochem Soc Trans *24*, 407-412.

Cannon, B., and Nedergaard, J. (2004). Brown adipose tissue: function and physiological significance. Physiol Rev *84*, 277-359.

Cao, W., Daniel, K.W., Robidoux, J., Puigserver, P., Medvedev, A.V., Bai, X., Floering, L.M., Spiegelman, B.M., and Collins, S. (2004). p38 mitogen-activated protein kinase is the central regulator of cyclic AMP-dependent transcription of the brown fat uncoupling protein 1 gene. Mol Cell Biol *24*, 3057-3067.

Chakraborty, T., Ebel, F., Domann, E., Niebuhr, K., Gerstel, B., Pistor, S., Temm-Grove, C.J., Jockusch, B.M., Reinhard, M., Walter, U., *et al.* (1995). A focal adhesion factor directly linking intracellularly motile Listeria monocytogenes and Listeria ivanovii to the actin-based cytoskeleton of mammalian cells. EMBO J *14*, 1314-1321.

Chen, L., Daum, G., Fischer, J.W., Hawkins, S., Bochaton-Piallat, M.L., Gabbiani, G., and Clowes, A.W. (2000). Loss of expression of the beta subunit of soluble guanylyl cyclase prevents nitric oxide-mediated inhibition of DNA synthesis in smooth muscle cells of old rats. Circ Res *86*, 520-525.

Cinti, S. (2005). The adipose organ. Prostaglandins Leukot Essent Fatty Acids *73*, 9-15.

Culmsee, C., Gerling, N., Landshamer, S., Rickerts, B., Duchstein, H.J., Umezawa, K., Klumpp, S., and Krieglstein, J. (2005). Nitric oxide donors induce neurotrophin-like survival signaling and protect neurons against apoptosis. Mol Pharmacol *68*, 1006-1017.

Cypess, A.M., Lehman, S., Williams, G., Tal, I., Rodman, D., Goldfine, A.B., Kuo, F.C., Palmer, E.L., Tseng, Y.H., Doria, A., *et al.* (2009). Identification and importance of brown adipose tissue in adult humans. N Engl J Med *360*, 1509-1517.

Dull, T., Zufferey, R., Kelly, M., Mandel, R.J., Nguyen, M., Trono, D., and Naldini, L. (1998). A third-generation lentivirus vector with a conditional packaging system. J Virol *72*, 8463-8471.

Finucane, M.M., Stevens, G.A., Cowan, M.J., Danaei, G., Lin, J.K., Paciorek, C.J., Singh, G.M., Gutierrez, H.R., Lu, Y., Bahalim, A.N., *et al.* National, regional, and global trends in body-mass index since 1980: systematic analysis of health examination surveys and

epidemiological studies with 960 country-years and 9.1 million participants. Lancet *377*, 557-567.

Forner, F., Kumar, C., Luber, C.A., Fromme, T., Klingenspor, M., and Mann, M. (2009). Proteome differences between brown and white fat mitochondria reveal specialized metabolic functions. Cell Metab *10*, 324-335.

Francis, S.H., Busch, J.L., Corbin, J.D., and Sibley, D. (2010). cGMP-dependent protein kinases and cGMP phosphodiesterases in nitric oxide and cGMP action. Pharmacol Rev *62*, 525-563.

Friebe, A., and Koesling, D. (2003). Regulation of nitric oxide-sensitive guanylyl cyclase. Circ Res *93*, 96-105.

Frost, J.A., Xu, S., Hutchison, M.R., Marcus, S., and Cobb, M.H. (1996). Actions of Rho family small G proteins and p21-activated protein kinases on mitogen-activated protein kinase family members. Mol Cell Biol *16*, 3707-3713.

Furchgott, R.F., and Vanhoutte, P.M. (1989). Endothelium-derived relaxing and contracting factors. FASEB J *3*, 2007-2018.

Galic, S., Oakhill, J.S., and Steinberg, G.R. Adipose tissue as an endocrine organ. Mol Cell Endocrinol *316*, 129-139.

Gambaryan, S., Hauser, W., Kobsar, A., Glazova, M., and Walter, U. (2001). Distribution, cellular localization, and postnatal development of VASP and Mena expression in mouse tissues. Histochem Cell Biol *116*, 535-543.

Garbers, D.L., Chrisman, T.D., Wiegn, P., Katafuchi, T., Albanesi, J.P., Bielinski, V., Barylko, B., Redfield, M.M., and Burnett, J.C., Jr. (2006). Membrane guanylyl cyclase receptors: an update. Trends Endocrinol Metab *17*, 251-258.

Garbers, D.L., and Lowe, D.G. (1994). Guanylyl cyclase receptors. J Biol Chem *269*, 30741-30744.

Garcia Arguinzonis, M.I., Galler, A.B., Walter, U., Reinhard, M., and Simm, A. (2002). Increased spreading, Rac/p21-activated kinase (PAK) activity, and compromised cell motility in cells deficient in vasodilator-stimulated phosphoprotein (VASP). J Biol Chem *277*, 45604-45610.

Garthwaite, J., Charles, S.L., and Chess-Williams, R. (1988). Endothelium-derived relaxing factor release on activation of NMDA receptors suggests role as intercellular messenger in the brain. Nature *336*, 385-388.

Gertler, F.B., Comer, A.R., Juang, J.L., Ahern, S.M., Clark, M.J., Liebl, E.C., and Hoffmann, F.M. (1995). enabled, a dosage-sensitive suppressor of mutations in the Drosophila Abl tyrosine kinase, encodes an Abl substrate with SH3 domain-binding properties. Genes Dev *9*, 521-533.

Gertler, F.B., Niebuhr, K., Reinhard, M., Wehland, J., and Soriano, P. (1996). Mena, a relative of VASP and Drosophila Enabled, is implicated in the control of microfilament dynamics. Cell *87*, 227-239.

Goh, K.L., Cai, L., Cepko, C.L., and Gertler, F.B. (2002). Ena/VASP proteins regulate cortical neuronal positioning. Curr Biol *12*, 565-569.

Guilak, F., Awad, H.A., Fermor, B., Leddy, H.A., and Gimble, J.M. (2004). Adipose-derived adult stem cells for cartilage tissue engineering. Biorheology *41*, 389-399.

Guo, D., Tan, Y.C., Wang, D., Madhusoodanan, K.S., Zheng, Y., Maack, T., Zhang, J.J., and Huang, X.Y. (2007). A Rac-cGMP signaling pathway. Cell *128*, 341-355.

Haas, B., Mayer, P., Jennissen, K., Scholz, D., Diaz, M.B., Bloch, W., Herzig, S., Fassler, R., and Pfeifer, A. (2009). Protein kinase g controls brown fat cell differentiation and mitochondrial biogenesis. Sci Signal *2*, ra78.

Haffner, C., Jarchau, T., Reinhard, M., Hoppe, J., Lohmann, S.M., and Walter, U. (1995). Molecular cloning, structural analysis and functional expression of the proline-rich focal adhesion and microfilament-associated protein VASP. EMBO J *14*, 19-27.

Halbrugge, M., and Walter, U. (1989). Purification of a vasodilator-regulated phosphoprotein from human platelets. Eur J Biochem *185*, 41-50.

Hall, A. (1998). G proteins and small GTPases: distant relatives keep in touch. Science *280*, 2074-2075.

Hattori, H., Sato, M., Masuoka, K., Ishihara, M., Kikuchi, T., Matsui, T., Takase, B., Ishizuka, T., Kikuchi, M., and Fujikawa, K. (2004). Osteogenic potential of human adipose tissue-derived stromal cells as an alternative stem cell source. Cells Tissues Organs *178*, 2-12.

Hofmann, F., Ammendola, A., and Schlossmann, J. (2000). Rising behind NO: cGMP-dependent protein kinases. J Cell Sci *113 (Pt 10)*, 1671-1676.

Hou, Y., Ye, R.D., and Browning, D.D. (2004). Activation of the small GTPase Rac1 by cGMP-dependent protein kinase. Cell Signal *16*, 1061-1069.

Hu, E., Kim, J.B., Sarraf, P., and Spiegelman, B.M. (1996). Inhibition of adipogenesis through MAP kinase-mediated phosphorylation of PPARgamma. Science *274*, 2100-2103.

Hu, J., Roy, S.K., Shapiro, P.S., Rodig, S.R., Reddy, S.P., Platanias, L.C., Schreiber, R.D., and Kalvakolanu, D.V. (2001). ERK1 and ERK2 activate CCAAAT/enhancer-binding protein-beta-dependent gene transcription in response to interferon-gamma. J Biol Chem *276*, 287-297.

Huttelmaier, S., Harbeck, B., Steffens, O., Messerschmidt, T., Illenberger, S., and Jockusch, B.M. (1999). Characterization of the actin binding properties of the vasodilator-stimulated phosphoprotein VASP. FEBS Lett *451*, 68-74.

Huttelmaier, S., Mayboroda, O., Harbeck, B., Jarchau, T., Jockusch, B.M., and Rudiger, M. (1998). The interaction of the cell-contact proteins VASP and vinculin is regulated by phosphatidylinositol-4,5-bisphosphate. Curr Biol *8*, 479-488.

Ignarro, L.J., Cirino, G., Casini, A., and Napoli, C. (1999). Nitric oxide as a signaling molecule in the vascular system: an overview. J Cardiovasc Pharmacol *34*, 879-886.

In 't Anker, P.S., Scherjon, S.A., Kleijburg-van der Keur, C., de Groot-Swings, G.M., Claas, F.H., Fibbe, W.E., and Kanhai, H.H. (2004). Isolation of mesenchymal stem cells of fetal or maternal origin from human placenta. Stem Cells *22*, 1338-1345.

Jaffe, A.B., and Hall, A. (2005). Rho GTPases: biochemistry and biology. Annu Rev Cell Dev Biol *21*, 247-269.

Jonckheere, V., Lambrechts, A., Vandekerckhove, J., and Ampe, C. (1999). Dimerization of profilin II upon binding the (GP5)3 peptide from VASP overcomes the inhibition of actin nucleation by profilin II and thymosin beta4. FEBS Lett *447*, 257-263.

Kajimura, S., Seale, P., Kubota, K., Lunsford, E., Frangioni, J.V., Gygi, S.P., and Spiegelman, B.M. (2009). Initiation of myoblast to brown fat switch by a PRDM16-C/EBP-beta transcriptional complex. Nature *460*, 1154-1158.

Kajimura, S., Seale, P., and Spiegelman, B.M. (2010). Transcriptional control of brown fat development. Cell Metab *11*, 257-262.

Kiosses, W.B., Daniels, R.H., Otey, C., Bokoch, G.M., and Schwartz, M.A. (1999). A role for p21-activated kinase in endothelial cell migration. J Cell Biol *147*, 831-844.

Kloss, S., Rodenbach, D., Bordel, R., and Mulsch, A. (2005). Human-antigen R (HuR) expression in hypertension: downregulation of the mRNA stabilizing protein HuR in genetic hypertension. Hypertension *45*, 1200-1206.

Knowles, R.G., and Moncada, S. (1992). Nitric oxide as a signal in blood vessels. Trends Biochem Sci *17*, 399-402.

Koesling, D., Russwurm, M., Mergia, E., Mullershausen, F., and Friebe, A. (2004). Nitric oxide-sensitive guanylyl cyclase: structure and regulation. Neurochem Int *45*, 813-819.

Krause, M., Dent, E.W., Bear, J.E., Loureiro, J.J., and Gertler, F.B. (2003). Ena/VASP proteins: regulators of the actin cytoskeleton and cell migration. Annu Rev Cell Dev Biol *19*, 541-564.

Krause, M., Sechi, A.S., Konradt, M., Monner, D., Gertler, F.B., and Wehland, J. (2000). Fyn-binding protein (Fyb)/SLP-76-associated protein (SLAP), Ena/vasodilator-stimulated phosphoprotein (VASP) proteins and the Arp2/3 complex link T cell receptor (TCR) signaling to the actin cytoskeleton. J Cell Biol *149*, 181-194.

Kuznetsov, A.V., Veksler, V., Gellerich, F.N., Saks, V., Margreiter, R., and Kunz, W.S. (2008). Analysis of mitochondrial function in situ in permeabilized muscle fibers, tissues and cells. Nat Protoc *3*, 965-976.

Langin, D. (2010). Adipose tissue lipolysis revisited (again!): lactate involvement in insulin antilipolytic action. Cell Metab *11*, 242-243.

Lanier, L.M., Gates, M.A., Witke, W., Menzies, A.S., Wehman, A.M., Macklis, J.D., Kwiatkowski, D., Soriano, P., and Gertler, F.B. (1999). Mena is required for neurulation and commissure formation. Neuron *22*, 313-325.

Lincoln, T.M. (1989). Cyclic GMP and mechanisms of vasodilation. Pharmacol Ther *41*, 479-502.

MacMicking, J.D., Nathan, C., Hom, G., Chartrain, N., Fletcher, D.S., Trumbauer, M., Stevens, K., Xie, Q.W., Sokol, K., Hutchinson, N., *et al.* (1995). Altered responses to bacterial infection and endotoxic shock in mice lacking inducible nitric oxide synthase. Cell *81*, 641-650.

Maruta, H., Nheu, T.V., He, H., and Hirokawa, Y. (2003). Rho family-associated kinases PAK1 and rock. Prog Cell Cycle Res *5*, 203-210.

McBeath, R., Pirone, D.M., Nelson, C.M., Bhadriraju, K., and Chen, C.S. (2004). Cell shape, cytoskeletal tension, and RhoA regulate stem cell lineage commitment. Dev Cell *6*, 483-495.

Mellion, B.T., Ignarro, L.J., Ohlstein, E.H., Pontecorvo, E.G., Hyman, A.L., and Kadowitz, P.J. (1981). Evidence for the inhibitory role of guanosine 3', 5'-monophosphate in ADP-induced human platelet aggregation in the presence of nitric oxide and related vasodilators. Blood *57*, 946-955.

Mergia, E., Russwurm, M., Zoidl, G., and Koesling, D. (2003). Major occurrence of the new alpha2beta1 isoform of NO-sensitive guanylyl cyclase in brain. Cell Signal *15*, 189-195.

Murholm, M., Dixen, K., and Hansen, J.B. (2010). Ras signalling regulates differentiation and UCP1 expression in models of brown adipogenesis. Biochim Biophys Acta *1800*, 619-627.

Nechad, M. (1983). Development of brown fat cells in monolayer culture. II. Ultrastructural characterization of precursors, differentiating adipocytes and their mitochondria. Exp Cell Res *149*, 119-127.

Nedergaard, J., Bengtsson, T., and Cannon, B. (2007). Unexpected evidence for active brown adipose tissue in adult humans. Am J Physiol Endocrinol Metab *293*, E444-452.

Nedergaard, J., Herron, D., Jacobsson, A., Rehnmark, S., and Cannon, B. (1995). Norepinephrine as a morphogen?: its unique interaction with brown adipose tissue. Int J Dev Biol *39*, 827-837.

Nisoli, E., Clementi, E., Paolucci, C., Cozzi, V., Tonello, C., Sciorati, C., Bracale, R., Valerio, A., Francolini, M., Moncada, S., *et al.* (2003). Mitochondrial biogenesis in mammals: the role of endogenous nitric oxide. Science *299*, 896-899.

Nisoli, E., Clementi, E., Tonello, C., Sciorati, C., Briscini, L., and Carruba, M.O. (1998). Effects of nitric oxide on proliferation and differentiation of rat brown adipocytes in primary cultures. Br J Pharmacol *125*, 888-894.

Nisoli, E., Falcone, S., Tonello, C., Cozzi, V., Palomba, L., Fiorani, M., Pisconti, A., Brunelli, S., Cardile, A., Francolini, M., *et al.* (2004). Mitochondrial biogenesis by NO yields functionally active mitochondria in mammals. Proc Natl Acad Sci U S A *101*, 16507-16512.

O'Dell, T.J., Hawkins, R.D., Kandel, E.R., and Arancio, O. (1991). Tests of the roles of two diffusible substances in long-term potentiation: evidence for nitric oxide as a possible early retrograde messenger. Proc Natl Acad Sci U S A *88*, 11285-11289.

Pfeifer, A., Ruth, P., Dostmann, W., Sausbier, M., Klatt, P., and Hofmann, F. (1999). Structure and function of cGMP-dependent protein kinases. Rev Physiol Biochem Pharmacol *135*, 105-149.

Pittenger, M.F., Mackay, A.M., Beck, S.C., Jaiswal, R.K., Douglas, R., Mosca, J.D., Moorman, M.A., Simonetti, D.W., Craig, S., and Marshak, D.R. (1999). Multilineage potential of adult human mesenchymal stem cells. Science *284*, 143-147.

Pollard, T.D., and Borisy, G.G. (2003). Cellular motility driven by assembly and disassembly of actin filaments. Cell *112*, 453-465.

Price, L.S., Leng, J., Schwartz, M.A., and Bokoch, G.M. (1998). Activation of Rac and Cdc42 by integrins mediates cell spreading. Mol Biol Cell *9*, 1863-1871.

Prunet-Marcassus, B., Cousin, B., Caton, D., Andre, M., Penicaud, L., and Casteilla, L. (2006). From heterogeneity to plasticity in adipose tissues: site-specific differences. Exp Cell Res *312*, 727-736.

Prusty, D., Park, B.H., Davis, K.E., and Farmer, S.R. (2002). Activation of MEK/ERK signaling promotes adipogenesis by enhancing peroxisome proliferator-activated receptor gamma (PPARgamma) and C/EBPalpha gene expression during the differentiation of 3T3-L1 preadipocytes. J Biol Chem *277*, 46226-46232.

Reinhard, M., Giehl, K., Abel, K., Haffner, C., Jarchau, T., Hoppe, V., Jockusch, B.M., and Walter, U. (1995). The proline-rich focal adhesion and microfilament protein VASP is a ligand for profilins. EMBO J *14*, 1583-1589.

Reinhard, M., Halbrugge, M., Scheer, U., Wiegand, C., Jockusch, B.M., and Walter, U. (1992). The 46/50 kDa phosphoprotein VASP purified from human platelets is a novel protein associated with actin filaments and focal contacts. EMBO J *11*, 2063-2070.

Reinhard, M., Jarchau, T., and Walter, U. (2001). Actin-based motility: stop and go with Ena/VASP proteins. Trends Biochem Sci *26*, 243-249.

Reinhard, M., Rudiger, M., Jockusch, B.M., and Walter, U. (1996). VASP interaction with vinculin: a recurring theme of interactions with proline-rich motifs. FEBS Lett *399*, 103-107.

Robidoux, J., Martin, T.L., and Collins, S. (2004). Beta-adrenergic receptors and regulation of energy expenditure: a family affair. Annu Rev Pharmacol Toxicol *44*, 297-323.

Rosen, E.D., Walkey, C.J., Puigserver, P., and Spiegelman, B.M. (2000). Transcriptional regulation of adipogenesis. Genes Dev *14*, 1293-1307.

Safford, K.M., Safford, S.D., Gimble, J.M., Shetty, A.K., and Rice, H.E. (2004). Characterization of neuronal/glial differentiation of murine adipose-derived adult stromal cells. Exp Neurol *187*, 319-328.

Saiki, R.K., Gelfand, D.H., Stoffel, S., Scharf, S.J., Higuchi, R., Horn, G.T., Mullis, K.B., and Erlich, H.A. (1988). Primer-directed enzymatic amplification of DNA with a thermostable DNA polymerase. Science *239*, 487-491.

Saito, M., Okamatsu-Ogura, Y., Matsushita, M., Watanabe, K., Yoneshiro, T., Nio-Kobayashi, J., Iwanaga, T., Miyagawa, M., Kameya, T., Nakada, K., *et al.* (2009). High

incidence of metabolically active brown adipose tissue in healthy adult humans: effects of cold exposure and adiposity. Diabetes *58*, 1526-1531.

Sale, E.M., Atkinson, P.G., and Sale, G.J. (1995). Requirement of MAP kinase for differentiation of fibroblasts to adipocytes, for insulin activation of p90 S6 kinase and for insulin or serum stimulation of DNA synthesis. EMBO J *14*, 674-684.

Sawada, N., Itoh, H., Yamashita, J., Doi, K., Inoue, M., Masatsugu, K., Fukunaga, Y., Sakaguchi, S., Sone, M., Yamahara, K., *et al.* (2001). cGMP-dependent protein kinase phosphorylates and inactivates RhoA. Biochem Biophys Res Commun *280*, 798-805.

Schlossmann, J., Ammendola, A., Ashman, K., Zong, X., Huber, A., Neubauer, G., Wang, G.X., Allescher, H.D., Korth, M., Wilm, M., *et al.* (2000). Regulation of intracellular calcium by a signalling complex of IRAG, IP3 receptor and cGMP kinase Ibeta. Nature *404*, 197-201.

Schwarz, U.R., Walter, U., and Eigenthaler, M. (2001). Taming platelets with cyclic nucleotides. Biochem Pharmacol *62*, 1153-1161.

Seale, P., Bjork, B., Yang, W., Kajimura, S., Chin, S., Kuang, S., Scime, A., Devarakonda, S., Conroe, H.M., Erdjument-Bromage, H., *et al.* (2008). PRDM16 controls a brown fat/skeletal muscle switch. Nature *454*, 961-967.

Seale, P., Kajimura, S., Yang, W., Chin, S., Rohas, L.M., Uldry, M., Tavernier, G., Langin, D., and Spiegelman, B.M. (2007). Transcriptional control of brown fat determination by PRDM16. Cell Metab *6*, 38-54.

Sengenes, C., Bouloumie, A., Hauner, H., Berlan, M., Busse, R., Lafontan, M., and Galitzky, J. (2003). Involvement of a cGMP-dependent pathway in the natriuretic peptide-mediated hormone-sensitive lipase phosphorylation in human adipocytes. J Biol Chem *278*, 48617-48626.

Sharina, I.G., Krumenacker, J.S., Martin, E., and Murad, F. (2000). Genomic organization of alpha1 and beta1 subunits of the mammalian soluble guanylyl cyclase genes. Proc Natl Acad Sci U S A *97*, 10878-10883.

Sonnenburg, W.K., and Beavo, J.A. (1994). Cyclic GMP and regulation of cyclic nucleotide hydrolysis. Adv Pharmacol *26*, 87-114.

Sordella, R., Jiang, W., Chen, G.C., Curto, M., and Settleman, J. (2003). Modulation of Rho GTPase signaling regulates a switch between adipogenesis and myogenesis. Cell *113*, 147-158.

Timmons, J.A., Wennmalm, K., Larsson, O., Walden, T.B., Lassmann, T., Petrovic, N., Hamilton, D.L., Gimeno, R.E., Wahlestedt, C., Baar, K., *et al.* (2007). Myogenic gene expression signature establishes that brown and white adipocytes originate from distinct cell lineages. Proc Natl Acad Sci U S A *104*, 4401-4406.

Trautwein, C., Caelles, C., van der Geer, P., Hunter, T., Karin, M., and Chojkier, M. (1993). Transactivation by NF-IL6/LAP is enhanced by phosphorylation of its activation domain. Nature *364*, 544-547.

Tsutsui, M., Shimokawa, H., Otsuji, Y., Ueta, Y., Sasaguri, Y., and Yanagihara, N. (2009). Nitric oxide synthases and cardiovascular diseases: insights from genetically modified mice. Circ J *73*, 986-993.

Uldry, M., Yang, W., St-Pierre, J., Lin, J., Seale, P., and Spiegelman, B.M. (2006). Complementary action of the PGC-1 coactivators in mitochondrial biogenesis and brown fat differentiation. Cell Metab *3*, 333-341.

van Marken Lichtenbelt, W.D., Vanhommerig, J.W., Smulders, N.M., Drossaerts, J.M., Kemerink, G.J., Bouvy, N.D., Schrauwen, P., and Teule, G.J. (2009). Cold-activated brown adipose tissue in healthy men. N Engl J Med *360*, 1500-1508.

Vasioukhin, V., Bauer, C., Yin, M., and Fuchs, E. (2000). Directed actin polymerization is the driving force for epithelial cell-cell adhesion. Cell *100*, 209-219.

Virtanen, K.A., Lidell, M.E., Orava, J., Heglind, M., Westergren, R., Niemi, T., Taittonen, M., Laine, J., Savisto, N.J., Enerback, S., *et al.* (2009). Functional brown adipose tissue in healthy adults. N Engl J Med *360*, 1518-1525.

White, M.F., and Kahn, C.R. (1994). The insulin signaling system. J Biol Chem *269*, 1-4.

Zabel, U., Hausler, C., Weeger, M., and Schmidt, H.H. (1999). Homodimerization of soluble guanylyl cyclase subunits. Dimerization analysis using a glutathione s-transferase affinity tag. J Biol Chem *274*, 18149-18152.

Zhang, S., Han, J., Sells, M.A., Chernoff, J., Knaus, U.G., Ulevitch, R.J., and Bokoch, G.M. (1995). Rho family GTPases regulate p38 mitogen-activated protein kinase through the downstream mediator Pak1. J Biol Chem *270*, 23934-23936.

Zhuo, M., and Hawkins, R.D. (1995). Long-term depression: a learning-related type of synaptic plasticity in the mammalian central nervous system. Rev Neurosci *6*, 259-277.

Zuk, P.A., Zhu, M., Ashjian, P., De Ugarte, D.A., Huang, J.I., Mizuno, H., Alfonso, Z.C., Fraser, J.K., Benhaim, P., and Hedrick, M.H. (2002). Human adipose tissue is a source of multipotent stem cells. Mol Biol Cell *13*, 4279-4295.